Aus dem Departement für Physik
Universität Freiburg (Schweiz)

Nanoparticle Hybrid Systems
Synthesis of a Tailored Composite Model

INAUGURAL-DISSERTATION

zur Erlangung der Würde des *Doctor rerum naturalium*
der Mathematisch-Naturwissenschaftlichen Fakultät
der Universität Freiburg in der Schweiz

vorgelegt von
Hervé Dietsch
aus
Strasbourg (Frankreich)

Nr. 1537
Empa Druckerei
2006

Von der Mathematisch-Naturwissenschaftlichen Fakultät der Universität Freiburg in der Schweiz angenommen, auf Antrag der Jury:

Dissertationsleiter:	Prof. P. Schurtenberger, Universität Freiburg
Gutachter:	Dr. B. A. Keller, Empa Dübendorf
	Prof. R. Mezzenga, Universität Freiburg
	Dr. F. Prochazka, Université de Saint-Etienne (France)
Jurypräsident:	Prof. J. C. Dousse, Universität Freiburg

Freiburg, 09.10.2006

Dissertationsleiter: Prof. Dr. P. Schurtenberger

Fakultätsdekan: Prof. Dr. T. A. Jenny

A Jana, présente pour moi à tout moment, source de joie de vivre, secret de mon inspiration, de ma motivation et de mon bien-être.

Financial support was provided by the Commission Suisse pour la Technologie et l'Innovation (CTI), Project no 6056.2.

1

Abstract, Résumé, Zusammenfassung

1.1 Abstract

Spherical and monodisperse $\mathrm{Si O_2}$ silica colloidal particles in a range of 30 nm to 1 μm are prepared using sol-gel processes. Their surfaces are functionalized with silane agent allowing covalent bond formation or not with macromolecules chains of a crosslinked elastomer (PMMA or PAA), polymerized under UV light.
In order to track particle under shear, there is a need to produce fluorescent particle. As commercial organic dyes (FITC, RITC) show photobleaching, our motivation to get stable fluorescent particle under UV excitation leads to a new synthesis for CdSe quantum dots at low temperatures. This approach allows the synthesis at large scale and low costs of fluorescent particles emitting from yellow to red. Incorporation of these quantum dots, avoiding any loss in the fluorescence emission and using another silane agent, the 3-propyl trimethoxymercapto silane is also described.
An in-situ study and characterization of the nanocomposite is performed using tribology, rheology, 3-DLS and SANS techniques. After proving that agglomeration and/or aggregation are avoided in our process (3-DLS, SANS), mechanical (tribology, rheology) and thermal (DSC, ATG) studies showed the effect of the ratio $\frac{V_{NP}}{S_S}.\phi$ with V_{NP}, volume of a single particle, S_S, specific surface of a particle and ϕ, the volume fraction of incorporated particles, on the friction coefficient, and the glass temperature.

1.2 Résumé

Des colloïdes de silice sphériques et monodisperses sont préparés par voie sol-gel avec des diamètres compris entre 30 nm et 1 μm. Leur surface est fonctionnalisée par differents silanes permettant des liaisons covalentes ou non avec les chaînes d'un réseau élastomère (PMMA ou PAA), polymerisés in-situ sous lampe UV.
Afin de suivre la trajectoire de particules sous cisaillement, il est nécessaire de les rendre fluorescentes. Les marqueurs fluorescents organiques (FITC, RITC) photoblanchissent, notre motivation pour obtenir des particules fluorescentes stables a mené à une nouvelle synthèse pour l'obtention de CdSe quantum dots, à basse température. Cette approche permet la synthèse à grande échelle et à faible coût de particules fluorescente emmettant du jaune au rouge. L'incorporation de ces quantum dots évitant tout problème de baisse de l'émission et utilisant un autre

agent silane, le 3-propyltrimethoxymercapto silane est également décrite.
L'étude in-situ et la characterisation du nanocomposite obtenu est effectuée utilisant les instruments de tribologie, rhéologie, 3-DLS et SANS. Après preuve faite que toute agglomération et/ou aggrégation est évitée dans notre procédé (3-DLS, SANS), des études mécaniques (tribologie, rheologie) et thermiques (DSC, TGA) ont montrés l'effet du ratio $\frac{V_{NP}}{S_S}.\phi$ avec V_{NP}, le volume d'une particule, S_S, la surface specifique d'une particule et ϕ, la fraction volumique de particules incorporées, sur le coefficient de friction et la température de transition vitreuse.

1.3 Zusammenfassung

Spherische und uniform dispergierte $\mathrm{Si O_2}$ Silica-Partikel werden durch eine Sol-Gel Synthese mit Durchmesser zwischen 30 nm und 1 μm hergestellt. Die Oberfläsche wurde durch verschiedenen Silane funktionalisiert. Die Silane ermöglichen sowohl eine kovalente Bindung an die Polymerketten (PMMA oder PAA), von welches polymerisiert unter einer UV Lampe, als auch eine nicht kovalente Bindung.
Um die Partikel unter dem Einfluss von Scherkräften folgen zu können, braucht man fluorescierende Partikel. Die fluorescierenden organische "dyes" (FITC, RITC) "photobleachen", unsere Motivation um stabile fluorescierende Partikel zu haben hat zu einer neuen CdSe Quantum Dot Synthese mit nidriegen Temperaturen geführt. Diese erlaubt die Synthese von einer größeren Menge mit geringen Kosten von fluorescierende Partikeln, die zwischen gelb und rot emittieren. Die Einbettung von diesen Quantum Dot ohne Rückgang der Fluoreszenz auf der Oberfläche von den Silica-Partikeln ist auch beschrieben. Dafür braucht man ein anderes Silan: das 3-Propyltrimethoxymercapto Silane.
Die in-situ Studie und die Nanokomposite Characterizierung ist mit Tribologie, Rheologie, 3-DLS und SANS durchgeführt. Nach dem Beweis, dass Agglomerierung und/oder Aggregierung in unserem Prozess vermieden ist, zeigen mechanische (Tribologie, Rheologie) und thermische (DSC, ATG) Untersuchungen den Einfluss von der Ratio $\frac{V_{NP}}{S_S}.\phi$ mit V_{NP}, Volume einem Partikel, S_S, die spezifische Oberfläche von einem einzelnen Partikel und ϕ, den Volumenanteil von eingebetteten Partikeln auf den Reibungskoefficient und die Glastemperatur.

Contents

1 Abstract, Résumé, Zusammenfassung . . . 1
1.1 Abstract . . . 1
1.2 Résumé . . . 1
1.3 Zusammenfassung . . . 2

2 Introduction . . . 5

3 Monodisperse functional silica particles: Synthesis and Characterization . . . 9
3.1 Synthesis of silica nanoparticles in basic environment . . . 11
3.1.1 Principe: Stöber method . . . 11
3.1.2 Controlled growth . . . 15
3.1.3 Experimental examples . . . 18
3.2 Silane modification . . . 21
3.2.1 Chemical structure and reactivity of the particle surface . . . 21
3.2.2 Surface modification . . . 23
3.3 Characterization of silica nanoparticles and their modified products . . . 25
3.3.1 Determination of the particle sizes and specific surfaces . . . 25
3.3.2 $^{29}\mathrm{Si}$ NMR . . . 27
3.3.3 Long term stability of the dispersed nanoparticles . . . 28
3.4 Conclusion of chapter 3 . . . 29

4 Synthesis of fluorescent silica particles . . . 31
4.1 Organic dyes . . . 31
4.1.1 Fluorescein isothiocyanate (FITC) . . . 31
4.1.2 Rhodamine isothiocyanate (TRITC) . . . 33
4.2 Quantum dots . . . 34
4.2.1 Different routes to the synthesis of quantum dots . . . 34
4.2.2 Synthetic route to a large amount of CdSe quantum dots at low temperatures for label applications . . . 38
4.2.3 Incorporation of quantum dots . . . 47
4.3 Conclusion of chapter 4 . . . 51

5 Synthesis of monodisperse distributed $\mathrm{SiO_2}$-Polymer hybrid system . . . 53
5.1 Polymerization and copolymerization . . . 53
5.1.1 Different type of polymerizations . . . 54
5.1.2 Photopolymerization . . . 56

5.2 Synthesis of a SiO_2-PAA hybrid system with commercial products 62
5.3 Conclusion of chapter 5 67

6 Characterization: light scattering, thermal, rheological and mechanical behaviors of the hybrid system 69
6.1 In-situ polymerization as a route towards transparent nanocomposites: Time-resolved light and neutron scattering experiments 69
6.2 Influence of the filler size and volume on the glass temperature and friction coefficient in a silica particles-PMMA hybrid composite 82
6.3 Synthesis and rheological study of tailored monodisperse and monodistributed SiO_2-PMMA composites 88

7 Conclusion 101

References 109

Curriculum Vitae 125

List of publications and communications 127

Acknowledgements 129

2

Introduction

Polymer and nanoparticles hybrid systems have been produced for decades for use in a variety of high performance materials [87] [134].
Developing new polymer materials to change their properties is not always the easiest way to proceed. Polymer blends or nanoparticle hybrid systems allow getting new material properties such as high impact resistant polymers and special coatings. Syntheses of new polymer or copolymer require much more time than by mixing several existing products and that is why combining inorganic-materials with polymers presents important new extensions.

The combination of nanosized inorganic particles with macromolecular polymer chains allows designing new products combining properties of both, applications are diverse:

- waterborne (for example clays and polyurethane [65]),
- special paints (conducting paints using carbon nanotubes [129]),
- special adhesives (for example pressure sensitive adhesives or hot melts) with gas permeation barrier using organically modified montmorillonite and polyurethane [89],
- redispersible latices powder,
- special coatings: hard coatings [82], coatings with special effects (mimic of nacre [116]),
- biotechnology, biomedical products [21],
- drug delivery (biodegradable polymeric nanoparticles [120]), medical diagnostics,
- problem solving electronics,
- magnetics [48],
- optoelectronics [119].

Industrially relevant polymer-particle hybrid systems are almost never dilute. A fundamental understanding of processes in dense nanoparticle systems (10-100 nm) requires excellence in synthesis, characterization and modeling.

The goal of the project was to study interactions, local structure and mobility of such hybrid systems. The purpose at Empa was more concentrated on the establishment of a tailored monodisperse hybrid system and so aimed to synthesize and characterize the hybrid system.
To build a model system, there was a need to control all the synthesis step and to work with high defined materials.

The first part of this thesis work focuses on the well-known Stöber sol-gel synthesis method [123] and chemistries used to produce silica particles in the 20-1000 nanometer range.
Historically, Gerhard Kolbe did the first sol-gel synthesis of $\mathrm{SiO_2}$ silica particles during his PhD work in 1956, but he did not publish the synthesis of nanoparticles, which let the opportunity to Stöber *et al* to find again this synthesis process twelve years later.
Stöber studied the influence of solution concentrations to get diverse particle sizes in a range between 50 nm and 2 μm but neglige two important points: the influence of the temperature of synthesis [127] (which control a homogeneous nucleation), which controls polydispersity and the ratio $\frac{[\mathrm{H_2O}]}{[TEOS]}$, relevant parameter to control the formation speed and the final size of the particles obtained.

An improvement allowing to produce quickly large particles ($\geq$ 400 nm) is described. An overview of characterization in terms of size, shape and specific surface is given. Big specific surface on the nanoparticles allows grafting a large variety of functional groups on the particle surface using silane agent.

Synthesis of fluorescent particles is described in the second chapter, an approach using classical organic dyes for fluorescent labeling is explained. Photobleaching problems occurs and that is why another solution using $\mathrm{CdSe(ZnS)}$ core-shell nanocrystals is preferred. Due to their important price, $\mathrm{CdSe(ZnS)}$ core-shell quantum dots have not been used so much as fluorescent marker and as a solution against photobleaching. A new synthesis of the $\mathrm{CdSe(ZnS)}$ core-shell semiconductor quantum dots and its incorporation with $\mathrm{SiO_2}$ silica particles is described.

In a third part, we associated polymer and particles to get hybrid systems. The description of the synthesis of a highly monodisperse and tailored system is explained in detail in the publication *Synthesis and rheological study of tailored monodisperse and monodistributed* $\mathrm{SiO_2}$*-PMMA composites*, which has been recently submitted.
This synthesis was based on the work of Ford *et al* [59], who were the first who synthesized monodistributed particles in a polymer medium for optical applications presented in the work of a collaborator of Ford: Jethmalani *et al* [56] [57] [58]. The system used in this research group are quite similar as ours, they use silica-poly(methyl methacrylate) and silica-poly(methyl acrylate) hybrid systems, but using commercial silica colloids and multi dialysis steps.
More recently, two PhD student Muriel Mauger and Julien Berriot concentrated on the characterization of these hybrid systems. Mauger *et al* [74] characterized silica@TPM-PMMA copolymer with optical tools like transmission electron microscopy (TEM and Atomic Force Microscopy (AFM)). Pictures showed an good dispersion but could not quantified the dispersion and distribution stage of the particles in the matrix. Berriot *et al* concentrated on silica@TPM-

ethyl acrylate elastomer, probably for wheel use. His characterization were more relevant using Small Angle Neutron Scattering (SANS) [13] to understand and determine the molecular mechanisms that are at the origin of the specific properties of hybrid systems. ^{1}H Nuclear Magnetic Resonance (NMR) [10] allows checking the percentage of TPM silane agent bound on the particle surface and a glass temperature study using rheological tool [11] [79] [12].

An in-situ characterization using 3 dimension light scattering and small-angle neutron scattering tools proves the non-existence of agglomerate during the polymerization process, this result led to a the formation of a highly transparent nanocomposite and a publication, collaboration between the University of Fribourg and Empa. Quantitative informations about the time dependence of the resulting mechanical and structural properties during the synthesis were obtained from these experiments. An observation of a qualitative change between diffusive and subdiffusive motion for the dispersed nanoparticles at the gel point is observed. Small-angle neutron scattering experiments clearly demonstrate that the initial liquid-like order of the nanoparticles is maintained during the polymerization process, and that there is no indication for particle aggregation. These results allow the simplification of the well known relation of Mayo-Lewis concerning copolymers kinetics presented in chapter 5.11.

The fourth and last scientific part details the characterization performed at Empa on the hybrid systems, changes in terms of tribological, rheological and thermal behaviors are presented and interpreted.
A major problem in the current ”nano”research is the size establishing the border between interactions on the local structure and intrinsic interactions. This makes the comparison between a microparticle-polymer hybrid system and a nanoparticle-polymer hybrid system difficult. ”Nano” implies per definition large surface area, which means more interaction because of more interface between particles and macromolecules. Larger interface is of course obtained for a comparable volume fraction of particles, so that we could establish a ratio between volume of particle embedded and surface area of this volume of particles (determined through BET or calculated by the use of the particle size and density).
This work is presented in a communication in the Journal of Tribology (JT) showing the influence on the glass temperature (Tg) and friction coefficient for different particle sizes and concentrations embedded in PMMA.

3

Monodisperse functional silica particles: Synthesis and Characterization

The first part of this thesis was achieved using commercial SiO_2 silica nanoparticles:

- $Aerosil\ OX\ 50$ at a powder state, $Degussa$, Germany
- Lyophilized $Ludox\ TMA$, suspension in water, $Sigma\text{-}Aldrich$

Both types of nanoparticle were chosen because of their availability ($Degussa$ kindly sent 2 kg flame produced $Aerosil\ OX\ 50$ for free, $Ludox\ TMA$ was sent in 2 days) and their different sizes staying in the classical "nanosize domain" (between 10 and 100 nm).

Lyophilizations were performed using freeze drying technique (figure 3.1), which avoids chemical aggregation (covalent bond formation between two or more particles).

The difference between chemical aggregation (particle dried without freeze drying technique) and physical aggregation (using freeze drying technique) is shown on the two $Ludox\ TMA$ TEM pictures on the figure 3.2.

Agglomeration and formulation problems did not allow performing monodisperse polymer-particle hybrid system based on commercial silica particles.

There was a necessity to develop the synthesis of SiO_2 silica nanoparticles at Empa for four reasons:

- Particle with a diameter lower than 400 nm at a powder-state cannot be dispersed again (experiment with sedimentation and DLS measurement gave this limit for SiO_2 silica particles).
- Most of commercial particles are not well defined and polydisperse. The TEM picture of commercial $Aerosil\ OX\ 50$ clearly showed polydisperse SiO_2 particles (see figure 3.3)

Fig. 3.1: Freeze drying technique: particles in water were frozen with liquid N_2 before evaporating water under vacuum

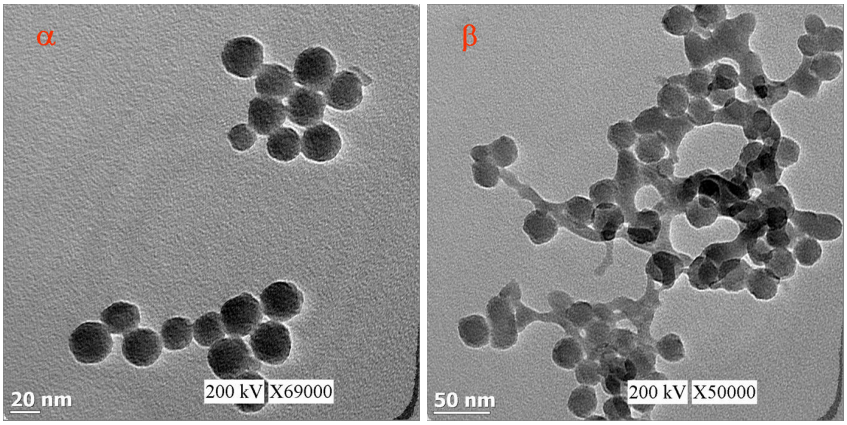

Fig. 3.2: Difference between agglomerate (α) and aggregate (β): example using TEM pictures of $Ludox\ TMA$, $Sigma\text{-}Aldrich$

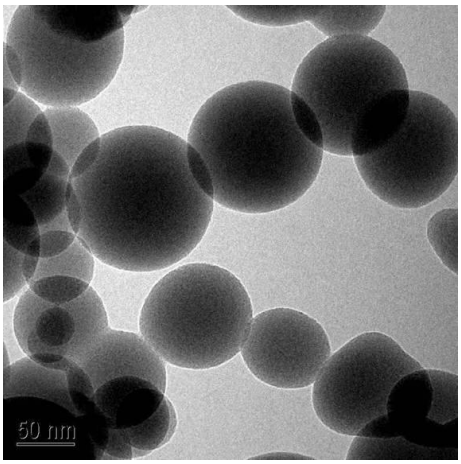

Fig. 3.3: TEM picture of $Aerosil\ OX\ 50$, $Degussa$

- Particles at a powder state present danger for health because free-floating nanoparticles are considered to be toxic for human beings [69].
- Synthesis of particles at Empa allowed controlling size over a larger size range.

An explanation for this 400 nm diameter boarder is that large specific surfaces of small particles implies large particle-particle interactions.

It is also important to notice that particles with diameter larger than 400 nm show self-sedimentation after a few days, which is not the case for small particles (D $<$ 150 nm).
Sedimentation would imply an irreversible agglomeration for small particles, larger particles (D $>$ 400 nm) were always dispersed again using an ultrasonic finger.

3.1 Synthesis of silica nanoparticles in basic environment

3.1.1 Principe: Stöber method

Silica particles of different sizes were fabricated by the sol-gel process, a synthesis in basic environment was proposed.

Stöber *et al* [123] published a synthetic process for the fabrication of monodisperse silica particles via hydrolysis of tetraethylorthosilicate ($TEOS$) in an ethanol solution. This reaction is catalyzed by ammoniac.

Hydrolysis and condensation of alkoxide silicon led to monodisperse spheres of silica.

The reaction scheme of the synthesis is shown in figure 3.4.

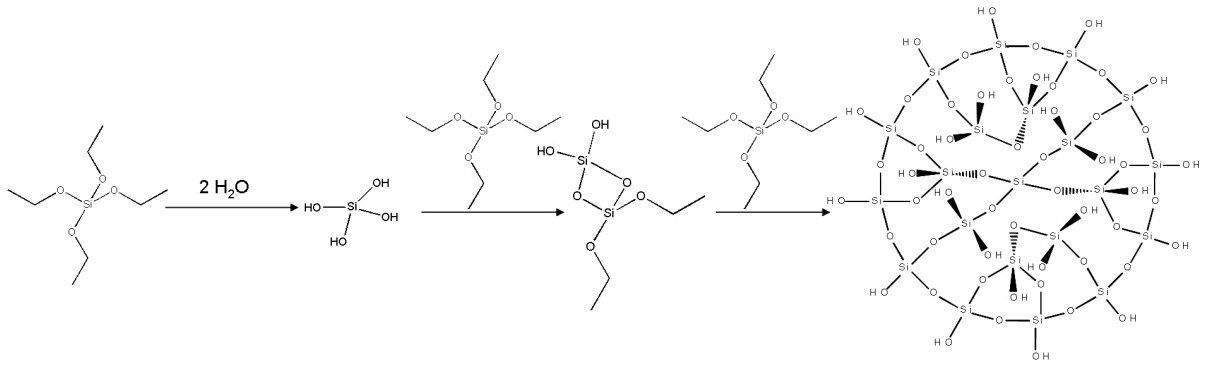

Fig. 3.4: Reaction scheme of Stöber reaction

The particle diameters depend on $TEOS$, water, $\mathrm{NH_3}$ concentrations and temperature. At low temperature, the ratio of nucleation to growth decreases [127] and leads to a larger distribution in the particle size.

Twenty years later, Bogush [16] proposed an empiric equation predicting particle diameter (in nanometer) as a function of educt concentrations (mol.L^{-1}) at 25°C (see equation 3.1).

$$D = A.[\mathrm{H_2O}]^2.exp(-B.\sqrt{[\mathrm{H_2O}]}) \tag{3.1}$$

with

$$A = \sqrt{[TEOS]}.(82 - 151.[\mathrm{NH_3}] + 1200.[\mathrm{NH_3}]^2 - 366.[\mathrm{NH_3}]^3) \tag{3.2}$$

and

$$B = 1.05 + 0.523.[\mathrm{NH_3}] - 0.128.[\mathrm{NH_3}]^2 \tag{3.3}$$

Particles with a maximum diameter of 2 μm can be synthesized with this method [93].

In practice, monodisperse particles (without any second or multi nucleations) could be synthesized up to 1.5 μm within a reasonable time scale for the synthesis.

The formed particles were porous and had densities between 1.6 and 1.9 g.cm^{-3} (measured by a "dry and weight" technique).
For the particles with diameters larger than 400 nm, the density could be increased by annealing in a oven at 900°C.

The size distribution of particles was narrowed at higher temperature [127] because there is a control of the nucleation and condensation steps, which are shown in the drawing 3.5 - 3.9 at different time.

Figures 3.5-3.9 compares at different time t the formation of silica particles at 20°C and 40°C.

Figure 3.5 depicts the formation of nuclei at low and high temperatures after a time t_1 (corresponding to a few minutes and depending on concentrations) of reaction.
t_1 is the moment, where almost all nuclei have been formed at 40°C, whereas only a few nuclei are formed working at 20°C.

Figure 3.6 shows the beginning of the condensation step on the nuclei already formed at t_1. In the batch at 20°C, new nucleations occur whereas at 40°C, only condensation reaction on existing nuclei occur.

Figures 3.7 and 3.8 show the drawings which explains that the condensation step goes on at 40°C, which is not the case at 20°C, where new nucleations and condensation occur simultaneously.

Figure 3.9 is the representation, where all $TEOS$ has been consumed. In the batch of colloids synthesized at 20°C, less particles are synthesized than in the batch at 40°C, particles are also larger and polydisperse in this first batch.

Excessive evaporation of ethanol prevented particle production at temperatures higher than 40°C, which leads to smaller particles ; Bogush's equation is no more valid under these temperature conditions.

At low temperature, hydrolysis kinetics and condensation are slow, involving the increase of nucleation and so the increase of polydispersity.

The reaction kinetics (equation 3.4) is a first order reaction of the $TEOS$ concentration according to the book of Sugimoto [124].

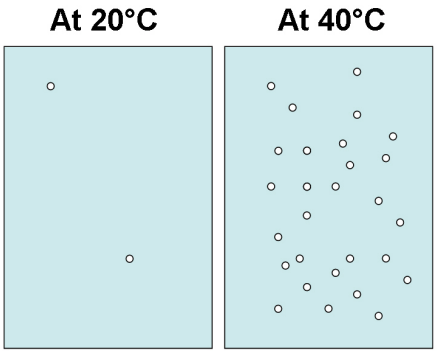

Fig. 3.5: time t1

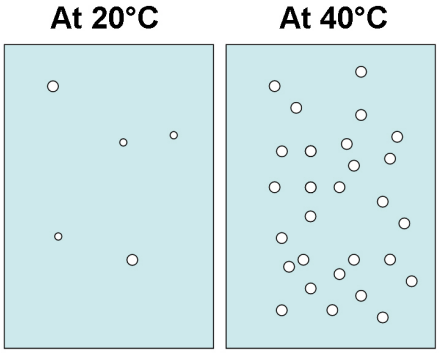

Fig. 3.6: time t2

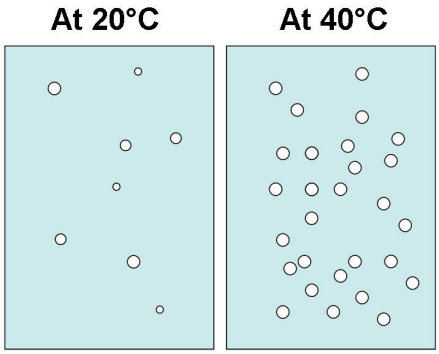

Fig. 3.7: time t3

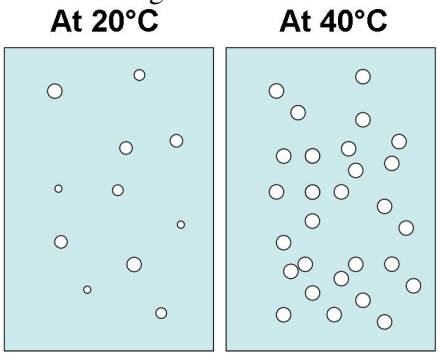

Fig. 3.8: time t4

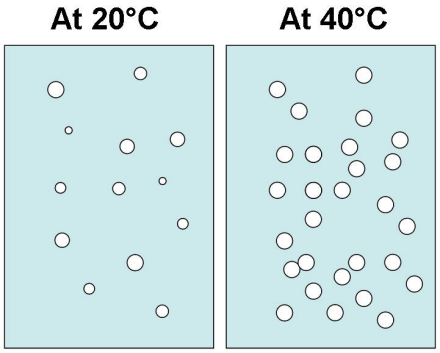

Fig. 3.9: time t5

$$\begin{aligned} \frac{d[\mathrm{Si\,O_2}particle]}{dt} &= \kappa_{TEOS}.[TEOS] \\ &= \kappa'.e^{\frac{-E_a}{RT}}.[\mathrm{H_2O}]^{1.18}.[\mathrm{N\,H_3}]^{0.97}.[TEOS] \end{aligned} \tag{3.4}$$

$$ln[\mathrm{Si\,O_2}] = \kappa_{TEOS} - ln[TEOS]_{t=0} \tag{3.5}$$

κ_{TEOS} depends on the temperature and the initial concentration of water and ammoniac and κ' is constant (2.36 s^{-1}(mol.dm^{-3})$^{-2.15}$).

The problem concerning this kinetic approach is that it does not take into account the very important ratio $\frac{[\mathrm{H_2O}]}{[TEOS]}$, which is a relevant parameter to accelerate the condensation process. The importance of this ratio is explained and illustrated for the synthesis of submicroparticles in chapter 3.1.3.

3.1.2 Controlled growth

Bogush *et al* [17] showed that it was possible to grow the silica particles by adding $TEOS$ in a solution containing already silica spheres.

The particles size depends on the total volume of added $TEOS$,

$$d = d_0.(\frac{n}{n_0})^{\frac{1}{3}} \tag{3.6}$$

where d is the final average diameter, d_0 the initial diameter of the particles, n_0 the initial quantity of $TEOS$ and n the total quantity of $TEOS$ added.

It is important to avoid a second or multi nucleation, an example of multi nucleation is presented in the SEM pictures in figure 3.10, which would mean a polydispersity in the particle size, Giesche described the preparation of monodisperse silica particles via a controlled continuous process [45].

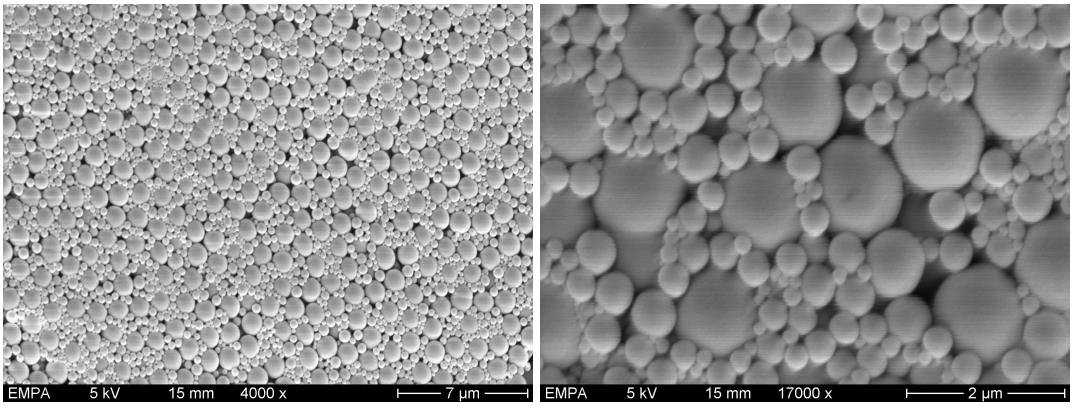

Fig. 3.10: SEM pictures of multi nucleations

This method was interesting because it allowed to limit the silanol concentration in solution, but required a peristaltic pump and a long time of synthesis (see figure 3.12).

Synthesis time was necessary because $TEOS$ must be added very slowly to avoid any second nucleation or chemical aggregation.

Second or multi nucleation(s) could be avoided by three ways:

- increase of the ionic force in order to reduce the number of nucleation centers [17]
- increase of particle surface in solution [24]
- limiting silicilic acid concentration [124]

Increasing ionic force has the consequence to slow the particle stability which can induce aggregation.

Increasing particle surface in solution leaves more silanol groups available for condensation, which limits further nucleations.

Nevertheless, this synthetic technique can quickly require a long time time if the desired particle size is larger than 400 nm.

The following calculation illustrates the time necessary to obtain different particle diameters.

Eight hours were required between two injections of the same volume of $TEOS$ (+ 2 mol equivalent water) to perform the reaction (time to consume all $TEOS$ in the condition 1 mol $TEOS$ for 2 mol water).

Practical example:

SiO_2 silica particles with a diameter of 100 nm were synthesized by injecting 135g $TEOS$ (0.65 mol) into a mixture of ethanol/ammoniac 25 wt$\%$ in water (519.1 g /50.5 g), i. e. a 11.28 mol ethanol /0.74 mol ammoniac /2.10 mol water at 40°C.

We obtained about 38.9 g of particles with a diameter of 99.8 nm $\pm$ 1.3 (DLS). TEM pictures (figure 3.11) showed porous particles, an annealing would have increased density (about 2.2 instead of 1.9) and made them perfect spheres but would avoid good dispersion of the agglomerates again.

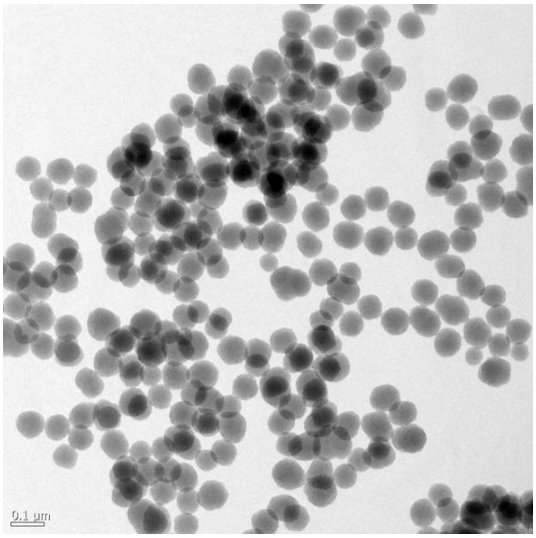

Fig. 3.11: TEM picture of SiO_2 particles with a diameter about 100 nm

In order to obtain particles with 200 nm in diameter, there was a need to choose as $[\frac{200}{100}]^3 = 8$ injections (see equation 3.6).

Drawing 3.12 represents the required timescale based on equation 3.6 needed to obtain larger particles starting from particles with 100 nm in diameters (d_0).

Notice that this graphics does not have any kinetic value and is based on the fact that two injections of the same volume of $TEOS$ (morning and evening) per day are done.

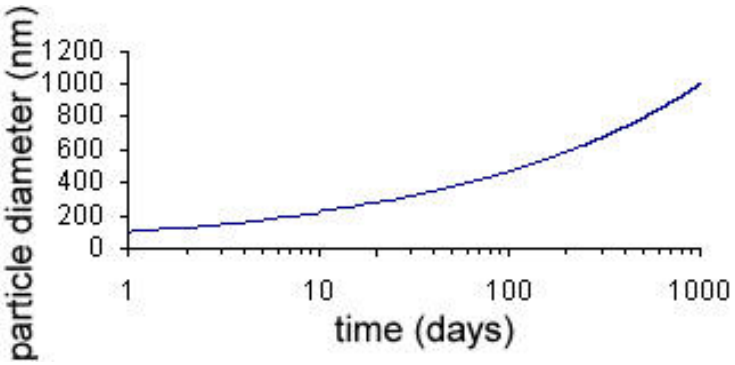

Fig. 3.12: Particle diameter size as a function of the number of day of work

However, there were ways to accelerate this reaction by dividing the initial volume after a few injection or injecting more $TEOS$ than the initial volume or using a growth solution (see US Patent 4,983,369) instead of only water, which catalysed the reaction and was actually the synthesis that was adapted for the growth of our largest particles.

Injecting $TEOS$ into a mixture containing mostly water and ammoniac (low concentration of ethanol) leads to a rapid consummation of the $TEOS$ used, which means acceleration of the condensation reaction.

3.1.3 Experimental examples

"Nanosized" particles synthesized with classical method

Particles of 15 nm in diameter were synthesized using 0.4 mol.L^{-1} ammoniac (25 $\%$ verified by Karl Fischer technique), 0.4 mol.L^{-1} $TEOS$ and 0.908 mol.L^{-1} water (coming from the ammoniac solution) at 40°C.

Under such conditions, the Bogush equation predicts a diameter of 30.44 nm (A = 120.278 and B = 1.239, see equations 3.2 and 3.3).

As we were working at 40°C, we expected half of this diameter (15 nm), which was grown with 5 more injections of $TEOS$ and 2 mol equivalent water (0.32 mol $TEOS$ + 0.64 mol water per injection). We expected to obtain a final average particle diameter of about 26 nm.

Dynamic Light Scattering measurements (DLS) performed at an angle of 90° gave an average diameter of 31.3 nm ± 0.9 (5 measurements). Monodispersity was confirmed with the TEM pictures and DLS measurements (figure 3.13).

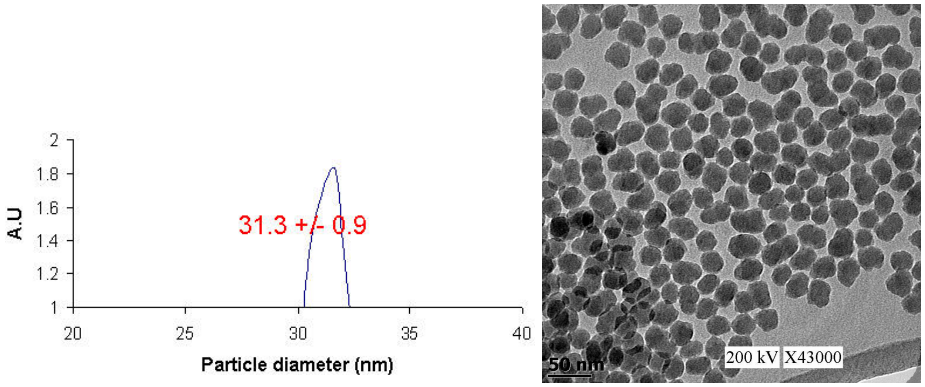

Fig. 3.13: Monodisperse silica particle size distribution and TEM picture

Particles synthesized by the described route were not perfect spheres due to their porosity.

The particle density was quite low and determined by weighting a 10 cm^3 fraction from silica solution in ethanol.

The colloidal solution density $\rho_{solution}$ was obtained using equation 3.7.

$$\rho_{solution} = x.\rho_{Si\,O_2} + (1-x).\rho_{ethanol} \tag{3.7}$$

The weight percentage of silica particles in ethanol solution (x) was determined by drying silica sol in an oven at 300°C, the obtained concentration was in our example 10.93 wt%.

The density of ethanol ($\rho_{ethanol}$) is 0.785 g.cm^{-3} at 25°C and so the silica particle density $\rho_{Si\,O_2}$ could be calculated using equation 3.7, we obtained 1.38 g.cm^{-3}.

Knowing diameter and density of silica nanoparticles ($D_{Si\,O_2}$=31.5 nm and $\rho_{Si\,O_2}$=1.38 g.cm^{-3}), the specific surface could be calculated with inserting the values of equation 3.11.

$$S_{\mathrm{Si\,O_2}} = \frac{6m}{\rho_{\mathrm{Si\,O_2}}.D_{\mathrm{Si\,O_2}}} = \frac{6}{1.38.10^6.31.5.10^{-9}} \tag{3.8}$$

This specific surface allowed to calculate the number of hydroxyl (-OH) groups at the surface per gram of particles.

The silanol concentration per gram is the product of the specific surface with the silanol concentration per square meter.
There are between 6 and 10 silanol groups per nanosquaremeter ($\mathrm{Si\text{-}OH.nm^{-2}}$) at the silica surface [54].

This result could have been determined (was not done at Empa) with the Li-Alant method [3], which uses the reaction scheme 3.9.

$$4\mathrm{SiOH} + \mathrm{LiAlH_4} \longrightarrow -\mathrm{SiOLi} + (\mathrm{SiO})_3\mathrm{Al} + 4\mathrm{H_2} \tag{3.9}$$

This result allows working stoichiometric for the surface modifications. With this method, the sample is dried at 120°C under vacuum (0.2 hPa) for 1 hour. After cooling, it is possible to determine the quantity of -OH on the particle surface with lithiumanalat ($\mathrm{LiAlH_4}$) in organic solution (diglyme) with hydrogen manometer measurement.
This means that we have between $1.1.10^{21}$ and $1.38.10^{21}$ molecules of -OH contained in one gram of silica particles, which means between 1.83 and 2.29 mmol -OH per gram $\mathrm{SiO_2}$.

Submicroparticles synthesized with a modified Stöber synthesis

The next example shows a way to obtain particles with diameter of 1 μm.

The main advantages of these particles are that they can be lyophilized and dispersed or redispersed again without any further agglomeration/aggregation and that they can be detected under a classical optical microscope.

A water/ammoniac (25 wt% in water /ethanol 99 % (38 mL/48 mL/14 mL)) mixture was stirred at 700 rpm and heated to 40°C, 48 mL of $TEOS$ were injected as quick as possible into the mixture.
Ten minutes later an aliquot of particles was taken and analyzed using DLS.
Particles with diameter of about 190 nm in diameter were obtained.

A stock solution of 1 L was prepared, for this purpose, 533 mL water were mixed with 215 mL ethanol and 252 mL ammoniac (23 wt$\%$ (Karl-Fischer)).

33 mL of this solution were added to the 190 nm in diameter particles in their reaction mixture without any purification.
Five minutes later 16 mL $TEOS$ were injected.
The reaction was repeated and allow obtaining particles with 1 μm in two days of injections (instead of 500 days with classical Stöber like synthesis!).

By those two methods, several particles with sizes varying between 31.5 nm and 1000 nm were synthesized. Stöber understood that the fabrication of nanoparticles is catalysed by $\mathrm{NH_3}$ in an ethanol solution in the presence of water, but did not study the influence of the ratio $\frac{n_{\mathrm{H_2O}}}{n_{TEOS}}$, which is necessary for control in the synthesis of large $\mathrm{SiO_2}$ particles.

In order to evaluate the influence of this parameter, six different samples with sizes of 31.5 nm, 50.8 nm, 106.7 nm, 515 nm, 760 nm and 1000 nm were selected.
These particles were then modified for the incorporation in the polymer matrix.

Figure 3.14 shows an overview of different particle size obtained.

Tailoring particle size represents the main advantage to be able to study the size with the microscope used.
Figure 3.14 is a representation using transmission electron microscopy, suitable for the entire range scale ; scanning electron microscopy for particles with diameters larger than 200 nm and optical microscope used for particles with diameter larger than 800 nm.

This size range was used for the realization of the paper *Synthesis and rheological study of tailored monodisperse and monodistributed* $\mathrm{SiO_2}$*-PMMA composites* [35], presented in chapter 6.

3.2 Silane modification

3.2.1 Chemical structure and reactivity of the particle surface

Silica particles are ideally described as a network composed of $\mathrm{Si\text{-}O\text{-}Si}$ siloxane bonds.

Three other kinds of silica are existing containing between one and three hydroxyl -OH groups, which did not react during the particle formation: silanol, silanediol and silanetriol (figure 3.15).

The silanols on the surface are necessary for the chemical reaction. The acido-basic proper-

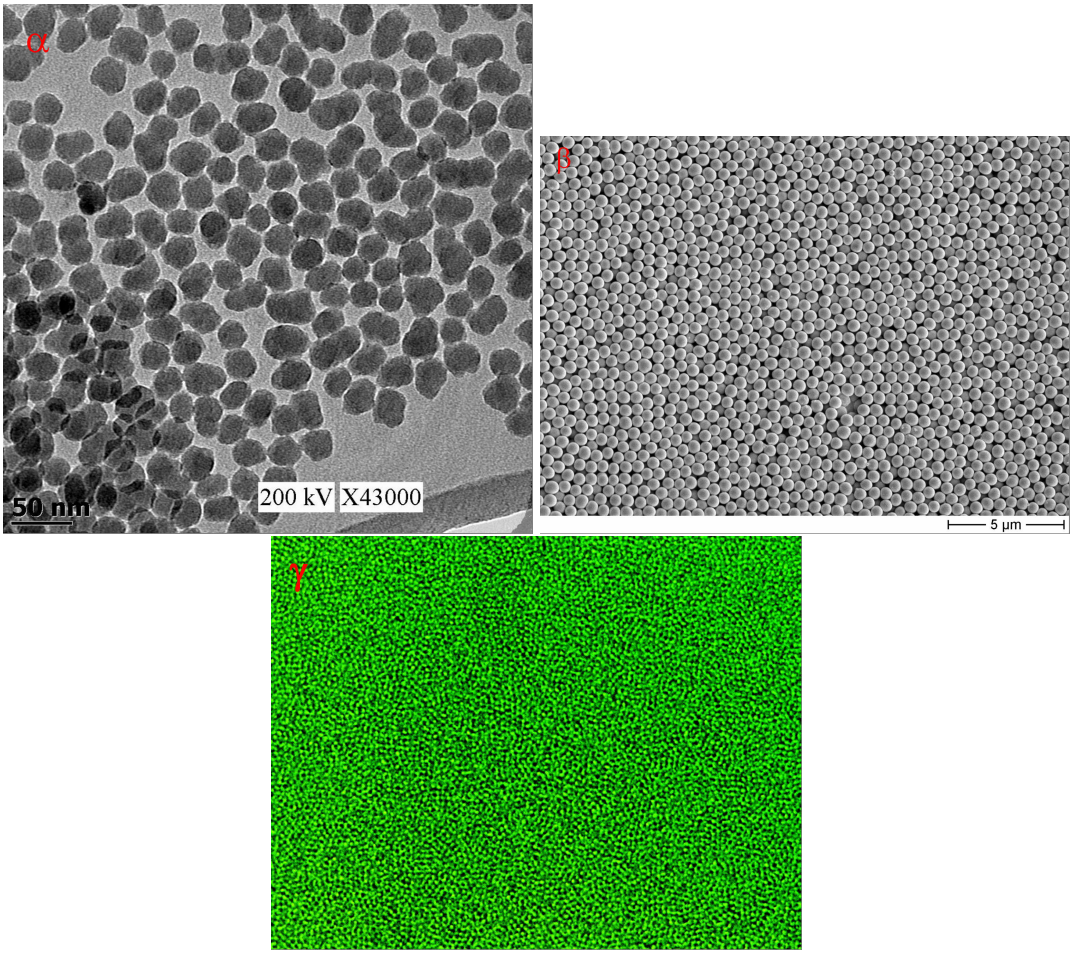

Fig. 3.14: TEM, SEM and OM pictures of particles with respective diameter: α) 31.5 nm, β) 515 nm and γ) 1μm

ties (dependencies of the pH) involve the presence of electrical charges on the surface and are at the origin from the colloidal silica stability.

Silanetriol and silanediol were only present in small number, most of the surface bound are silanols or siloxanes [59].

Isolated silanols have the highest reactivity, they can be distinguished from the other silanol groups with infrared spectroscopy (IR) or ^1H nuclear magnetic resonance (NMR) [50], [66].

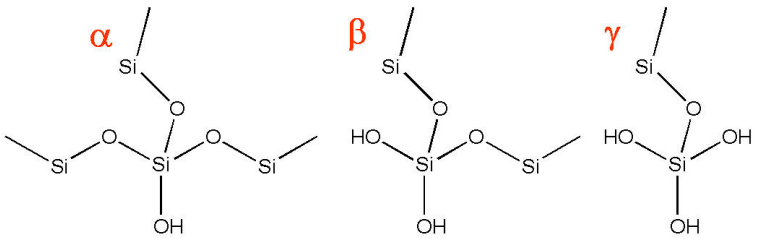

Fig. 3.15: α) silanol, β) silanediol and γ) silanetriol

3.2.2 Surface modification

The surface of silica particles must be modified to fabricate a composite. Surface modification was performed with the grafting of a silane agent of general formula 3.16.

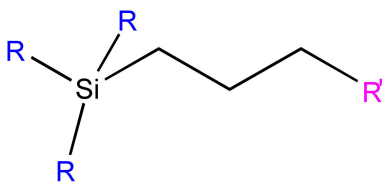

Fig. 3.16: General formula of silane agents, with R=OCH_3, as OC_2H_5, as Cl, as CH_3 and respectively R'=SH, as NH_2, as CH_3, as NCO, etc...

Silane agents containing either chloride or methyl groups as R group were not used at Empa, only multialkoxysilane were used:

Examples:

3-aminopropyl triethoxysilane (APTES, figure 3.2.2) and 3-methacryloxy-propyl- trimethoxysilane (TPM, figure 3.18) [96].

Using TPM silane agent leads to copolymerization of the particles with MMA or MAA monomer.

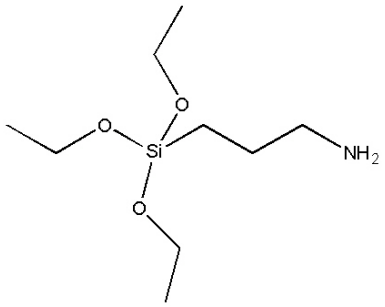

Fig. 3.17: 3-aminopropyltriethoxysilane, APTES ($ABCR$, Germany)

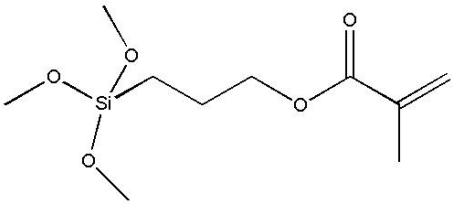

Fig. 3.18: 3-methacryloxy-propyl-trimethoxysilane, TPM ($Sigma\text{-}Aldrich$)

With BET or TEM size distribution data, the specific surface was determined and the reaction is performed under stoichiometric condition.

This reaction is based on the hydrolysis of the silane agent on the adsorbed water of the particle surface.

It was performed without free water in the solution to avoid the aggregation of silica particles at 50°C-60°C under stirring.
Hydrolysis and condensation on the surface could be performed in all alcohols.

Presence of a basic agent in the solution catalyses the reaction because it removes the hydrogen available on the silanol surface and leads to the formation of ethanol methanol or hydrochloric acid (depending on the -R group).

Figure 3.2.2 presents the general reaction scheme between silanol groups present on the silica surface with silane agents.

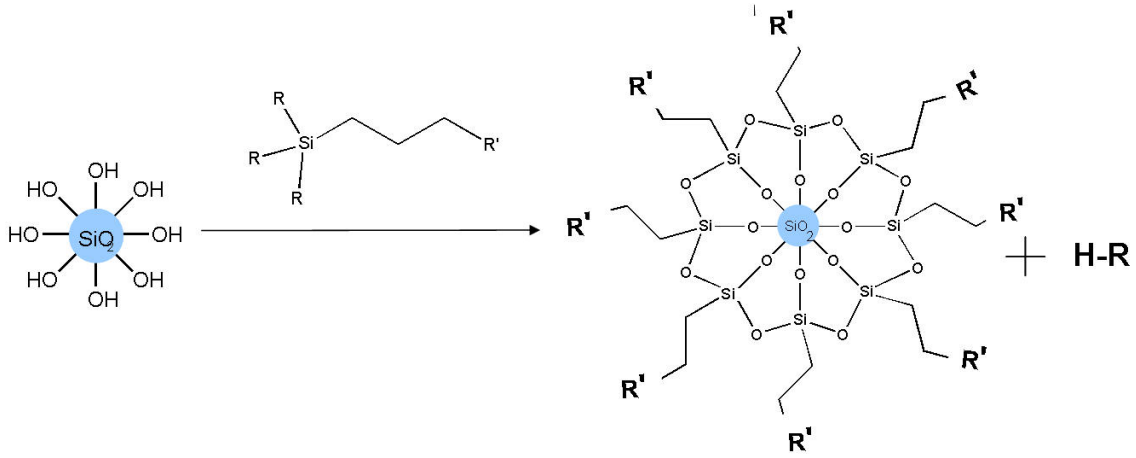

Fig. 3.19: General scheme for particle surface modification with silane agent

Notice that the expected size of the particle lies between 30nm and 1000nm and the approximative size of a silane agent is 1 nm (scale not respected for the drawing).

Silane agents containing -R = Cl were not used because of unwanted hydrochloric acid (HCl) formation.

3.3 Characterization of silica nanoparticles and their modified products

3.3.1 Determination of the particle sizes and specific surfaces

$\mathrm{SiO_2}$ silica particles and their modified products can be characterized in terms of size distributions with transmission electron microscope (TEM) and dynamic light scattering (DLS).

Aerosil OX 50 (*Degussa*) was dispersed in water and then lyophilized, as well as *Ludox TMA* (*Sigma-Aldrich*), under 0.4 mBar pressure to be able to disperse them in a more volatile solution for the TEM sample preparation.

Specific surface (in $\mathrm{m^2.g^{-1}}$) was obtained with the average diameter of these particles (Table 6.1).

Two batches were selected as examples batch α and batch β.

APTESNP means APTES (figure 3.2.2) modified nanoparticles, MEMONP means TPM (figure 3.18) modified nanoparticles and FNP, FITC modified fluorescent APTESNP nanoparticles.

Nanoparticles α	batch α	APTESNP α	MEMONP α	FNP α
Average diameter (nm)	86.46	79.22	81.15	79.59
Nanoparticles β	batch β	APTESNP β	MEMONP β	FNP β
Average diameter (nm)	26.6	26.9	not measured	27.2

Tab. 3.1: Average Diameter of the nanoparticles obtained by TEM pictures

N_s particles of a volume V_s occupy a volume V described in equation 3.10.

$$V = V_s N_s = \frac{4}{3}\pi < R >^3 N_s \tag{3.10}$$

with $< R >$ denoting the average radius of a sphere. The corresponding specific surface S of this N_s calculated by equation .

$$S = 4\pi < R >^2 N_s \tag{3.11}$$

The specific surface was then obtained with these two relations, as given in equation 3.12.

$$S = \frac{3V}{< R >} \tag{3.12}$$

The values of calculated specific surfaces of the nanoparticles are summarized in table 3.2.

The specific surface could also be measured using standard B.E.T. (or BET for Brunauer, Emmett, and Teller) technique. Results obtained are presented in the table 3.3.

Name	m (g)	ρ ($g.m^{-3}$)	V (m^3)	$< R >$ (m) (from TEM data)	S ($m^2.g^{-1}$)
Batch α	1	2.20E+06	4.545E-12	4.33E-08	31.54
MEMONP α	0.2997	2.20E+06	1.362E-12	3.96E-08	34.43
APTESNP α	0.2965	2.20E+06	1.348E-12	4.06E-08	33.61
FNP α	0.301	2.20E+06	1.368E-12	3.98E-08	34.27
Batch β	0.3181	2.17E+06	1.466E-12	1.33E-08	103.95
APTESNP β	0.2885	2.17E+06	1.329E-12	1.35E-08	102.79
FNP β	0.2129	2.17E+06	9.811E-13	1.36E-08	101.65

Tab. 3.2: Specific surface of nanoparticles

Nanoparticles α	α	APTESNP α	MEMONP α	FNP α
Specific Surface α ($m^2.g^{-1}$)	51.53	44.21	44.47	41.19
Nanoparticles β	β	APTESNP β	MEMONP β	FNP β
Specific Surface β ($m^2.g^{-1}$)	119.7	109.7	not measured	106

Tab. 3.3: BET measurements of nanoparticles specific surface

Differences obtained between the two methods are due to the approximation of spherical particles with an average diameter, which does not take into account the particle size distribution.

Another explanation is that the roughness of particles is also measured with the BET apparatus, whereas TEM size analysis just considers a hydrodynamic radius.

A positive result is that TEM pictures proved that surface modifications did not induce aggregation (no covalent bond between particles).
The measured specific surface is lower after surface modification due to the fact that particles are larger and their specific surface is decreasing. No modification in the density for the modified particles is considered.

3.3.2 ^{29}Si NMR

^{29}Si NMR data were obtained for the unmodified commercial $Aerosil\ OX\ 50$ and for the two different APTES and the TPM functionalized $Aerosil\ OX\ 50$ silica nanoparticles, modified in ethanol at 50°C.

These measurements show different Si signals arising from the silica particles and from the silanisation process, which is a proof that silane agents were adsorbed on the particle surface.

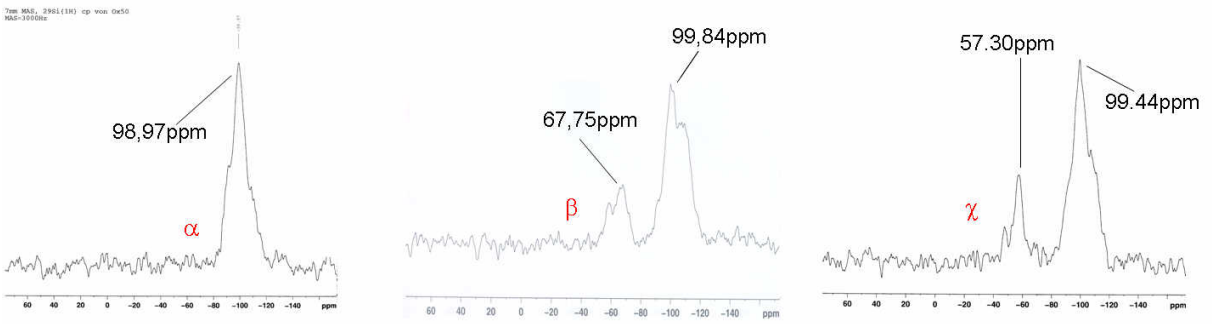

Fig. 3.20: Solid-state ^{29}Si NMR spectroscopy of silica nanoparticles modified by silane coupling agents

^{29}Si NMR spectra (figure 3.20) clearly indicate that the reaction took place.
Measurements were also performed on the fluorescein marked APTES particles (see chapter 4 for their synthesis), but since the FITC content was only 0.333 % in weight, no specific signal was detected.

Figure 3.20 (α) shows the spectrum of unmodified silica nanoparticles. The corresponding signal is also detected in β and χ, and corresponds to the silicium signal of the particles.
Other signals are assigned in β at 67.75 ppm to the APTES silane coupling agent and in χ at 57.30 ppm to the TPM coupling agent.

^{29}Si NMR results proved that the silanisations in ethanol took place but we were not able to specify if aggregation also occurred.

However, transmission electron microscopy (TEM) images analysis showed that the modified nanoparticles did not form more aggregates than the commercial $Aerosil\ OX\ 50$ silica nanoparticles did.

3.3.3 Long term stability of the dispersed nanoparticles

Particles dispersed with an ultrasonic finger (Ultrasonic Homogenizer $Bandelin\ Sonopuls$) generally show (depending on particle size and solution polarity) a poor stability.

A rapid phase separation was observed in organic solvents like toluene for unmodified particles. This phase separation appeared after one day with the APTES modified particles.

The long term stability could not be reached for particles at a powder state:
Since silica powders without any surface treatment cannot form a stable suspension in organic

hydrophobic solution, because of the hydrophilic surface of unmodified SiO_2 silica particles.

A surface treatment using a hydrophobic and charged silane agent (1H, 1H, 2H, 2H-perfluoroalkyltriethoxysilane) allowed to form a stable dispersion but prohibited any further reaction with polymer chains.

Nevertheless, it was possible to disperse a powder of particles with diameters larger than 400 nm in the case of SiO_2 particles.
Powder state should always be avoided for particles with diameters lower than this value for a good dispersion in any solvent.

3.4 Conclusion of chapter 3

Table 3.4 summarizes chapter 3 comparing silica particles at a powder state (flame produced or dried particle) and particle in solutions (sol-gel chemistry).

The first points presented in this table are the drawbacks and advantages of both types of particles.
The production of monodisperse SiO_2 particles without agglomeration and/or aggregation always requires sol-gel synthesis.

The second point presented is that the sol-gel approach allows a direct modification in the synthesis milieu, which simplifies the modification process.

The general conclusion of this chapter is that in order to obtain a tailored system, there is a necessity to define first tailored silica particles.
For this purpose, sol-gel synthesis has been chosen using controlled temperature (40°C) and concentrations of educts, particles in a range between 30 nm and 1000 nm could be synthesized in hundreds of grams.

SiO_2 silica particles		
Types of particles	powders	colloidal solutions
Schematic representation	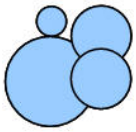	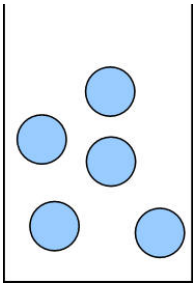
Advantages and drawbacks		
Availability	commercial *Degussa, Sigma-Aldrich*	home-made
Price	low	high, (solvent costs)
Quantity produced	industrial range	labor range
Size distribution	polydisperse	monodisperse
Good dispersion in solution	no, always agglomerates	yes, already dispersed
Dangers for health	Yes, because of volatility	no danger
	Quality colloidal solutions (home syntheses) are more expensive but more defined	
SiO_2 surface modification		
Ultrasonic required	Yes	No in synthetic milieu
Dialysis required	No	Yes
Modification in the particle size distribution	no data	Not at all
Quantity produced	small	small

Tab. 3.4: Comparison between different kinds of SiO_2 silica particles

4

Synthesis of fluorescent silica particles

An important part of this thesis was the fabrication of fluorescent particles, which can be observed by optical tools.

Fluorescence is an optical phenomenon in which the energy difference between the absorbed (high energy) and emitted (low energy) photons implies a molecular vibration.
In other terms, electrons gain energy from a light source and undergo a transition from an occupied orbital to an empty orbital (absorbtion), high energy levels can then decay to lower levels by emitting radiation (emission or luminescence) as shown in the figure 4.1.

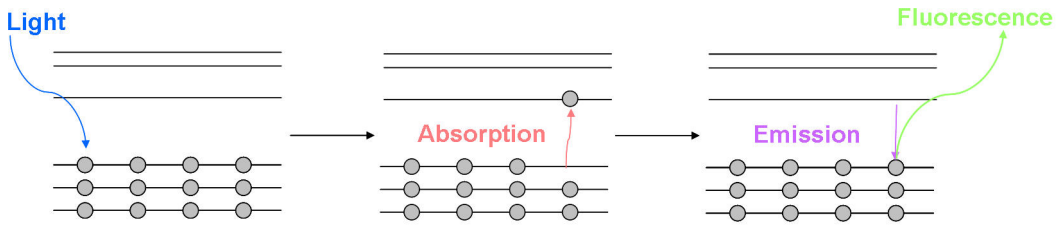

Fig. 4.1: Representation of optical absorption and emission

In our case, absorbed photon and emitted light (luminescence) are in the visible range.
The first idea was to use organic dyes like fluorescein (figure 4.2) or rhodamine (figure 4.5).
Reasonable prices and well established reaction scheme encourage us to work with these dyes.

4.1 Organic dyes

4.1.1 Fluorescein isothiocyanate (FITC)

The reaction scheme for synthesis of fluorescein isothiocyanate (FITC, figure 4.2) labeled fluorescent nanoparticles (FITCNP) is described in the figure 4.3.

SiO_2 silica particles in a diameter range of 30 nm to 1 μm were synthesized with the process described in chapter 3.

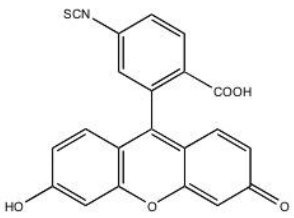

Fig. 4.2: Fluroesceinisothiocyanate (FITC)

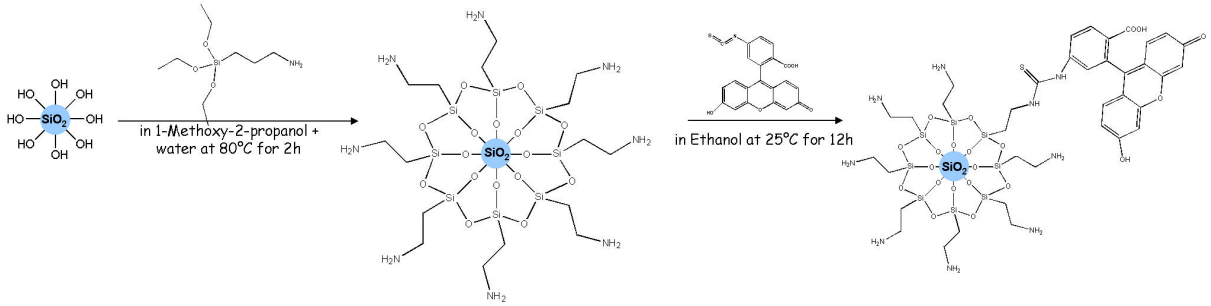

Fig. 4.3: Reaction scheme of SiO_2@FITC

Figure 4.4 shows an optical microscope fluorescent picture of a 1 μm diameter large modified SiO_2 FNP particle.

Amino surface groups were obtained via a silanisation process using 3-aminopropyl-triethoxysilane [38] (APTES, see chapter 3, figure 3.2.2).
Silanol functional entities were exchanged by this reaction to provide a reactive center for coupling with the fluorescent marker [15], [91] fluorescein isothiocyanate (FITC, figure 4.2).
The reaction scheme is described in the figure 4.3.

The main problem of fluorescein tagged fluorescent particles arises from the fast decrease of the fluorescence under excitation resulting from photobleaching [55].
The observed photobleaching instability does not allow studying the hybrid system under a confocal microscope.

A considerable improvement in photostability was obtained in the past by increasing the photostability of marked particles by increasing the concentration of fluorescein [55] or by using more stable fluorochromes [15], [108] or by modifying chemically the fluorochrome [140].

However, the required synthetis to achieve these goals are complex, and the expected im-

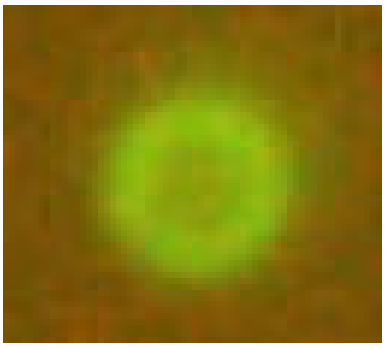

Fig. 4.4: Optical fluorescent microscope picture of a SiO_2@FITC particle

provement in photostability was not satisfying us.

4.1.2 Rhodamine isothiocyanate (TRITC)

The most popular red fluorescent markers are derivates from rhodamine e.g. TRITC (Tetramethylrhodamineisothiocyanate, figure 4.5).

In our case, tetramethylrhodamine isothiocyanate mixed isomers ($Sigma\text{-}Aldrich$) were used as received for synthesis.

The coupling reaction was similar to the one using FITC as fluorescent marker described on the figure 4.3 based on an amino-isothiocyanate reaction.

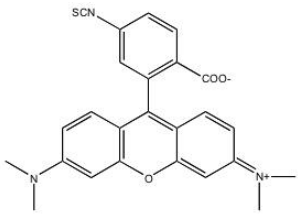

Fig. 4.5: Tetramethylrhodamineisothiocyanate (TRITC)

Compared to fluorescein, the main advantage of this fluorescent marker lies in its higher photostability and pretty high quantum yield (often used as a reference).
On the other hand, we were not convinced us to continue working with this marker because it was not suitable for long time (more than 15 minutes) experiments.

Our search for systems with a superior performance led to the evaluation of semiconductor nanocrystals. These materials are commonly known as quantum dots and show in contrast to organic dyes a very high resistance against photobleaching when exposed to UV radiation.

4.2 Quantum dots

4.2.1 Different routes to the synthesis of quantum dots

Among the different ways to fabricate quantum dots, the high temperature synthesis reported by Murray *et al* [81] leads to quantum dots with the best quality in terms of particle size distribution and optical properties.

However, the high cost and the moisture sensitivity of the dimethylcadmium ($\mathrm{Cd(CH_3)_2}$) used in this synthesis makes it difficult. Quantum dots using cadmium salts as precursors are easier to handle and the educts are available at low costs.

Cadmium acetate ($\mathrm{Cd(C_2H_5)_2}$, $\mathrm{2H_2O}$ $Sigma\text{-}Aldrich$) and Se powder ($Sigma\text{-}Aldrich$) were used in our synthetic approach.

Cadmium chloride ($\mathrm{CdCl_2}$) or cadmium iodide ($\mathrm{CdI_2}$) have also been studied as possible substitutes [63], Peng and Peng [95] did not manage to make high-quality CdSe nanocrystals using $\mathrm{CdCl_2}$ in spite of its perfect solubility in the reaction mixture at elevated temperatures. This can be due to the high stability of cadmium chloride in the solvents used.

Wong and Stucky [137] proved that under the same synthetic conditions, chloride and iodide salts of Cd do not lead to fine structure in their absorbance spectra, which means that crystalline quantum dots cannot be formed using these salts.

The first approach followed was using the experimental conditions that published Wong [137].

Details of his set-up were missing so that we presume that the temperature conditions were changed.

Large sized quantum dots (blood red in color with a diameter of approx. 10 nm) could be synthesized with this protocol.

This method is efficient but hazardous as it requires higher temperature than the flash point of trioctylphosphine oxide ($TOPO$) surfactant.

Another approach was tried using the US patent (WO 2004/008550 A2) of Young and Naumann (example 1 [0048] page 10 of the patent). This synthesis is interesting because it requires lower temperatures, but cannot lead to high luminescent quantum dots.

Wong and Stucky like synthesis

The reaction developed by Wong [137] needs three reactors:

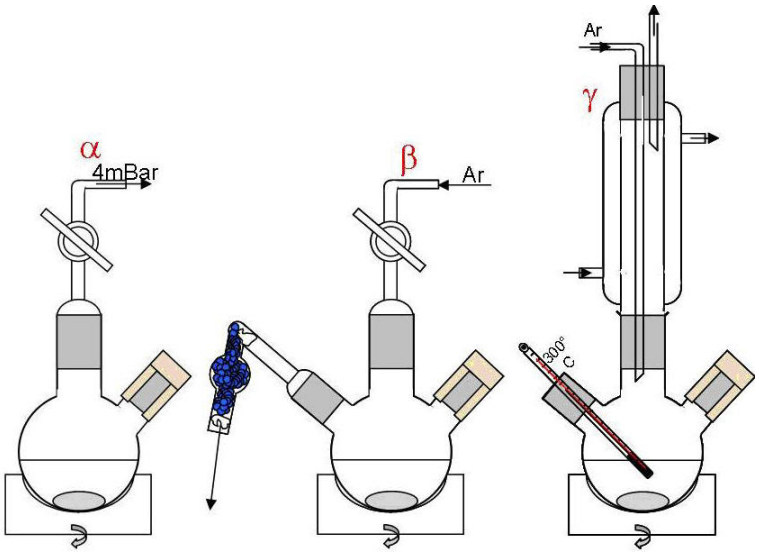

Fig. 4.6: α) $Cd(C_2H_5O_2)_2$; $2H_2O$ in $TOPO$ β) Se powder in TOP γ) $TOPO$

Cadmium salt is dissolved in $TOPO$ at 140°C in the first one (α) which is placed under 4 mBar vacuum for thirty minutes in order to wash the $TOPO$ and to evacuate water, which crystallized our salt. During this time, Se powder is mixed in trioctylphosphine (TOP) under argon atmosphere at 25°C in the second reactor (β).
The solution from α is injected into β and heated at 100°C under argon. The third reactor (γ) containing $TOPO$ is heated at 140°C under 4 mBar vacuum for two hours and then at 250°C under argon. The resulting mixture of β is injected, as fast as possible, in the boiling $TOPO$ of γ and then cooled in an ice bad. Dark red $CdSe$ quantum dots (D = 9 nm) are obtained by this synthesis.

Young and Naumann like synthesis

The synthesis is based on the US patent (WO 2004/008550 A2) from Young and Naumann and the example 1 [0048] page 10. Synthesis was performed using stoichiometric quantities of $Cd(C_2H_5O_2)_2$ and Se in a two-neck flask, five to ten times more dodecylamine (DDA) were added in the flask and washed with an argon atmosphere.

Under stirring (700 rpm), as few TOP as possible was injected through a septum to dissolve the cadmium salt, selenium and DDA, at this moment the mixture was slowly heated and aliquots were taken at 100°C, 110°C, 120°C, 125°C, 130°C, 135°C, 140°C, 145°C, and 150°C (figure 4.7).

Fig. 4.7: CdSe quantum dots with diameter between 1 and 8 nm.

The sizes of quantum dots depend on both temperature at which they are formed and the quantity of ionic surfactant (DDA) that is used.

Visual control is suitable for a direct determination of the quantum dot size.

Finally, an own synthetic route was developed at Empa, which led to the paper, *Synthetic route to a large amount of* CdSe *quantum dots at low temperatures for label applications*, submitted to *Nanotechnology* on September 18^{th} 2006.

Table 4.2.1 is an overview of the different synthetic route of Murray, Wong, Young and Dietsch comparing five points:

- Educts used (price and moisture sensitivity)
- Temperature range (explosion risks)
- If inert gas was used (CdO formation lows quantum yield)
- Number of reactors necessary (required facilities and space)
- Quantity that can be produced with one reaction (industrial application)

Authors	Murray	Young	Wong	Dietsch
Educts	Se *TOP* $Cd(CH_3)_2$	Se *TOP* $Cd(CH_3COO)_2$	Se *TOP* $Cd(CH_3COO)_2$	Se *TOP* $Cd(CH_3COO)_2$
	$Cd(CH_3)_2$ is inflammable, expensive, detonable and moisture sensitive.			
	TOPO	*DDA*	*TOPO*	*TOPO*
	TOPO technical grade (90%) contains rest products from its synthesis, which catalyses the reaction.			
Temperature range	190°C-320°C	25°C-180°C	250°C-350°C	60°C-170°C
	Temperature conditions higher than TOPO technical grade (90%) flashpoint.			
Inert gas ?	Yes Absolutely required because of $Cd(CH_3)_2$	No, not at all bad quantum yield, CdO formation	$Cd(CH_3COO)_2$ + *TOPO* without inert gas, bad quantum yield, CdO formation	Yes Every flasks under Ar or N_2
How many reactors ?	3 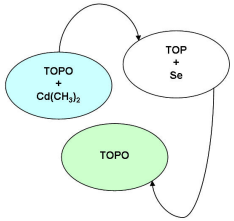	1 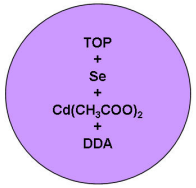	3 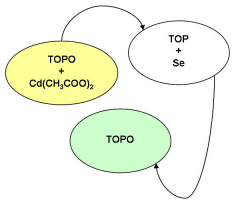	2 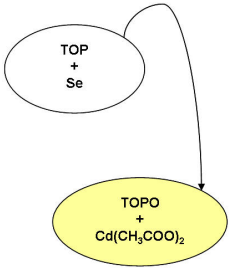
Quantity produced in one reaction	small (a few mg)	large (a few g)	small (a few mg)	large (a few g)

Tab. 4.1: Comparison of the different synthetic routes towards $CdSe$ quantum dots

Table 4.2.1 shows the relevancy of our synthesis using non explosive educts, working at temperatures lower than the $TOPO$ flashpoint (estimated between 180°C-200°C) and a way to synthesize large quantities of CdSe quantum dot cores.

4.2.2 Synthetic route to a large amount of CdSe quantum dots at low temperatures for label applications

Hervé Dietsch[1], Didier Lootens[2] Beat A. Keller[1*]
[1] Laboratory for Nanoscale Materials Science EMPA - Materials Science and Technology, Ueberlandstrasse 129, CH-8600 Dübendorf, Switzerland
Submitted to the *Nanotechnology* on September 18^{th} 2006
[2]Sika AG, Tüffenwies 16, CH-8048 Zürich, Switzerland *Beat.keller@empa.ch

Abstract

Commercial quantum dots are expensive for label applications, particularly for nanosized objects, which imply large surface area to be covered.
Current syntheses of nanocrystals require high temperature exceeding 250°C, which only allow synthesizing a few milligrams.
A synthesis using low price educts and low temperature is described, grams of quantum dots with limited quality in terms of quantum yield are synthesized using high concentration of surfactant ($TOPO$).
This facile way of producing fluorescent CdSe quantum dots can be performed in every chemistry laboratory using cadmium acetate and Se powder as precursors at temperatures, which can be kept as low as 180°C (below surfactant's flashpoint).
The photoluminescence of the resulting material can be further improved by a ZnS shell using diethylzinc and bis(trimethylsilyl) sulphide as zinc and sulphide sources. By controlling the temperature between 110°C and 180°C, crystalline particles of 2 to 8 nm can be synthesized. The proposed reaction yields a high quantity of low cost quantum dots, which can typically be used for or grafting on colloidal nanoparticles large specific surfaces. A proof that these nanocrystals are good enough for labeling applications is also demonstrated.

Introduction

Since their discovery (1) and due to their high resistance against photobleaching (approximately 100 times as photostable as rhodamine), crystalline semi conductor quantum dots (QD) aroused a growing interest as fluorescent markers.
Organometallic compounds which were since the 90's used as precursors in the synthesis of semicrystalline quantum dots are expensive, hazardous, and require special safety equipment, e.g. a glove box, during synthesis, which led to new approach based on alternate II-VI quantum

dot syntheses using cheaper educts cadmium carboxylate, chloride, iodide, and acetate for example.
The group of Peng were the first in 2001, which started those new "greener and cheaper" chemical synthetic routes (2).
They manage to produce CdSe nanocrystals with relatively good monodisperse distribution (5-10$\%$ standard deviation) and good photoluminescence reaching 20-30$\%$. Two years later, they produced nanocrystals using successive ion layer adsorption and reaction (SILAR) at quite low temperature (240°C), which results to high quality core shell nanocrystals with comparable quantum yields as their previous work.
In this work, we report the lower temperature used for quantum dots syntheses.
Other research groups, Reiss *et al* (3) and Mohamed *et al* (4) focuse on the monodispersity of the nanocrystals formed to obtain a thin and well defined emission, for biological applications.
Amelioration of the syntheses was also been proposed by Barrelet *et al* (5) using single source molecular precursors to get CdS and ZnS nanowires. One pot synthesis of core-shell nanocrystals were the subject of concentration of Mekis *et al* (6) and Pradhan *et al* (7).
Our interests is not to produce high quality quantum dots with cheap precursors but to synthesize within a batch quantum dots in gram quantity in order to label large quantities of silica particle in a range between 30 and 1000 nm (8), for this purpose, we refer to the work of Nann *et al* (9, 10) and on the incorporation of quantum dots and silica particles.
The emitted wavelength of a quantum dot can be tuned from ultraviolet up to infrared by the size of particles. However, this property also makes QD's difficult to study. The basis of the tunability is the quantum confinement of electrons and holes of the semiconductor particles. The energy level scheme then becomes atom-like with many discrete levels, which show an increasing energy separation with decreasing particle radius. If the size becomes smaller than the Bohr exciton radius a quantum confinement effect, i.e. fluorescence is observed.
For CdSe quantum dots the bulk Bohr radius was estimated as approximately 5.5 nm (11). Emission from CdSe particles has been detected for semiconductor crystals with diameters of 2.3 nm at 470 nm, and for 5.5 nm at 610 nm, respectively (12).

Particles of different size can be simultaneously excited at a wavelength of ca. 400 nm using a single ultraviolet light source. This allows for detection of several colors at the same time without spectrum overlap, which makes semiconductor QD's good fluorescent markers for in-vivo imaging.

Wu *et al* (13) used quantum dots as an alternative to organic dyes in biology fluorescent labeling experiments. It has been found that the capping of CdSe quantum dots with a thin layer of ZnS increases the quantum efficiency to values exceeding 50 $\%$ (14-15). These systems were used in the past for biological applications in which $\mathrm{CdSe(ZnS)}$ core-shell quantum dots were functionalized with proteins to label human cervical adenocarcinoma (HeLa) cells in receptor-mediated endocytosis studies (16). Bruchez *et al* (15) used silica coated $\mathrm{CdSe(ZnS)}$ core-shell quantum dots to identify mouse fibroblasts. The advantage of this process over traditional labeling with fluorescent polymer particles is the higher density of silica (1.96 g.cm^{-3} for silica

vs. 1.05 g.cm^{-3} for polystyrene), which facilitates centrifugal separation. In addition silica particles are more hydrophobic and therefore easier to modify and also more resistant against microbial attack. The oxidic nature of the material also prohibits the particles from swelling and porosity change.

Dye-doped silica nanoparticles have been prepared via two general synthetic routes: the Stöber and microemulsion processes. Stöber *et al* (17) described their classical method for synthesizing silica nanoparticles ranging from 50 nm to a few micrometers and good monodisperse size distribution in 1968. Typically, the reaction starts with the hydrolysis of a silica alkoxide precursor such as tetraethylorthosilicate ($TEOS$) in an ethanol/ammonium hydroxide mixture to form silicic acid, which subsequently starts to undergo condensation to form the (amorphous) silica particles. The covalent attachment of organic fluorescent markers has been described in the literature (18). The standard protocol of this procedure usually involves in a first step the chemical modification of the marker dye with a coupling agent. The most popular reaction is the attachment of an amino group via silanisation by 3-aminopropyl-triethoxysilane (APTES). The doping process is initiated by co-hydrolyzing followed by condensation of APTES and $TEOS$ to form the dye-doped silica particle (9-10).

Due to wide range of possible reaction partners, this concept offers the possibility for incorporation of a variety of different dye molecules into the silica particles. Our particular interest is to label Stöber-based silica particles with $\mathrm{CdSe(ZnS)}$ core-shell quantum dots and disperse them in a polymer matrix in order to obtain a hybrid system with easy-to-identify individual structural entities. Although quantum dots exhibit higher resistance to photobleaching and are more photostable than organic dye molecules, a superior quantum yield can only be achieved for core-shell systems. Generally, the performance of quantum dots is considerably improved after deposition of a semiconductor shell with a larger band gap than the core (12).

Commercial $\mathrm{CdSe(ZnS)}$ core-shell quantum dots from Evidot, Inc. exhibit a quantum yield of approximately 32 $\%$, whereas that of Rhodamine (often used as reference for quantum yield measurements (19) can reach a value of 95 $\%$ (Rhodamine 6G (20)). Although it is possible to use silica particles with covalently attached organic dyes for the purpose to fabricate organic/inorganic hybrid materials with luminescent properties, most of the systems proved to be unsuitable because of rapid photobleaching. On the other hand, the preparation of monodispersed semiconductor particles, which show a lower tendency for bleaching, is a process that usually involves toxic materials and working under high-temperature conditions (14). Quantum dots are available in various sizes, shapes and with the proper surface chemical groups for later secondary reactions. However, if the particles are needed in large quantities for a certain purpose, the considerable cost of commercially available QD's often limits the range of experimental studies. Considering these restraints, we were motivated by our special requirements in synthetic process conditions and the rather large amount of material that was necessary for our experimental studies to search for less hazardous synthetic conditions and more cost effective chemicals.

Experimental Section

Instruments:

Fluorescent microscope:

An Axioskop (Zeiss, Germany) fluorescent microscope equipped with a charge-coupled device camera and a HBO50W fluorescent lamp was used to monitor the fluorescent emission of 1 micrometer large silica particles coated with the described $\mathrm{CdSe(ZnS)}$ core-shell quantum dots. The objective lens used for this purpose was a Zeiss Neofluar 100X/1.30 Oil Iris.

UV-Vis spectrophotometer:

A Varian Cary 50 (USA) UV-VIS spectrophotometer is used to measure the absorbance spectra of the quantum dots. Fluorescence spectrometer: Emission spectra were obtained using a Fluorolog fluorescent spectrometer from Horiba Jobin Yvon LtD (UK) with a minimal bandwidth of 0.5 nm (corresponds to the slit size).

Materials:

Cadmium acetate ($\mathrm{Cd(CH_3COO)_2}$; $\mathrm{2H_2O}$), trioctylphosphine oxide ($TOPO$, 90 $\%$ technical grade), selenium (99.999 $\%$ Se powder) and trioctylphosphine (TOP) were all purchased from $Sigma\text{-}Aldrich$. Methanol and butanol (both from VWR international) were of analytical grade and used as received.

In a typical example, the reaction is carried out with two similar systems of two-neck-flasks. The first flask contained the cadmium acetate precursor
$\mathrm{Cd(CH_3COO)_2}$; $\mathrm{2H_2O}$ (0.337g, 1.266 mmol) with fifteen molar equivalents (7.34 g, 19 mmol) $TOPO$. The flask was purged several times with argon and maintained under mild argon flow conditions. The second flask contained Se powder (5 g, 63.32 mmol) kept under argon.
Trioctylphosphine TOP solution (50 mL, 0.112 mol) was injected in the second flask through a septum. The Se/TOP dispersion was stirred for 12 hours under ambient conditions to form 1.26 mol.L^{-1} of trioctylphosphine/selenide ($TOPSe$) solution. Because of the oxygen/humidity sensitivity of the $TOPSe$ material, the latter reaction step was performed in a glove box which was conditioned for anaerobic and water-free conditions.
A Model 855-AC from Indulab AG was used in our laboratory for this purpose. As a result of the described procedures we obtained 50 mL of 1.26 mol.L^{-1} $TOPSe$ stock solution. 1 mL of this stock solution was injected into the mix of the cadmium acetate/$TOPO$ solution and stirred at 110°C (383 °K). After 5 minutes, an aliquot of 1 mL yellow quantum dots were removed from the flask. Afterwards, the temperature was stepwise increased and other aliquots

were taken.
Orange colored quantum dots were formed at 140°C (413 °K). The red color particles could be harvested at 180°C (453 °K).

An equimolar ratio between Cd and Se was maintained throughout the synthetic process. A small dependence of the formation temperature of a certain particle size on the $TOPO$ concentration was observed, but generally the formation conditions were found as very reproducible. Since quantum dots were formed relatively slowly in the mixture, they could easily be withdrawn and then stored in a refrigerator. If the particles are immediately used for further synthetic purposes, l0 mL quantity of methanol was twice added to the reaction mixture to remove $TOPO$ from the surface of the nanocrystals. After centrifugation, washing with clean methanol and several drying steps, the material could be redispersed in organic solvents like n-alkanes, chloroform tetrahydrofuran or toluene, respectively. The quantum yield of the dispersed particles strongly depends on the $TOPO$ concentration. However, a performance trade-off in using larger quantities of $TOPO$ surfactant caused in the necessity to put more emphasis to washing it from the CdSe. In a next step, ZnS shells were grown on CdSe particles using a classical method synthetic route from the literature (12).

A maximum quantum yield enhancement of up to a factor 20 was published for similarly fabricated particles. An alternative way to build $\mathrm{CdSe(ZnS)}$ core-shell quantum dots was recently published by Steckel *et al* (21).

Although diethylzinc ($\mathrm{Zn(C_2H_5)_2}$) was used in both synthetic routes as zinc source, we decided to follow the original procedure published by Dabbousi *et al* (12). A standard synthetic protocol for the synthesis of $\mathrm{CdSe(ZnS)}$ core-shell quantum dots was developed. First, the solution containing CdSe cores was washed 3 times with clean methanol and dried. Afterwards, 5 mg of the core powder were dispersed in 2 mL hexane. 10 g $TOPO$ was heated at 140 °C under vacuum for two hours in order to remove any remaining water. The CdSe cores solution in hexane was then injected through a septum under held under argon atmosphere into the batch containing the dried $TOPO$ surfactant. The excess hexane was then pumped off with the CdSe quantum dot cores left dispersed in a melt of $TOPO$. Equimolar amounts of $\mathrm{Zn(C_2H_5)_2}$ (10 μL, 0.1 mmol) and $\mathrm{(TMS)_2S}$ (18 μL, 0.1 mmol) were mixed with 7 mL TOP under a water free and inert atmosphere prepared in a glovebox (855-AC anaerobic chamber, Plas-Labs, USA). The mixture was loaded into a syringe, added dropwise to the CdSe/$TOPO$ mixture and the resulting reaction batch kept at 140 °C for 15 min. The synthesis vessel was cooled after 5 hours reaction time.
As a result of the shell build-up, the color of the $\mathrm{CdSe(ZnS)}$ core-shell was different from the CdSe cores. For example, initially yellow CdSe quantum dot cores became slightly orange in color (bathochromic shift) after the reaction. The resulting $\mathrm{CdSe(ZnS)}$ quantum dots were isolated and dispersed in an organic solution using the same procedure described for the CdSe cores.

Fig. 4.8: CdSe quantum dots (size between ca. 1.5 nm and 9 nm from left to right). The bare particles have been irradiated with UV light to show the photoemission

Results:

Quantum Yield Determination:

The quantum yield of a sample QY_s was calculated by comparing measured emission to a reference QY_r. When the solvent is the same for the sample and the reference, the following equation can be used to determine the quantum yield of a sample:

$$QY_s = QY_r . \frac{I_x . a_r}{I_y . a_s} \tag{4.1}$$

where I and a are the integrated area of the emission and absorbance band, respectively. I and a values are determined experimentally from the emission and absorption spectra of the reference and sample. The quantum yields of the dyes and the refractive indices of selected solvents were used from the literature. This equation can be simplified because all our measurements were performed in n-butanol (VWR International) with no further purification. Gelation of $TOPO$ is avoided by surface stabilization of n-butanol. Figure 4.8 represents nine samples of quantum dot solutions redispersed in n-butanol.

We can obtain about 3 g quantum dots with the described synthesis, which is a factor 100 times more than the existing syntheses.
Absorption and emission spectra of CdSe quantum dots as function of wavelength and temperature are shown in figure 4.9.

The fluorescence spectra show a broad emission indicating that the CdSe quantum dots are polydisperse. Although this result is far from perfect for various applications, particularly for

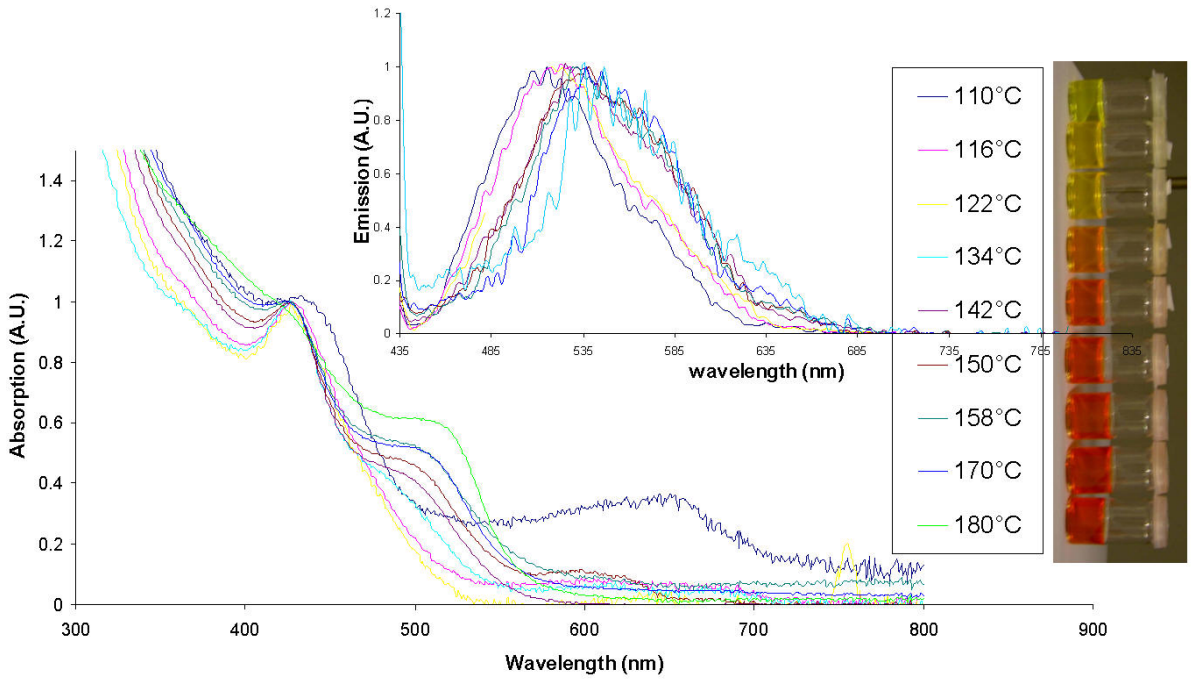

Fig. 4.9: Absorption and emission spectra of the $CdSe$ quantum dots.

systems in quantum optics, it is a less severe problem in cases where the nanocrystals are used as fluorescent markers. The estimated quantum yield enhancement of our core-shell synthesis product does not exceed a factor of three to four as compared with the emission from bare $CdSe$ core particles. Figure 4.10 shows the emission of $CdSe(ZnS)$ core-shell particles and $CdSe$ cores measured at the same concentration in butanol, size increase and the emission is slightly tuned at higher wavelength because of the shell size, increasing the particle size.

The photoluminescence quantum yield of core-shell nanocrystals can reach up to 50-80 $\%$ (12) (22). However, in most cases values between 10 and 40 $\%$ (15) (23) (24) (25) can be realistically expected. We obtained 4.5 $\%$ for our core-shell nanocrystals, which is low compared to high temperature syntheses work, but sufficient enough for the marker application. And this is proved in figure 4.11, which shows SiO_2 particles decorated with our $CdSe(ZnS)$ core-shell nanocrystals and detected by irradiation with UV light.

Acknowledgements

We thank for support from the Commission for Technology and Innovation (CTI, Switzerland) through its Technology-Oriented Program TOP NANO 21 (contract no. 6056.2 TNS).

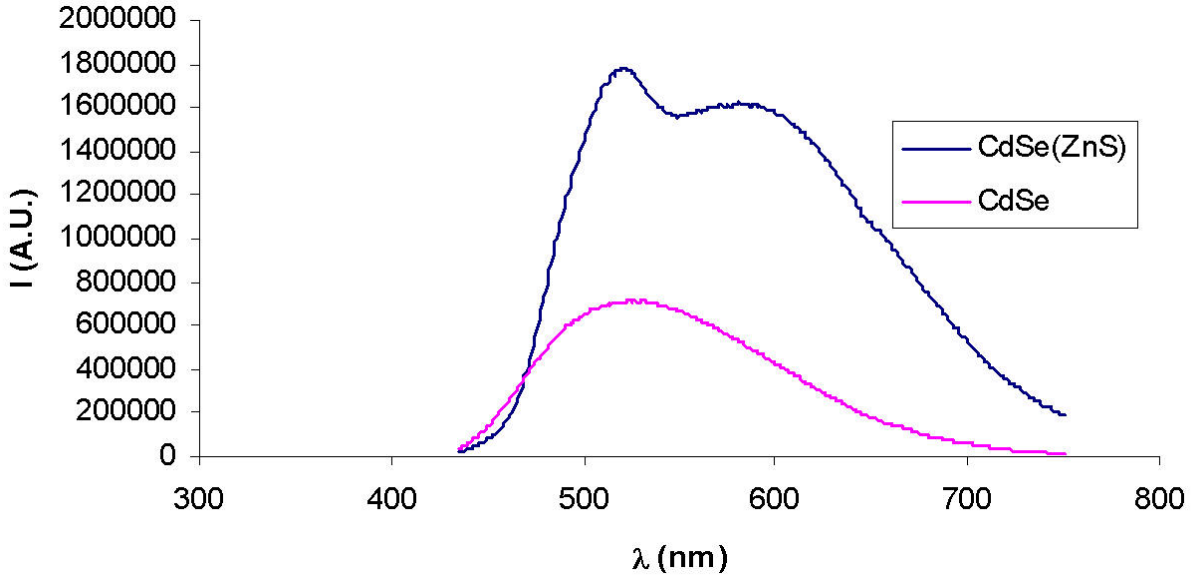

Fig. 4.10: Emission spectra of the $CdSe$ and $CdSe(ZnS)$ quantum dots.

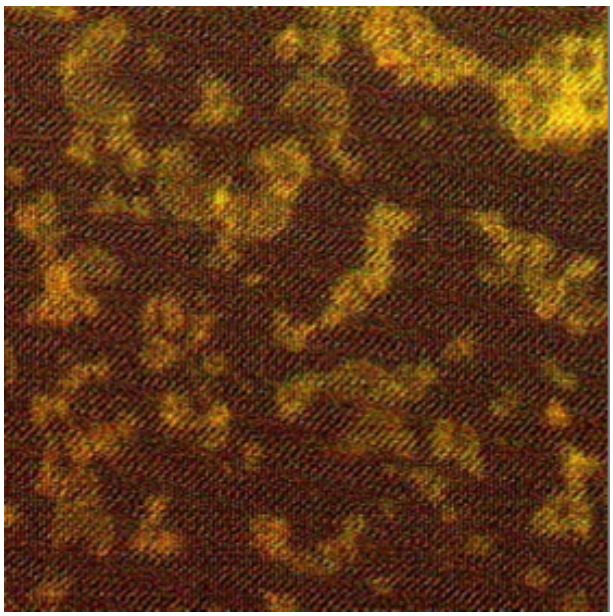

Fig. 4.11: Emission of SiO_2@$CdSe(ZnS)$ core-shell fluorescent particles

Conclusions

A simple synthesis of CdSe quantum dots using a high concentration of $TOPO$ reaction medium is proposed for gram scale syntheses. The low price of educts and the low temperature conditions make this synthesis particularly straightforward to perform. Cadmium acetate salt is chosen because it is relatively inexpensive and easy to handle (no need to work under controlled atmosphere and no moisture sensitivity). In addition, we were able to work with low temperatures (110°C - 180°C), which reduces the danger potential of this synthesis and allows even sparsely equipped chemical laboratories to perform it.
Reaction temperature and time were used to define the size and color of the resulting quantum dots. All reactions were performed under inert gas ($\mathrm{N_2}$ or Ar) atmosphere, which leads to highly luminescent quantum dots. We were also able to synthesize many different sizes, i.e. colors with only one batch by withdrawing aliquots at set temperatures.
In terms of quantity, we were able to obtain about 100 times more quantum dots than the currently described syntheses, suitable for labeling but not suitable for FRET or biological applications.

References

(1) Murray, C. ; Norris, D. and Bawendi, M.G. J. Am. Chem. Soc. 1993, 115, 8706
(2)Qu, L.H. ; Peng, Z.A. and Peng, X.G. Nanoletters 2001, 1, 333
(3) Reiss, P. ; Bleuse, J. and Pron, A. Nanoletters 2002, 2, 781
(4) Mohamed, M.B. ; Tonti, D. ; Al-Salman, A. ; Chemseddine, A. and Chergui, M. J. Phys. Chem. B 2005, 109, 10533
(5) Barrelet, C.J. ; Wu, Y. ; Bell, D.C. and Lieber, C.M. J. Am. Chem. Soc. 2003, 125, 11498
(6) Mekis, I. ; Talapin, D.V. ; Kornowski, A. ; Haase, M. and Weller, H. J. Phys. Chem. B 2003, 107, 7454
(7) Pradhan, N. and Efrima, S. J. Am. Chem. Soc. 2003, 125, 2050
(8) Dietsch H. and Keller, B:A:, in preparation.
(9) Nann T. and Mulvaney P., Angew. Chem. Int. Ed., 2004, 43, 5393
(10) Darbandi M., Thomann R. and Nann T., Chem. Mater., 2005, 17, 5720
(11) Empedocles, S. and Bawendi, M.G., Acc. Chem. Res. 1999, 32, 389
(12) Dabbousi, B.O. ; Rodriguez-Viejo, J. ; Mikulec, F.V. ; Heine, J.R. ; Mattoussi, H. ; Ober, R. ; Jensen, K.F and Bawendi, M.G. J. Phys. Chem. B 1997, 101, 9463
(13) Wu, X. ; Liu, H. ; Liu, J. ; Haley, K.N. ; Larson, J.A. ; Ge, N. ; Peale, F. and Bruchez, M.P. Nature Biotechnology 2003, 21, 41
(14) Hines, M.A. and Guyot-Sionnest, P. J. Phys. Chem. 1996, 100, 468
(15) Bruchez, M.P. ; Moronne, M. ; Gin P. ; Weiss, S. and Alivisatos, A.P. Science 1998, 281, 2013
(16) Chan, W.C.W. and Nie, S. Science 1998, 281, 2016
(17) Stöber, W. ; Fink, A. and Bohn, E. J. Colloid Interface Sci. 1968, 26, 62
(18) Verhaegh, A.M.N. and van Blaaderen, A. Langmuir 1994, 10, 1427

(19) Karstens, T., and Kobs, K. J. Phys. Chem. 1980, 84, 1871
(20) Georges, J. ; Arnaud, N., and Parise, L. Applied Spectroscopy 1996, 50, 1505
(21) Steckel, J.S. ; Zimmer, J.P. ; Coe-Sullivan, S. ; Stott, N.E. ; Bulovic, V. and Bawendi, M.G. Angew. Chem. Int. Ed. 2004, 43, 2154
(22) Peng, X. ; Schlamp, M.C. ; Kadavanich, A. ; Alivisatos, A.P. J. Am. Chem. Soc. 1997, 119, 7019
(23) Mattoussi, H. ; Mauro, J.M. ; Goldman, E.R. ; Anderson, G.P. ; Sundar, V.C. ; Mikulec, F.V. ; Bawendi, M.G. J. Am. Chem. Soc. 2000, 122, 12142
(24) Sundar, V.C. ; Lee, J. ; Heine, J.R. ; Bawendi, M.G. ; Jensen, K.F. Adv. Materials 2000, 12, 1102
(25) Coe-Sullivan, S. ; Woo, W.K. ; Bawendi, M.G. and Bulovic, V. Nature 2002, 420, 800

4.2.3 Incorporation of quantum dots

Quantum dots are per definition particles with a diameter in the order of the compound's exciton Bohr radius. Semiconductor nanocrystals have typically diameters between 2 and 8 nm.
Due to this property, the optical emission of quantum dots shows a strong dependence of the particle diameter.
The representation of a discrete quantum state is a typical property of nanoscale particles and not observed in bulk materials.

Quantum dots are very small in comparison with the silica particles, which were used in a range of 30 nm to 1 μm. Sizes in figure 4.12 are not to be scaled.

Fig 4.12 shows four different possibilities to synthesize silica@quantum dots. The first method, "dots core" was already used by making a synthesis in emulsion where dots are into the silica [23], (silica@dots silver [133]) or by imprisoning some quantum dots into aggregates of silica [104].

More recently, and via a microemulsion procedure, the group of Dr. Nann achieved CdSe-(ZnS)-$\mathrm{SiO_2}$ with silica particle diameters of about 10 nm on a single $\mathrm{CdSe}(\mathrm{ZnS})$ quantum dot core [33].
One year before, Nann and Mulvaney already managed to incorporate a single quantum dot in a larger spherical silica particle [84].

The efficiency of this technique of incorporation was regrettably very weak for our application because a single quantum dot does not emit enough radiation to label silica particles.

Another synthesis consists of depositing quantum dots on the surface of silica (figure 4.12 b).
This synthesis required a silane coupling agent which was grafted on the surface of quantum dots or silica to make the surface reactive. This process is used for any type of nanoparticles.

a) Incorporation in particles of silica, (dots core)

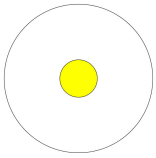

b) Absorption on surface, (dots shell)

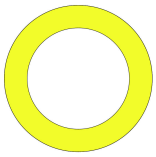

c) Incorporation between to silica layers (dots sandwich)

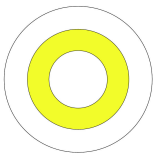

d) Partial adsorption on the surface, (dots surface patch)

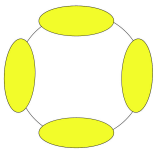

Fig. 4.12: Different ways of quantum dot incorporation into silica particles.

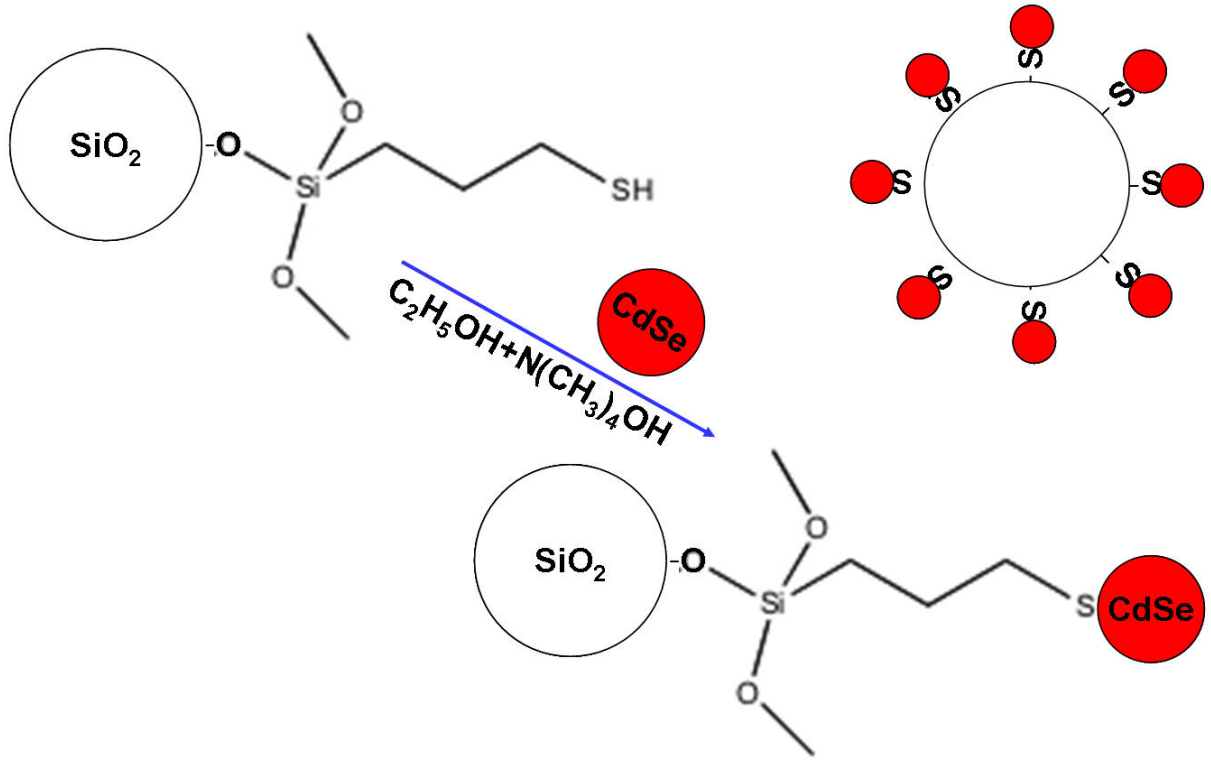

Fig. 4.13: Reaction scheme of $SiO_2@CdSe(ZnS)$ core-shell synthesis

For the metal particles, 3-aminopropyltrimethoxysilane (APTES) can be used as coupling agent because of the constant of complexation of the amino group on the metal.
In the case of semiconductors, a mercapto group was used to couple only quantum dots [28], [44].

The stability of quantum dots in organic solvents is assured by the adsorption of a surfactant: $TOPO$, HDA or DDA. $TOPO$ as a technical grade ($TOPO$, 90 %) was chosen because it catalyses the reaction (source M.I.T.).
Surfactant could be replaced by a mercapto group so that quantum dots could be dispersed in an aqueous environment.
It was then possible to graft quantum dot on the surface of the silica particles. The reaction scheme is described on the figure 4.13.

The synthesis described limits the possibility to attach quantum dots on the surface of silica. We suggested to synthesize monodisperse, fluorescent particles of silica by adsorbing quantum dots on the surface of our particles.
This synthesis was previously used [40] to cover particles of silica with gold nanoparticles. In this synthesis, the authors covered the silica of MPTS (cf. synthesis), and then incorporate

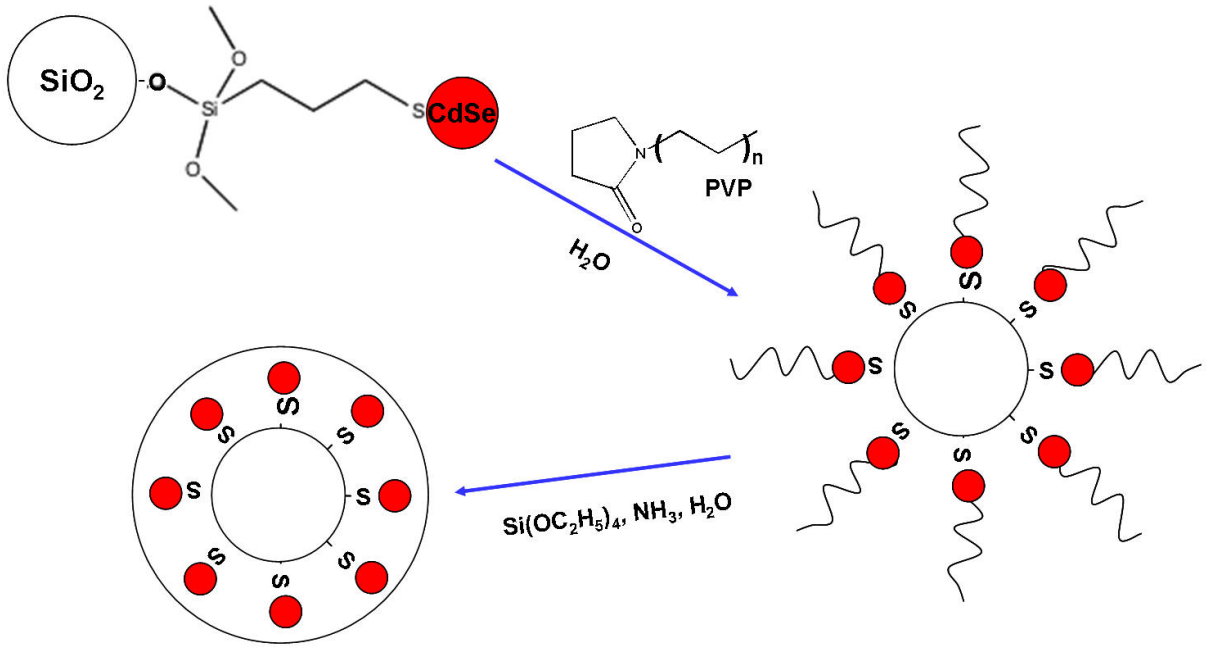

Fig. 4.14: SiO_2@CdSe(ZnS)@SiO_2 sandwich particles synthesis

nanoparticles.

This reaction requires a shell on the CdSe cores. Without it, the particle exhibits surface quenching and the emitted fluorescence is very low.
CdSe(ZnS) core shell quantum dots were synthesized in Empa laboratory.

This core shell particles have the main advantage that not only one but a few hundreds of fluorescent quantum dots are grafted onto a SiO_2 silica particle.
The disadvantage of this synthesis is that we cannot graft anymore a single silane agent onto the particle's surface, which suppresses copolymerization possibilities through TPM agent for example.

A solution of this problem is to build another silica layer onto the particle surface and so obtaining a sandwich system. The reaction we performed is described in the figure 4.14.

Experimental procedure to get SiO_2@CdSe(ZnS) particles

CdSe(ZnS) core shell quantum dots were synthesized like described in the paper [36].

A mixture containing 10 wt% tetramethylammoniumhydroxide $N(CH_3)_3OH$ (25 wt% in methanol, *Aldrich*) and 90 wt% 3-propyl trimethoxymercaptosilane (MPTS) was prepared and

stirred for five minutes.
100 μL of this mixture was added to 1 mL $\mathrm{CdSe(ZnS)}$ core shell quantum dots from the synthesis batch and stirred vigorously. Fluorescence was checked because any loss would mean presence of water and requires a new synthesis.

After twelve hours, 1 mL absolute ethanol was added and fluorescence was checked again. No apparent loss could be observed, which mean a shell of MPTS silane was built on the quantum dot surfaces.

2 mL containing about 100 mg particles with diameters of 1 μm were then combined in a ultrasonic bath with the MPTS surface modified quantum dots for 20 minutes.
Particles were then washed with methanol, which eliminates all $TOPO$ solved in methanol + ethanol. Notice that there was an exchange on the surface releasing the $TOPO$ surfactant from the quantum dot surface and adsorbing the MPTS agent because of the mercapto group.

Figure 4.13 is a schematic representation of the reaction, which would be the ideal case. We remarked that it was easier to coat first the quantum dots with MPTS agent before incorporating silica particles due to photobleaching problems.
Quantum dots are sensible without surface protection to water and ethanol, which were both present in the suspension of large silica particles.
A disadvantage of this synthesis was that the large MPTS quantity used to coat all the surface of quantum dots led to the formation of bridges between silica particles (figure 4.11), due to the condensation of the ethoxysilanes.

4.3 Conclusion of chapter 4

The synthetic procedures to get fluorescent particles using organic dyes were successful. Rhodamine red dyes have compared to fluorescein higher photostability and pretty high quantum yield. However these markers were not suitable for long time (more than 15 minutes) experiments.
Rhodamine or fluorescein show the highest photostability for organic dyes, which was still suitable in a limited way for our purposes. Both dyes are suitable for spacial repartition of agglomeration in a polymer matrix.

Quantum dots are photo-chemically stable even for several hours of exposure to the UV excitation light. They fluoresce brighter and longer than organic dyes under the same conditions.

However, the surface modification of quantum dots to encapsulate them into silica nanoparticles is a challenge. Nevertheless, this step is required to embed them in the desired polymer matrix. This requires alcohols and water, which low the emission of the obtained particles.

5

Synthesis of monodisperse distributed SiO_2-Polymer hybrid system

A hybrid system is per definition a mixture of two or more components of different origin or composition.
In our case, hybrid system describes a mixture consisting of particle and polymer.

The chosen system was built with silica particles, synthesized using sol-gel processes described in chapter 3 and two different polymer matrices:

- a commercial, polyacrylic acid (PAA) from $Sigma\text{-}Aldrich$.
- an Empa synthesized, polymethylmethacrylate (PMMA), based on methylmethacrylate (MMA) monomer, from VWR International.

5.1 Polymerization and copolymerization

Definition of polymerization and copolymerization:

Polymerization is per definition the process of reacting monomer molecules together to form linear chains or a three-dimensional network of polymer chains.

Copolymerization is the polymerization of two or more monomers, which combines in the ideal case properties of both polymers. The resulting product may be a random copolymer, an alternating copolymer, or a block copolymer.

In this section, we describe the polymerization of methylmethacrylate (MMA) and its copolymerization with TPM modified SiO_2 particles (SiO_2(TPM)) based on a previous work.
A kinetic model is also proposed.

Hybrid system based on commercial dispersion of silica colloids in the nanorange and MMA monomer was performed in the group of Ford [126] a decade ago, this work described the idea

and a way to get a hybrid SiO_2-PMMA copolymer without drying at any moment the nanoparticles used using double dialysis tubing.
This synthesis was resumed at one dialysis step at Empa.

5.1.1 Different type of polymerizations

Anionic [138] and cationic [30] [29] (also called ionic) polymerizations can be made in a laboratory scale, it is difficult to perform this kind of polymerizations on an industrial scale.

Anionic polymerization is a ”living polymerization”, where the polymer chain length can be perfectly controlled.
Anionic polymerization of methacrylic monomers [131] and methylmethacrylate were already performed in the past [143].
However an anionic polymerization requires an expensive synthetic system to be built, which does not allow producing large quantities of materials.

Free radical polymerization and photopolymerization are easier to perform than ionic polymerization. These two types of polymerization need an initiator.

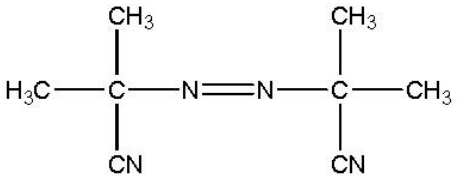

Fig. 5.1: Azobisisobutyronitrile (AIBN)

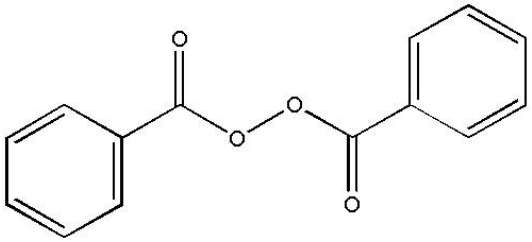

Fig. 5.2: Benzoyl peroxide (BPO)

Free radical polymerization using typically azobisisobutyronitrile (AIBN, figure 5.1) or benzoyl peroxide (BPO, figure 5.2) as initiator can be performed in any chemistry laboratory work-

ing with a classical reflux set-up (figure 5.3) under inert gas (N_2 or Ar).

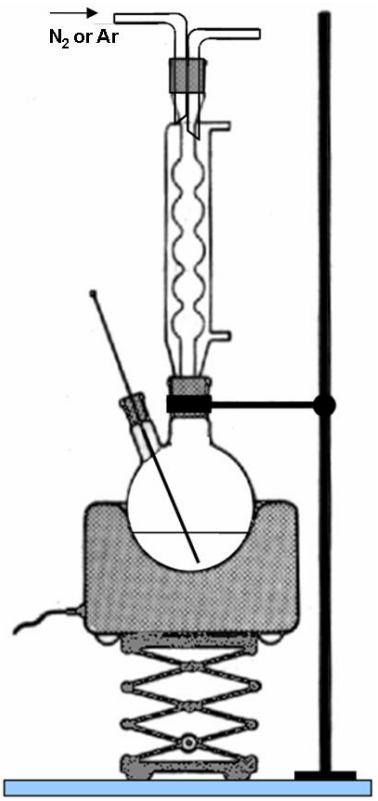

Fig. 5.3: Reflux set-up

Radical polymerization has two main disadvantages:

The first one is the so-called Tromsdorff effect, also more commonly named autoacceleration. It occurs during polymerizations with high concentrations of monomer (i.e. small amount or no solvent).
The reaction proceeds normally for a while, then suddenly the rate of polymerization increases dramatically.
The size (molecular weight) of polymer chains grown during the accelerated period is much larger than those chains grown earlier and therefore the resulting macromolecules polydispersity is higher.

The second main disadvantage is that the classical radical initiators require a decomposition step, which is necessary for the initiation of the formation of a macromolecule. During the decomposition step, gas is released allowing the formation of free radicals. Gas can be either O_2, CO_2 (case for peroxide initiators) or N_2 (case for AIBN).

The decomposition of AIBN is presented in the reaction scheme 5.4. Two radicals (isobutyronitrile radicals) and nitrogen gas are resulting from this reaction.

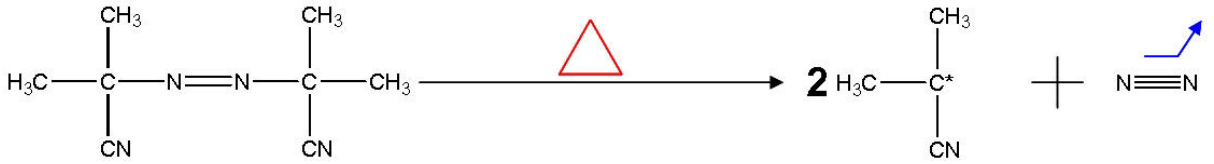

Fig. 5.4: Decomposition of AIBN initiator

Decomposition of BPO is presented in the reaction scheme 5.5. Two radicals (benzoyl and/or benzyl) are released and CO_2 gas is emitted.

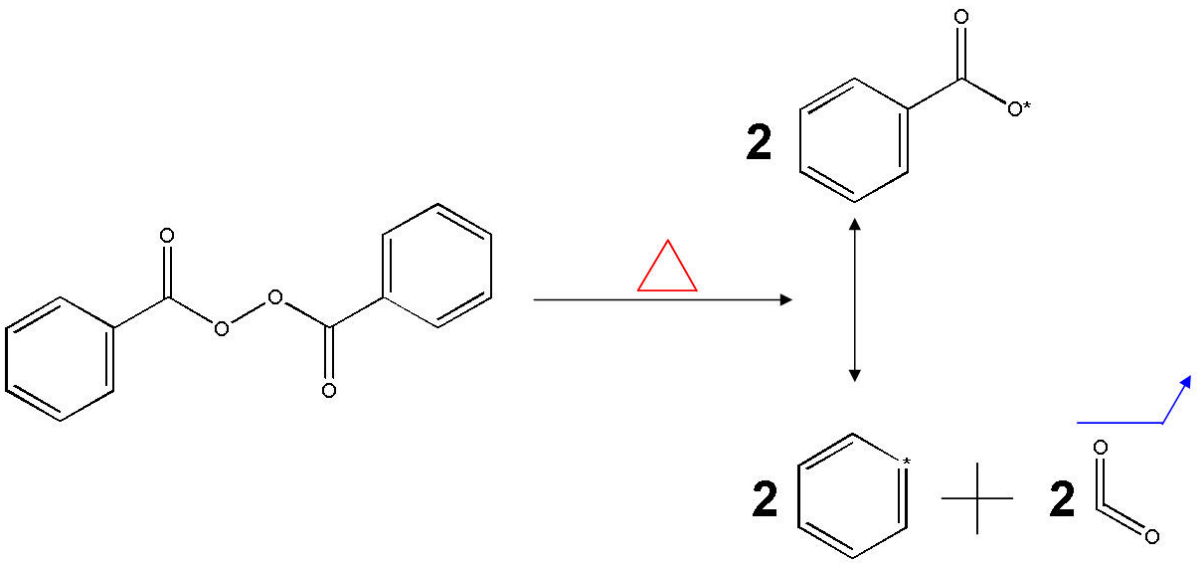

Fig. 5.5: Decomposition of BPO initiator

5.1.2 Photopolymerization

Polymethylmethacrylate (PMMA) was photopolymerized under UV light exposure.

Photopolymerization is drastically different from the polymerization induced by thermal energy. A thermal radical polymerization is relatively slow and generally implies evaporation of

the solvent.

Photopolymerization allows a rapid and solvent free reaction with the need of a photoinitiator. Photoinitiator capt emitted energy from the UV light, which leads to excited species, able to polymerize in a chain reaction.

Irgacure 184 ($\mathrm{I_{184}}$) was kindly provided by $Ciba\ SC$, Basel. This Ketone photoinitiator allows working without any gas released from the activated initiator $\mathrm{I_{184}}^*$. The mechanism of the reaction leading to the chain initiation is described in equations 5.1 and 5.2.

$$I_{184} + h\nu \longrightarrow I_{184}^* \tag{5.1}$$

$$I_{184}^* + M \longrightarrow I_{184} - M^* \tag{5.2}$$

$$M^* + M \longrightarrow M_2^* \tag{5.3}$$

$$M_n^* + M \longrightarrow M_{n+1}^* \tag{5.4}$$

where M is the monomer to be polymerized and the energetic condition presented in the following energy relation:

$$E_{I_{184}^*} - E_{I_{184}} > E_{M*} - E_M$$

Chain polymerization proceeds in the following reaction stages:
The first one (5.1) is the activation of the photoinitiator after excitation with UV light.
The second stage (5.2) is the initiation of the polymerization, also called the activation of the monomer.
The third one (5.3 and 5.4) is the chain propagation of the polymerization.
The last stage is the termination, which deactivates the chain to yield macromolecules, also

called polymers.

$$M_m^* + M_n^* \longrightarrow M_{m+n} \tag{5.5}$$

$$M_m^* + M_n^* \longrightarrow M_m + M_n \tag{5.6}$$

The macromolecules can be formed by two termination ways:
combination (5.5) or dismutation (5.6).

In copolymerization, two different types of monomers are present in the reaction vessel. Therefore, more reaction steps become possible.
This is shown below (equations 5.9-5.12) in the example of copolymerization of methylmethacrylate with TPM modified silica particles ($\mathrm{Si\,O_2}$(TPM)).
The activation of the photoinitiator (equation 5.1) stays the same.

Initiations that occur are presented in the equations 5.7 and 5.8.

$$I_{184}^* + MMA \longrightarrow I_{184} - MMA^* \tag{5.7}$$

$$I_{184}^* + \mathrm{Si\,O_2}(TPM) \longrightarrow I_{184} - \mathrm{Si\,O_2}(TPM)^* \tag{5.8}$$

Four main reactions (equations 5.9, 5.10, 5.11, 5.12) can happen in the propagation step.

$$MMA^* + MMA \xmapsto{k_{MMA-MMA}} (MMA)_2^* \tag{5.9}$$

$$MMA^* + \mathrm{Si\,O_2}(TPM) \xmapsto{k_{MMA-\mathrm{Si\,O_2}(TPM)}} MMA - \mathrm{Si\,O_2}(TPM)^* \tag{5.10}$$

$$\mathrm{Si\,O_2}(TPM)^* + MMA \xmapsto{k_{\mathrm{Si\,O_2}(TPM)-MMA}} \mathrm{Si\,O_2}(TPM) - MMA^* \tag{5.11}$$

$$\mathrm{Si\,O_2}(TPM)^* + \mathrm{Si\,O_2}(TPM) \xmapsto{k_{\mathrm{Si\,O_2}(TPM)-\mathrm{Si\,O_2}(TPM)}} (\mathrm{Si\,O_2}(TPM))_2^* \tag{5.12}$$

Rate constants ($k_{MMA-MMA}$, $k_{MMA-\mathrm{Si\,O_2}(TPM)}$, $k_{\mathrm{Si\,O_2}(TPM)-MMA}$, $k_{\mathrm{Si\,O_2}(TPM)-\mathrm{Si\,O_2}(TPM)}$) are defined in equations 5.13 for the respective reaction 5.9, 5.10, 5.11, and 5.12.

These rate constants are defined by:

$$\begin{aligned}
k_{MMA-MMA} &= \frac{[MMA]_2^*}{[MMA]^*.[MMA]} \\
k_{MMA-\mathrm{Si\,O_2}(TPM)} &= \frac{[MMA-\mathrm{Si\,O_2}(TPM)]^*}{[MMA]^*.[\mathrm{Si\,O_2}(TPM)]} \\
k_{\mathrm{Si\,O_2}(TPM)-MMA} &= \frac{[\mathrm{Si\,O_2}(TPM)-MMA]^*}{[\mathrm{Si\,O_2}(TPM)]^*.[MMA]} \\
k_{\mathrm{Si\,O_2}(TPM)-\mathrm{Si\,O_2}(TPM)} &= \frac{[\mathrm{Si\,O_2}(TPM)]_2^*}{[\mathrm{Si\,O_2}(TPM)]^*.[\mathrm{Si\,O_2}(TPM)]}
\end{aligned} \tag{5.13}$$

The reactivity ratios of individual monomers are expressed in these relations:

$$\begin{aligned}
r_{MMA} &= \frac{k_{MMA-MMA}}{k_{MMA-\mathrm{Si\,O_2}(TPM)}} \\
&= \frac{[MMA]_2^*.[\mathrm{Si\,O_2}(TPM)]}{[MMA-\mathrm{Si\,O_2}(TPM)]^*.[MMA]}
\end{aligned} \tag{5.14}$$

and

$$\begin{aligned} r_{\mathrm{Si\,O_2}(TPM)} &= \frac{k_{\mathrm{Si\,O_2}(TPM)-\mathrm{Si\,O_2}(TPM)}}{k_{\mathrm{Si\,O_2}(TPM)-MMA}} \\ &= \frac{[(\mathrm{Si\,O_2}(TPM))]_2^*.[MMA]}{[\mathrm{Si\,O_2}(TPM)].[\mathrm{Si\,O_2}(TPM)-MMA]^*} \end{aligned} \tag{5.15}$$

r, also commonly called *"copolymerization parameter"* describes the rate of reaction with another monomer.

The copolymerization equation (equation 5.16) also called Mayo-Lewis relation [75] gives the molar ratios of the two monomers in the resulting copolymer.

$$\frac{d[M_{MMA}]}{d[M_{\mathrm{Si\,O_2}(TPM)}]} = \frac{[M_{MMA}](r_{MMA}[M_{MMA}]+[M_{\mathrm{Si\,O_2}(TPM)}])}{[M_{\mathrm{Si\,O_2}(TPM)}]([M_{MMA}]+r_{\mathrm{Si\,O_2}(TPM)}[M_{\mathrm{Si\,O_2}(TPM)}])} \tag{5.16}$$

Approximations and simplifications

There is a possibility to omit a few terms in the case of a monodistributed polymer-particle hybrid systems.
We proved that our silica particles did not build aggregates [109], which means in terms of reaction that the activated TPM modified silica $\mathrm{Si\,O_2}$(TPM)* did not react with other modified particles (no aggregation). This results in negligible $r_{\mathrm{Si\,O_2}(TPM)}$ because $k_{\mathrm{Si\,O_2}(TPM)-\mathrm{Si\,O_2}(TPM)} \simeq 0$. This result simplified the Mayo-Lewis relation as shown in equation 5.17.

$$\frac{d[M_{MMA}]}{d[M_{\mathrm{Si\,O_2}(TPM)}]} = \frac{r_{MMA}[M_{MMA}]+[M_{\mathrm{Si\,O_2}(TPM)}]}{[M_{\mathrm{Si\,O_2}(TPM)}]} \tag{5.17}$$

where F_{MMA} and $F_{\mathrm{Si\,O_2}(TPM)}$ are the respective fraction of MMA and modified silica particles in the completed copolymer.
f_{MMA} and $f_{\mathrm{Si\,O_2}(TPM)}$ are the fractions of monomer in the reaction mixture, the mathematical terms expressions in equation 5.18 and 5.19 become valid.

$$\begin{aligned} F_{MMA} + F_{\mathrm{Si\,O_2}(TPM)} &= \frac{d[MMA]}{d[MMA] + d[\mathrm{Si\,O_2}(TPM)]} \\ &+ \frac{d[\mathrm{Si\,O_2}(TPM)]}{d[MMA] + d[\mathrm{Si\,O_2}(TPM)]} = 1 \end{aligned} \tag{5.18}$$

and

$$\begin{aligned} f_{MMA} + f_{\mathrm{Si\,O_2}(TPM)} &= \frac{[MMA]}{[MMA] + [\mathrm{Si\,O_2}(TPM)]} \\ &+ \frac{[\mathrm{Si\,O_2}(TPM)]}{[MMA] + [\mathrm{Si\,O_2}(TPM)]} = 1 \end{aligned} \tag{5.19}$$

Our modified Mayo-Lewis equation can so be simplified to formula 5.20.

$$\begin{aligned} F_{MMA} = 1 - F_{\mathrm{Si\,O_2}(TPM)} &= \frac{d[M_{MMA}]}{d[M_{MMA}] + d[M_{\mathrm{Si\,O_2}(TPM)}]} \\ &= \frac{r_{MMA}.f_{MMA} + f_{\mathrm{Si\,O_2}(TPM)}}{r_{MMA}.f_{MMA} + 2.f_{\mathrm{Si\,O_2}(TPM)}} \end{aligned} \tag{5.20}$$

The expression 5.20 gives the fraction of MMA in the completed copolymer, but does not consider the influence of the particle size (i.e. specific surface).
It is crucial to precise that $f_{\mathrm{Si\,O_2}(TPM)}$, the fraction of monomer, is in fact the fraction of TPM.

A particle with a radius R has a surface S defined as $S = 4.\pi.R^2$.
This implies that a larger particle has a larger surface and of course through the nanoeffect that at the same volume fraction of incorporated particles, the interface (where the TPM is located) is much lower for larger particles.

[SiO_2(TPM)] is defined in equation 5.21.

$$[SiO_2(TPM)] = \frac{\alpha.10^{18}}{\mathfrak{N}}.S_s.\phi_m = \frac{\alpha.10^{18}}{\mathfrak{N}}.\frac{3}{\rho.R}.\phi_m \tag{5.21}$$

with α as the number TPM groups per nm^2 particle surface, estimated between 8 and 10 groups.nm^{-2} [74],
$\mathfrak{N}$ as $\mathfrak{A}vogadros$ number = 6.022.10^{23} $groups.mol^{-1}$,
ρ as the SiO_2 density in g.m^{-3},
R as the SiO_2 particle radius in m,
and ϕ_m as the weight percent of SiO_2 particles in monomer.

From equations 5.21 and 5.20, the equation 5.22 can be deduced.

$$F_{MMA} = \frac{r_{MMA}.[MMA] + \frac{\alpha.10^{18}}{\mathfrak{N}}.\frac{3}{\rho.R}.\phi_m}{r_{MMA}.[MMA] + 2.\frac{\alpha.10^{18}}{\mathfrak{N}}.\frac{3}{\rho.R}.\phi_m} \tag{5.22}$$

Equation 5.22 is the explanation that in a PMMA-SiO_2 nanocomposite systems, the fraction of integrated MMA units in the final composite is dependent on the MMA monomer concentration, degree of particle modification, radius, density and weight fraction.

5.2 Synthesis of a SiO_2-PAA hybrid system with commercial products

Nanocomposites composed of fluorescent marked particles were fabricated using commercial products : SiO_2 particle powder ($Aerosil\ OX50$ and $Ludox\ TMA$) and commercial polyacrylic acid (PAA) (400 kg.mol^{-1}, $Aldrich$) polymer.

The first suggested solution was to create bifunctional nanoparticles, that could have been silanised with two different silane agents. This allows for copolymerizing and simultaneously detecting the nanoparticles under UV excitation.

Unfortunately, it was difficult to fabricate these particles, probably due to a different diffusion coefficient of the different silane agents. An alternative solution was found for this problem.

Direct transplantation of the FITC marked APTES modified SiO_2 (see chapter 4) on the surface of polyacrylic acid (PAA) with a substitution mechanism [97] was the proposed solution, presented in figure 5.6.
This reaction is an amidification.

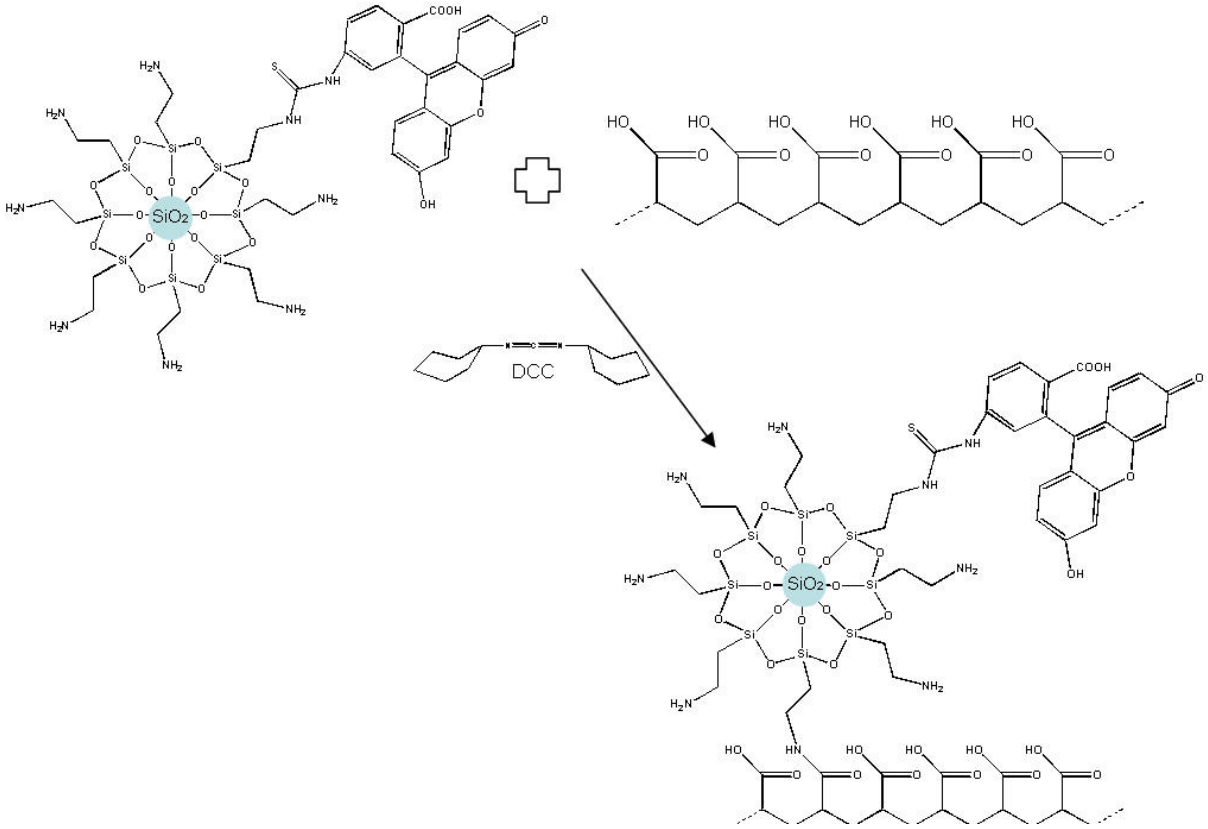

Fig. 5.6: Scheme of the incorporation of SiO_2@FITC in PAA

To control if the reaction took place, direct detection of the characteristic amide group (R-CO-NH-R') for this substitution with Raman and FTIR spectroscopy was performed.
The Raman spectra were measured for PAA in Dimethylformamide (DMF) and FITC modified SiO_2 particles labeled PAA in DMF (figure 5.7). At 1735 cm^{-1}, a new signal arising from the carboxylic group of an amide was identified.

A previously not detected additional signal between 3000 and 3600 cm^{-1} in the FT-IR spectrum (figure 5.8) was taken as proof for the existence of an amide group as expected from the proposed reaction scheme.

Fluorescence microscopy was used in the past to track colloidal particles with subnanometer

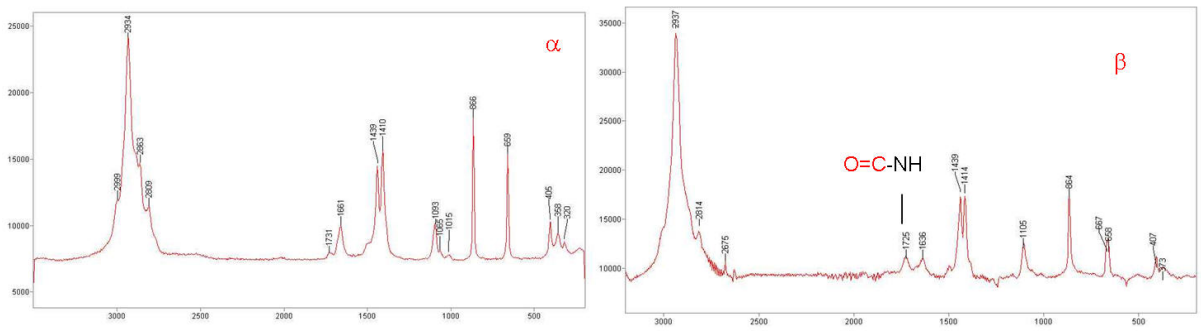

Fig. 5.7: Raman spectra of α) PAA in DMF and β) FNP labeled PAA in DMF

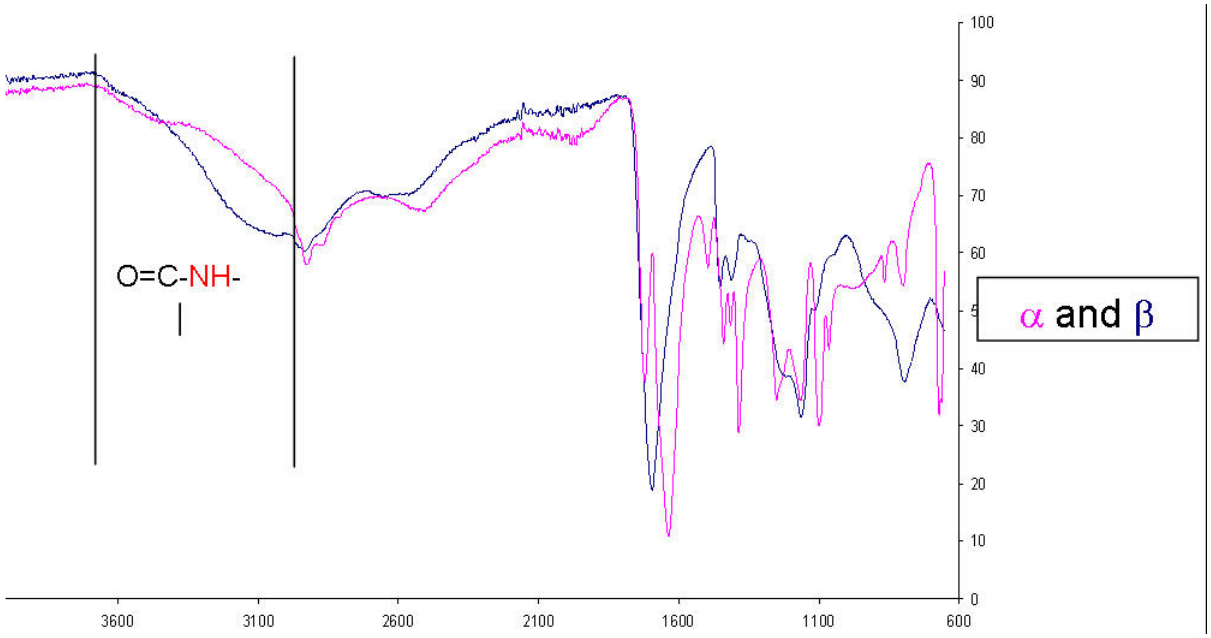

Fig. 5.8: FT-IR spectra of α) PAA in DMF and β) FNP labeled PAA in DMF

precision.
Speidel *et al* [121] realized a system based on a modified inverted microscope (Axiovert 35, Carl Zeiss) with an epifluorescence setup and a high numerical aperture (NA) objective lens (Plans Neofluoar 100X; oil immersion; NA, 1.3, Carl Zeiss).
A mercury lamp was used for fluorescence excitation (HBO100, Carl Zeiss).

However, since the same equipment is not available at EMPA, an Axioscop from Carl Zeiss with the same objective lens and mercury lamp with similar emission characteristics was employed for fluorescence excitation (HBO50, Carl Zeiss (50 W instead 100 W)).
Images of figure 5.9 was recorded using a high-resolution CCD camera (Leica DC 500) with a maximum pixel format of 3900 X 3090 (equiv. 12 million pixels).
The particles were not monodisperse and showed a high degree of agglomerates. Alignment of clusters, originating from intrinsic orientation of polymer chains was due to the fact that a rackel was used to create the polymer film. Since the fluorescent particles were covalently bound to the polymer chains, they were co-aligning.

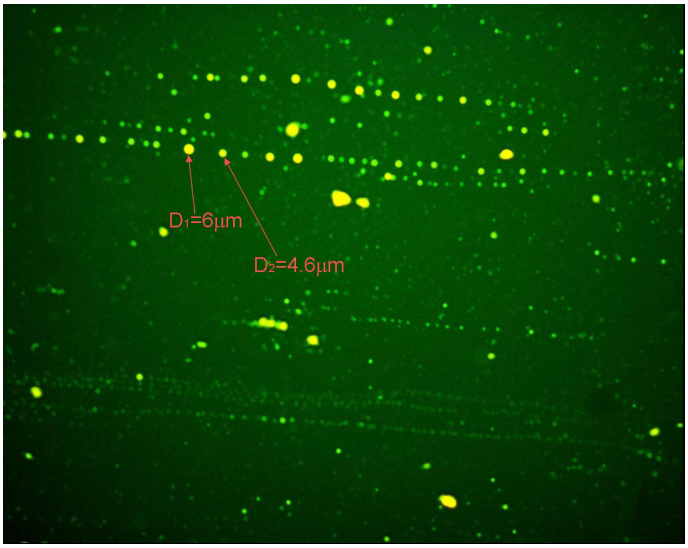

Fig. 5.9: Alignment of FITC modified SiO_2 clusters incorporated in PAA : 10 wt% of $Aerosil\ OX50$ incorporated

No orientation of particles or clusters was found in films deposited using a spin coating instrument.

Orientation is also not observed in cases where the particles had no covalent bound to the polymer chain.
Additional stabilization with surface active molecules does not significantly alter the degree of cluster formation. Particles dispersed in polar or non-polar solutions are generally treated with

an ultrasonic finger (US finger 750W 50 % 45 min) to avoid excessive agglomeration. In combination with dissolved polymers, this process does not offer a synthetic route for monodispersed nanoparticle hybrid materials and forced us to develop another synthetic way.

Figure 5.10 is a drawing, which represents the different synthetic steps to fabricate those two SiO_2-co-PAA hybrid systems, covalently bound or not.

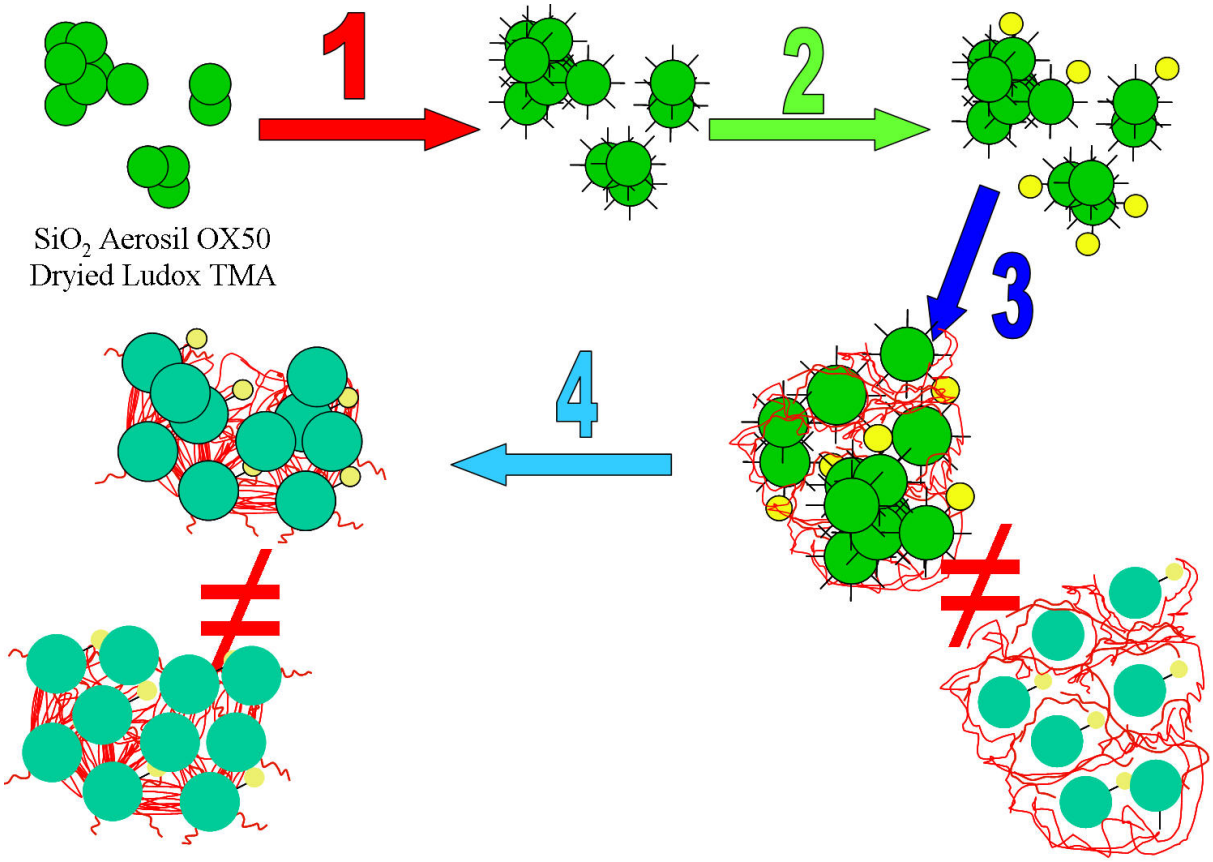

Fig. 5.10: Schematic representation of FITC modified SiO_2 clusters incorporated in PAA

The particle powder was dispersed using an ultra sonic finger in ethanol, under stirring at 700 rpm. Different synthetic steps are then necessary to fabricate the composite, represented in the drawing 5.10.

1. Required amount of APTES silane agent (see chapter 3.2) is injected in the stirred milieu regulated at 50 °C.
2. After eight hours, surface modified particles are marked with fluorescein or rhodamine (see chapter 4.1).

3. A transfer of the fluorescent particles obtained after drying to a solution of PAA in water allowed the fabrication of a non-covalently bound hybrid system.

4. Through chemical treatment (amidification), the covalent bound system is built.

Small powder particles cannot be redispersed (see chapter 3), which does not allow the fabrication of monodisperse, monodistributed model hybrid system by this synthetic procedure. This led to the development of a new strategy synthesizing SiO_2 particles and polymer.

5.3 Conclusion of chapter 5

A presentation of the synthesis of a tailored monodisperse and monodistributed SiO_2-PMMA particle-polymer composite system is presented in the following paper [35].

Figure 5.11 represents the synthetic route of the hybrid preparation.
A description in more details with the rheological study of the hybrid system is presented in chapter 6.3.

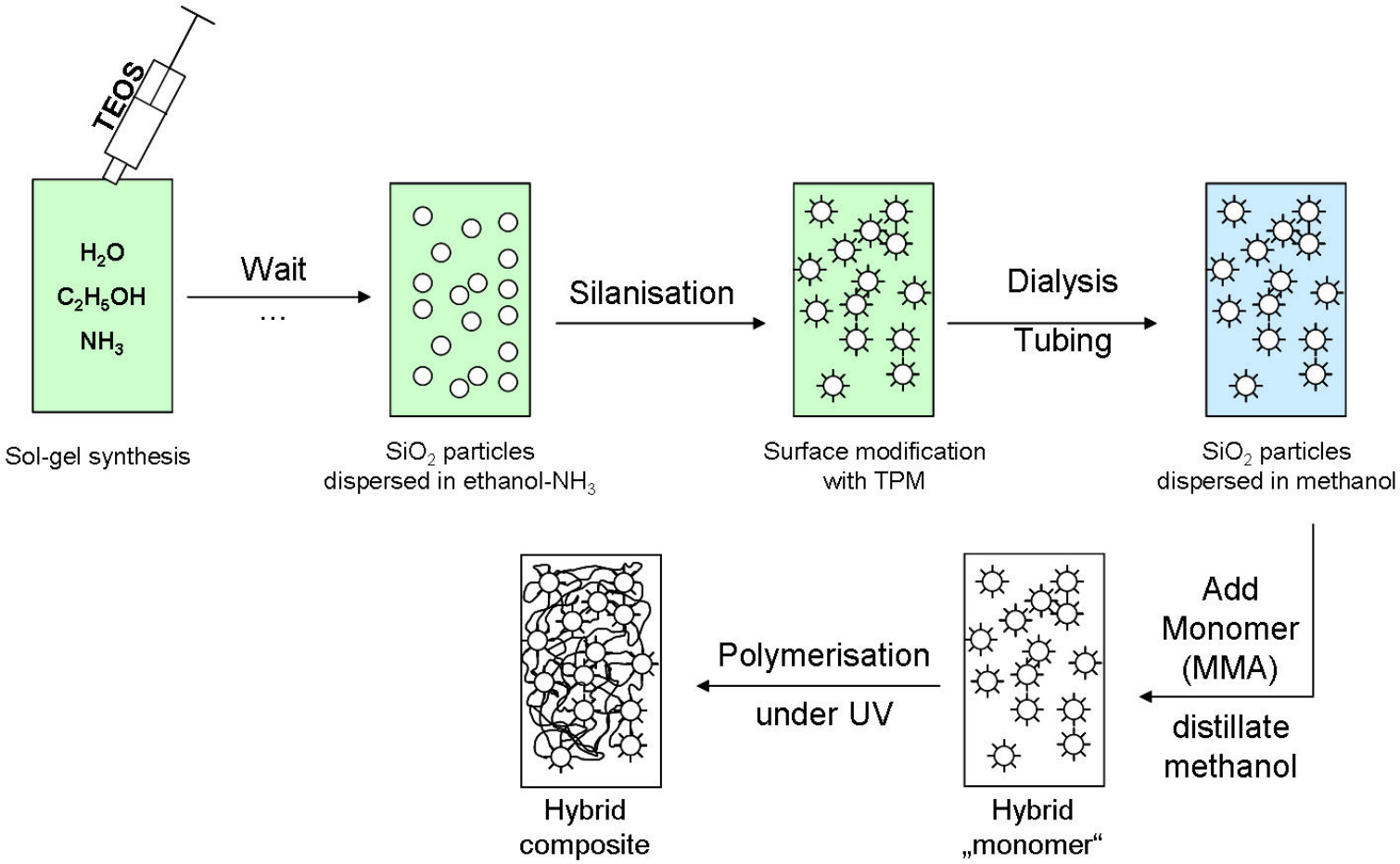

Fig. 5.11: The ”never dry approach”: principe of the synthesis

6

Characterization: light scattering, thermal, rheological and mechanical behaviors of the hybrid system

6.1 In-situ polymerization as a route towards transparent nanocomposites: Time-resolved light and neutron scattering experiments

This work, a collaboration between Empa and the University of Fribourg, led to a publication in *Colloids and Surfaces A, Physicochemical and Engineering Aspects*, 2006, 291, 110-116 [109].

Mirko Saric[1], Hervé Dietsch[2], and Peter Schurtenberger[1]*
[1]Department of Physics, Soft Condensed Matter Group, University of Fribourg, CH-1700 Fribourg, Switzerland, and
[2] Laboratory for Nanoscale Materials Science EMPA - Materials Science and Technology, Empa, CH-8600 Dübendorf, Switzerland

Abstract

We describe the formation of a highly transparent nanocomposite using an in-situ polymerization of monodisperse, 50 nm diameter, colloidal silica coated with 3-(trimethoxysilyl) propyl methacrylate (TPM) dispersed in methyl methacrylate (MMA). We demonstrate that it is possible to follow the polymerization process in a completely non-invasive way using time-resolved dynamic light scattering and small-angle neutron scattering. These experiments allow us to obtain quantitative information on the time dependence of the resulting mechanical and structural properties during the synthesis. We observe a qualitative change between diffusive and subdiffusive motion for the dispersed nanoparticles at the gel point, in agreement with the behavior of other colloidal systems undergoing a sol-gel transition. The small-angle neutron scattering experiments clearly demonstrate that the initial liquid-like order of the nanoparticles is maintained during the polymerization process, and that there is no indication for particle aggregation. This information is confirmed by TEM experiments of the final nanocomposite.

* Author to whom correspondence should be addressed:
peter.schurtenberger@unifr.ch, Department of Physics, University of Fribourg Chemin du musée 3 CH-1700 Fribourg Switzerland
Tel: +41 - 26- 300 9115
Fax: +41 - 26 - 300 9747

Introduction

Nanostructured organic-inorganic hybrid systems represent an exiting class of materials. The combination of nanoscale inorganic moieties with organic polymers allows us to combine the properties of nanoparticles and polymers and thus to design materials with enhanced or even completely new properties. Another important feature is the possibility of tuning the structure and morphology on the nanometric scale, which opens the door for innovative applications in both advanced and conventional technology fields. Selected examples for potential applications are the design of new components in electronic and optoelectronic devices, bioencapsulation or as active substrates in chromatography and catalysis. The unique properties of these materials such as their improved mechanical (1), thermal (2-5), electrical (6), magnetic (7), photochemical (8), and catalytic (9) performance in comparison to pure organic polymers as well as their high optical transparency (10) has created enormous interest among materials scientists and engineers. However, the control of the mixing between the two dissimilar phases remains a challenging task, and there still is a lack of data on structure-property relationships at a nanoscale level (11). We have thus started a systematic study in which we combine synthetic activities with an application of time-resolved scattering methods in order to understand and improve the formation mechanism of polymer-colloid nanocomposites.

A major obstacle on the way towards versatile nanocomposites with tailor-made properties arises from the poor miscibility of the two dissimilar phases. The properties of particulate-filled composites are generally determined by the component properties, composition, structure (spatial distribution), particle-particle interaction and particle-matrix interaction. Although it is well accepted that full dispersion (disaggregation) of the particles is of crucial importance for the performance of the composites, there is still no quantitative method to predict and/or measure the dispersability of the filler particles in the polymer matrix. The extent to which particles agglomerate depends both on the processing conditions (shear forces) as well as on the balance between the attractive and repulsive forces among the particles and the matrix. Depending on the chemical interaction between the species, one can differ between materials with strong (covalent, coordination or ionic), weak (Van-der-Waals, hydrogen-bonds) or without chemical interaction (12, 13).

In principle, there are various ways of creating stable and fully dispersed polymer-colloid nanocomposites with different properties, and Figure 6.1 shows some schematic drawings of selected examples. In practice, a simple dispersion of inorganic nanoparticles in a polymer matrix as depicted in figure 6.1 (a) is seldom feasible since polymers and inorganic fillers often

possess incompatible segments leading to micro- and/or macrophase separation and a concomitant clustering on various length scales (14). There are several possibilities in order to avoid these phenomena:

1. to attach an inert organic layer covalently to the surface of the particle in order to enhance the compatibility of the polymer-particle interface (16)

2. to encapsulate the nanoparticles by emulsion polymerization (10)

3. to attach functional or initiating groups which allow a covalent linkage to the polymer matrix

4. to graft polymer chains from the particle surface which leads to a steric stabilization of the nanoparticles and enhanced stability of the resulting material (17, 18).

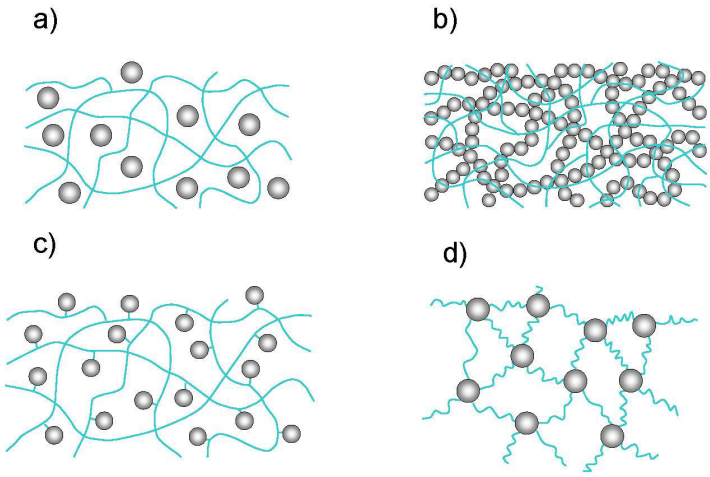

Fig. 6.1: Selected examples of stable polymer-colloid nanocomposites, where the particles (a) are present in a stable dispersion, (b) form an interpenetrating network, (c) are chemically linked to the polymer matrix, or (d) act as crosslinkers.

Here we now describe the use of method 3, where we functionalized nanoparticles and thus make them available as crosslinkers for the creation of a polymer gel through an in-situ polymerization. This should then lead to a situation as schematically shown in Figure 6.1 (d). We use a Poly(methyl methacrylate) (PMMA) based system. PMMA belongs to the important species of polyacrylic and methacrylic esters, and possesses high optical transparency, exceptional mechanical strength and form stability as some of its most important materials properties. In combination with nanoparticles, it is in addition possible to decrease the gas permeability, and

to enhance the physical performance and heat resistance without diminishing the optical transparency (10). Optically clear composites of silica-PMMA have been prepared by using silica particles that are much smaller than the wavelength of visible light or by matching the refractive index of the components (19, 20). However, the transparency of the composite decreases dramatically if aggregation occurs, since clusters of nanoparticles strongly scatter visible light. Several routes towards stable PMMA-silica-based nanocomposites have been followed in the past. In order to improve the compatibility of silica and vinyl polymer matrices, silane coupling agents have been grafted on colloidal silica surfaces (21, 22). PMMA-layered silicate nanocomposites were also prepared by in-situ suspension and emulsion polymerization (10).

Our approach for the nanocomposite preparation was to use surface modified silica nanoparticles suspended in a monomer solvent, followed by an in-situ polymerization (23). We used 3-(Trimethoxysilyl)-propylmethacrylate (TPM) surface modified silica nanoparticles that have a radius of 25 nm. For the radical polymerization we did not use an additional organic solvent, the monomer undertakes this function as well. After the reaction no further purification from the solvent is necessary, and a possible agglomeration due to the drying processes is avoided. The polymerization process is initialized by an initiator and UV-irradiation. The particles then act as crosslinkers, and any potential clustering and micro- or macrophase separation due to depletion effects arising from the growing polymer chains can be avoided. The resulting nanocomposites thus remain highly transparent.

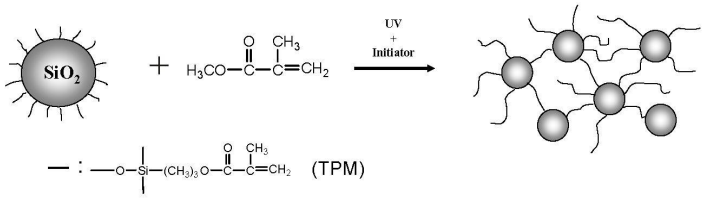

Fig. 6.2: Schematic representation of the in-situ polymerization process and the resulting chemically cross-linked particle-PMMA nanocomposite. Also shown is the surface modification of the Silica particles with TPM.

In this paper, we describe the use of dynamic light scattering (DLS) in order to monitor the Brownian motion of the TPM-silica particles during the polymerization process. DLS is a powerful tool to scan thermal fluctuations of dispersed probe particles that are related to the (local) viscoelastic properties of the system (24). In addition, we describe time-resolved SANS experiments that enable us to determine the evolution of the static structure and the possible formation of particle clusters during the in-situ polymerization. The combination of these two methods allows us to gain detailed information about the time evolution of the structure and dynamics of the medium on a microscopic level. It thus becomes possible to follow the poly-

merization process in a completely non-invasive and time-resolved way, and we obtain access to the kinetics and dynamics of the production process of nanocomposite materials and the resulting mechanical properties.

Experimental Section

Nanocomposite preparation.

3-(Trimethoxysilyl)-propylmethacrylate (TPM) grafted silica nanoparticles with an averaged diameter of 50 nm were prepared in methanol as described before (23) and transferred to methyl methacrylate by dialysis. The dispersions were polymerized in round 10 mm tubes. The system containing the colloidal silica dispersion and 0.2 wt$\%$ of the initiator (Irgacure 184, $Ciba\ SC$) was polymerized at ambient temperature over 2 h using an UV-lamp (UV SPOT 400T, Dr. Hönle, Germany) with a H2 UV-filter in order to reduce heating via Infrared absorption. The tube was rotated around its horizontal axis to guarantee complete mixing and equal UV-irradiation. The DLS experiments were preformed in-situ with the same sample holder. The samples for SANS experiments were prepared in standard Hellma quartz cells with a path length of 2 mm instead of round 10 mm tubes using the same polymerization protocol.

Nanocomposite characterization.

The time-resolved DLS experiments were carried out with an ALV DLS/SLS-5000 compact goniometer system with an ALV-5000 fast correlator and an argon-ion laser source (Coherent Innova 300) operating at a wavelength of 514.5 nm. For the time-resolved in-situ measurements with polymerizing samples we worked at a single scattering angle of θ = 60° and at a temperature of T = 20°C.

The measured intensity correlation function is defined as $g_2(\tau) = \frac{<I(t).I(t+\tau)>}{<I(t)>^2}$. The experimental correlation function is related to the normalized field autocorrelation function $g_1(\tau)$:

$$g_2(\tau) = 1 + A[g_1(\tau)]^2 \tag{6.1}$$

where A is a constant that depends on the experimental setup. The mean-square displacement (MSD) of the particles can be calculated from $g_1(\tau)$ (25):

$$g_1(\tau) = exp[-\frac{q^2}{6}[\Delta r^2(\tau)]] \tag{6.2}$$

The SANS measurements were performed at the SANS I instrument of the Swiss Neutron Source $SINQ$ at the Paul Scherer Institute and covered a range of scattering vectors q = $0.01-1.5$ nm^{-1}. Three settings were used, with combinations of sample-detector distance and neutron wavelength of 4.5 m and 0.8 nm, 12 m and 8 nm, and 20.27 m and 1.267 nm, respectively. The samples were measured in standard Hellma quartz cells with a path length of 2 mm. The SANS data was converted to an absolute scale with a 1 mm thick water sample as a secondary standard.

The polymerized nanocomposites were also investigated using transmission electron microscopy (TEM). A sample of a $\mathrm{Si O_2}$-PMMA composite film containing 13.3 wt$\%$ (6.2 Vol$\%$) of 50.8 nm diameter particles was cut with a diamond blade "Cryotim 45°" from Diatome, Switzerland (www.diatome.ch). The thickness was then reduced to a nominal value of 50 nm using an ultramicrotome Leica UCT equipped with an "ultra 35°" knife at a cutting speed of 1 mm.s^{-1}. The thus obtained thin section was then transferred onto a 200 mesh carbon grid and investigated using bright field TEM images made on a CM100 Philips microscope operated at 80 kV.

Results and Discussion

Time-resolved DLS experiments were performed on a dispersion of 3.3 wt$\%$ TPM-silica nanoparticles in a MMA monomer solvent during radical polymerization at a fixed scattering angle of 60°C and a temperature of 20°C. The corresponding intensity autocorrelation functions are presented in figure 6.3. Due to the very high scattering contrast of the $\mathrm{Si O_2}$ particles, the dominant contribution to the scattered light intensity arises from the nanoparticles, and the resulting correlation functions reflect the particle dynamics even after polymerization. For the initial suspension, i.e. before the polymerization is initiated at $t = 0$, the TPM-silica nanoparticles are able to undergo free Brownian motion characterized by a single exponential decay for $g_2(t) \sim exp(-t/\tau_c)$.
The characteristic decay time τ_c is then given by the product of the diffusion coefficient D_0 and the magnitude of the square of the scattering vector, i.e., by $\tau_c = (D_0 q^2)^{-1}$. The addition of the initiator and the irradiation with UV-light then triggers the radical polymerization of the monomer. Poly(methyl methacrylate)-polymer chains (PMMA) now start to grow freely in the monomer solution, but also covalently bonded to the particles surface. This is schematically illustrated in Figure 6.4 (a). With ongoing UV-irradiation the correlation functions thus shift towards longer decay times, indicating that the particle motion slows down gradually. This is due to the fact that the polymers attached to the particles increase the hydrodynamic radius of the colloids, and the growing polymer chain length in the matrix results in an increase of the background viscosity.

However, as the polymerization time increases even further, we observe a qualitative change in the shape of the correlation functions. The characteristic decay is no longer single exponen-

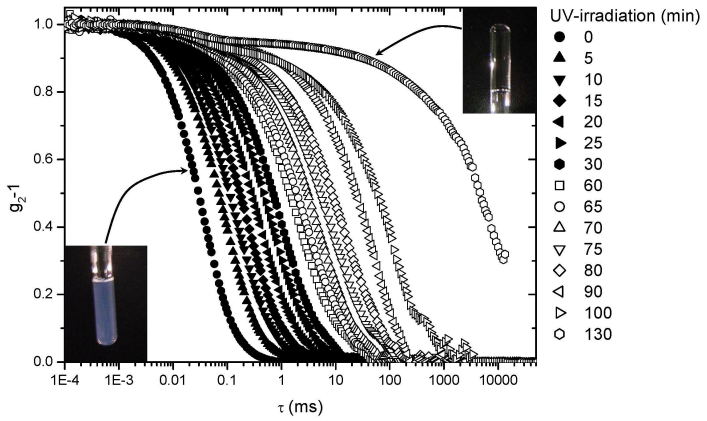

Fig. 6.3: Normalized intensity correlation function of 3.3 wt% TPM-silica nanoparticles measured at a scattering angle = 60° at different polymerization times. Solid symbols indicate Brownian motion of nanoparticles, whereas open symbols indicate subdiffusive motion. Also shown as insets are photographs of the initial and final samples.

tial, but appears to become stretched, and a plateau with a subsequent second decay develops. The height of this plateau increases with time due to the network formation and crosslinking of the particles. This dramatic change in the particle dynamics is accompanied by a tremendous increase of the viscosity of the sample and a subsequent transition to a solid-like state. However, the sample remains fully transparent at all times as demonstrated by the two photographs of the initial and final sample shown as insets in Figure 6.3, where the latter also demonstrates the solid-like character of the final nanocomposite.

For a quantitative understanding of the temporal evolution of the microscopic particle dynamics in the course of the polymerization process we analyzed the particle mean square displacement $< \Delta r^2(t) >$ as calculated from all correlation functions $g_2 - 1$ shown in Figure 6.3 using eqn. 6.2. The data shown in Figure 6.4 (b) and 6.4 (c) demonstrate that the nanoparticles initially, i.e. without UV-irradiation, show a behavior typical for Brownian diffusion over the whole accessible time range. This is characterized by a linear $< \Delta r^2(t) >$, where $< \Delta r^2(t) >$ is given by $< \Delta r^2(t) >= 6D_0t$. With increasing duration of the UV-irradiation the polymer chains grow and start to form a network. The initial short time behavior changes qualitatively from diffusive to subdiffusive motion and can be described by a power law $< \Delta r^2(t) > \propto t^p$, where the exponent p decreases from $p \approx 1$ to a value of $p \approx 0.7$ during the network formation. At the same time, the particle motion becomes constrained, and a plateau in the MSD develops.

The MSD obtained from samples at longer polymerization times, where the formation of a viscoelastic solid is induced, all show the same qualitative behavior. Their initial time depen-

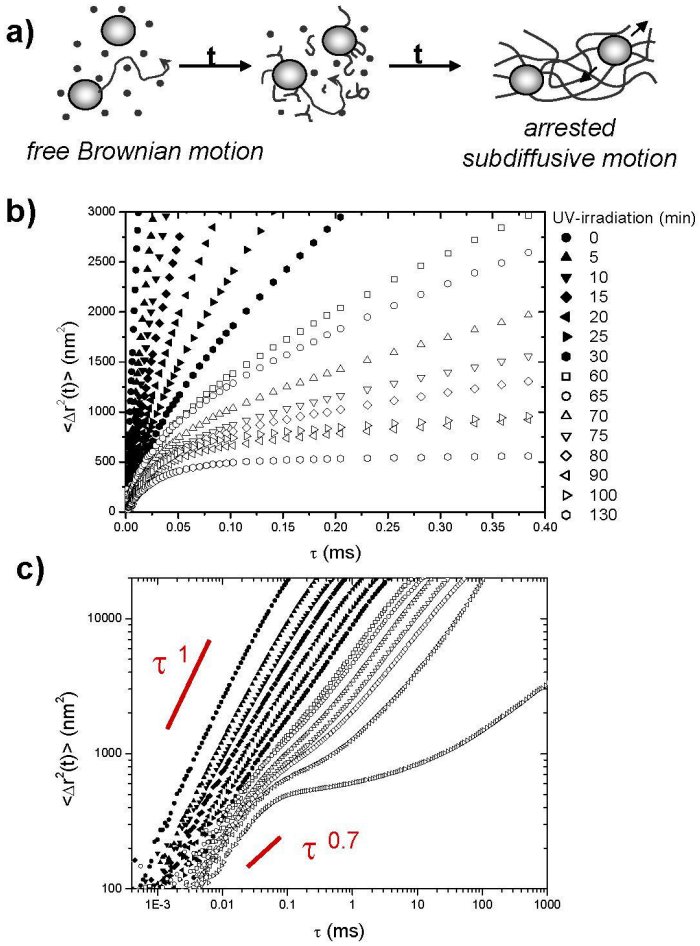

Fig. 6.4: (a) Schematic representation of the UV-initiated polymerization process, where the particles are initially freely suspended in the monomer solvent. Polymerization then results in growing polymers both in the melt as well as covalently attached to the particle surface. The functionalized particles act as crosslinkers, and a fully crosslinked polymer gel is formed. (b) Initial time dependence of the mean-square displacement of 3.3 wt% nanoparticles suspended in MMA monomer solvent at different polymerization times at 20°C. (c) Complete representation of the measured MSD over the full range of accessible time scales for all data shown in b).

dence is well described by a stretched exponential of the form:

$$\langle \Delta r^2(t) \rangle = \delta^2 [1 - e^{-(t/\tau_c)^p}] \tag{6.3}$$

indicating that for the silica colloids the particle excursion is restricted to a maximum MSD δ^2. Similar expressions for the short time dynamics of colloidal particles have for example been found for colloidal gels (24, 26-27) or tracer particles in crosslinked polymer gels (28) or actin networks (29). The good agreement between the experimental data and the description of constrained subdiffusive motion of the nanoparticles given by eqn. 6.3 is demonstrated in figure 6.5, where we plot a master curve obtained by normalizing t with τ_χ and $< \Delta r^2(t) >$ by δ^2.

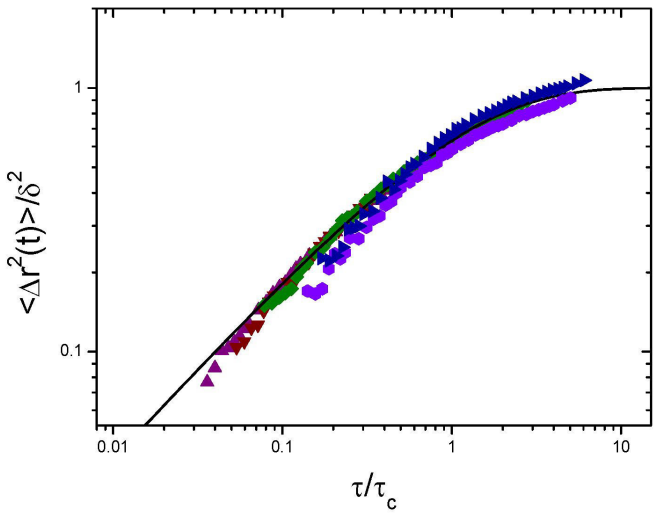

Fig. 6.5: Master curve $< \Delta r^2(t) > /\delta^2$ vs. t/τ_χ for the MSD obtained for samples at longer polymerization times, i.e., where viscoelastic solids have formed.

It has already been previously pointed out that the constrained motion of tracer particles in viscoelastic solids or liquids must reflect the elasticity of the background medium, and this has been used successfully in the application of the so-called microrheology concept to the characterization of complex fluids and solids (24). Therefore, we can use the MSD and in particular the crossover from Brownian to constrained subdiffusive motion in order to obtain additional information about the network formation in the nanocomposite. This is illustrated in figure 6.6, where we plot the temporal evolution of the exponent p and the characteristic relaxation time τ_c

from an analysis of the MSD shown in figure 6.4 (b).

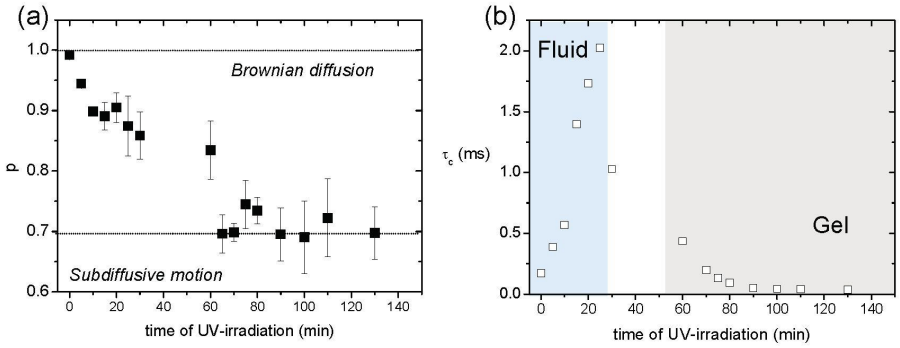

Fig. 6.6: Time evolution of parameter p (a) and τc (b) from an analysis of the MSD obtained for the 3.3 wt% TPM-silica nanoparticles in MMA during radical polymerization using eqn. 6.3

During the first 30 minutes, p decreases only slightly from a value of 1 indicating Brownian motion, but c increases dramatically by almost an order of magnitude as a result of the slowing down of the particle motion in the growing polymer solution. After this initial polymerization period, the situation changes completely. The relaxation time now starts to decrease strongly, while p continues to decrease to a final value of 0.7. This reflects the fact that the nature of the nanoparticle dynamics now qualitatively changes. The particles no longer undergo Brownian motion in a viscous polymer fluid, but become chemically crosslinked to a polymer network. Therefore τ_c no longer reflects the diffusion coefficient of the polymer-coated particles, but rather the local viscoelastic properties of the polymer network. As pointed out previously, both τ_c and δ^2 are linked to the elastic modulus of the resulting gel. A simple argument would be that the work necessary for a particle to move over a distance δ is equal to the thermal energy kT of the particle. This allows us to at least estimate the elastic shear modulus G via

$$G = \frac{kT}{6\pi a \delta^2} \tag{6.4}$$

where G has the meaning of a local shear modulus and a is the particle radius (29, 31). If we use the data summarized in figure 6.4 (b) for the longest polymerization time of 130 min, we obtain a value for $\delta^2 \approx 5$ nm^2, which yields a shear modulus of $G \approx 2$ kPa. This is quite reasonable in view of the fact that at this point the system is far from being fully polymerized yet. The fact that we have not yet reached the end of the polymerization process is also visible from the shape of the MSD when plotting the full range of accessible time scales (figure 6.4 (c)).

Here we see that the MSD shows an apparent plateau, but that a second very slow relaxation process is still present, indicating that the system is rather viscoelastic and not completely solid or glass-like.

The DLS experiments have allowed us to achieve a non-invasive characterization of the particle dynamics during the formation of a silica-PMMA nanocomposite via in-situ polymerization. However, they do not provide information about the degree of agglomeration that often occurs in nanocomposites. Therefore we have conducted time-resolved SANS-measurement during the in-situ polymerization of a nanocomposite with a high particle loading of 13.3 wt% TPM-silica nanoparticles (figure 6.7 (a)). The initial colloidal suspensions show a q-dependence typical for hard sphere colloids at moderate volume fractions. This becomes apparent from a determination of the effective structure factor $S_{eff}(q)$ of the initial suspension,

$$S_{eff}(q) = \frac{I(q)}{c.P(q)} \tag{6.5}$$

where $I(q)$ and c are the scattered intensity and concentration of the suspension and $P(q)$ the independently determined particle form factor, respectively, shown in the inset of figure 6.7 (a). $S_{eff}(q)$ exhibits a weak correlation peak at a value of $q \approx 0.12$ nm^{-1} and a decrease to an asymptotic value at $q = 0$ of $S_(0) \approx 0.4$. Applying a simple hard sphere model using the approximation of Carnahan and Starling (32) for $S_(0)$, this would yield an effective hard sphere volume fraction of $\phi_{hs} \approx 0.11$, not too far from the "dry" volume fraction of $\phi \approx 0.08$ that we would estimate based on the weight concentration of 13.3 wt% for the given densities of the SiO_2 nanoparticles and the MMA solvent, and taking into account the TPM coating of the colloids. Moreover, using a value of $q^* \approx 0.12$ nm^{-1} and a hard sphere model, the estimated value of $2aq^* = 6.1$ for the peak position in S(q) would also be consistent with a hard sphere volume fraction of approximately $\phi \approx 0.1$ (33).

The initiation of the polymerization process has no influence on the measured q-dependence of the scattered intensity in the time-resolved SANS experiments (figure 6.7 (a)). This clearly indicates the absence of any measurable agglomeration process, which we have already concluded based on the fact that the nanocomposite remains transparent at all times. The fact that the fictionalization of the silica nanoparticles combined with an in-situ polymerization results in the formation of a stable nanocomposite with well-dispersed colloids is further supported from subsequent TEM measurements shown in figure 6.7 (b). This figure presents pictures with two different magnifications that clearly demonstrate the absence of inhomogeneities at all length scales.

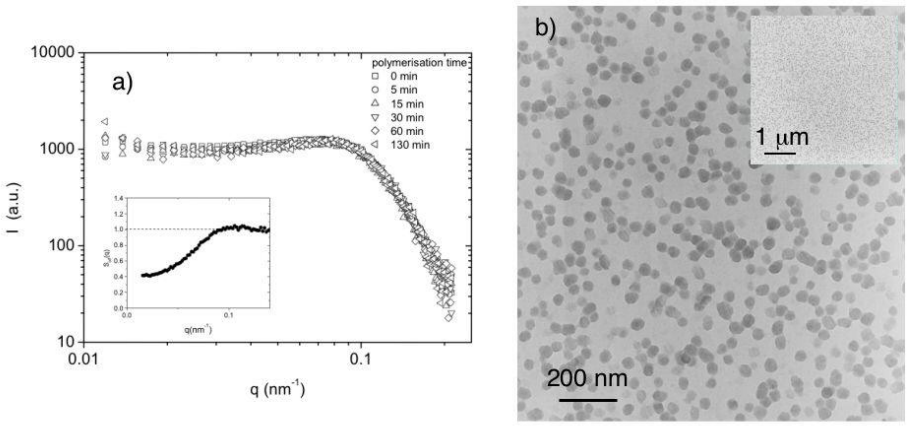

Fig. 6.7: (a) Dependence of the q-dependence of the scattering intensity I(q) from time-resolved SANS experiments with TPM-functionalized SiO_2 nanoparticles at a concentration of 13 wt% dispersed in MMA at different polymerization times. Also shown as an in-set is the effective structure factor $S_{eff}(q)$ of the initial particle dispersion. (b) TEM micrographs of the final nanocomposite at two different magnifications.

Conclusions

The combination of functionalistic monodisperse silica nanoparticles with TPM and an in-situ polymerization of the monomer solvent results in the formation of completely stable and highly transparent nanocomposite materials up to particle concentrations of 13 wt%.
Time-resolved dynamic light scattering and small-angle neutron scattering experiments have allowed us to follow the in-situ polymerization of the nanocomposites in a completely non-invasive way. They provide a quantitative description of the particle dynamics during the polymerization process and the subsequent formation of a chemically crosslinked polymer gel, and they have allowed us to assess the lack of agglomeration and absence of inhomogeneities. Moreover, DLS has yielded additional information on the development of the mechanical properties of the system as the polymers and network form. In principle, the microrheology approach will allow us to go beyond a simple determination of the modulus and arrive at a full time-resolved description of the frequency dependent storage and loss moduli (24). While this is beyond the scope of this first study, it is worth pointing out the potential of these combined experiments in the investigation of the kinetics of polymerization and structure formation due to the completely non-invasive character of the scattering experiments and the fact that we achieve structural characterization and temporal resolution on the required length and time scales.

Acknowledgements

The authors are grateful to Beat Keller for encouraging and stimulating discussions. We thank Nicolas Sary, UniFr, who performed the TEM experiments, and Helmut Gnägi, Diatome.ch, who kindly prepared the thin sections for the TEM samples. Financial support was provided by the Commission Suisse pour la Technologie et l'Innovation (CTI), Project no 6056.2.

References

(1) Okada, A. ; Usuki, A. Mater. Sci. Engng. C. 1995, 3, 109.
(2) Gilman, J.W. Appl. Clay Sci. 1999, 15, 31.
(3) Gilman, J.W. ; Jackson, C.L. ; Morgan, A.B. ; Harris, Jr.R. ; Manias, E. ; Giannelis, E.P. ; Wuthenow, M. ; Hilton, D. ; Phillips, S.H. Chem. Mater. 2000, 12, 1866.
(4) Porter, D. ; Metcalfe, E. ; Thomas, M.J.K. Fire. Mater. 2000, 24, 45.
(5) Zanetti, M. ; Lomakin, S. ; Camino, G. Macromol. Mater. Engng. 2000, 279, 1.
(6) Armes, S.P. Polym. News 1995, 20, 233.
(7) Godovski, D.Y. Adv. Polym. Sci. 1995, 119, 79.
(8) Wirnsberger, G. ; Scott, B.J. ; Chmelka, B.F. ; Stucky, G.D. Adv. Mater. 2000, 12, 1450.
(9) Hanprasopwattana, A. ; Srinivasan, S. ; Sault, A.G. ; Datye, A.K. Langmuir 1996, 12, 3173.
(10) Huang, X. ; Brittain, W.J. Macromol. 2001, 34, 3255.
(11) Messersmith, P.B. ; Stupp, S.I. J. Mater. Res. 1992, 7, 2559.

(12) Judeinstein, P. ; Sanchez, C. J. Mater. Chem. 1996, 6, 511.
(13) Schubert, U. ; Hüsing, N. Synthesis of inorganic materials, Weinheim, Wiley-VCH, 2000.
(14) Bates, F. S. ; Fredrickson, G. H. Annu. Rev. Phys. Chem. 1990, 41, 525.
(15) Chujo, Y. ; Saegusa, T. Adv. Polym. Sci. 1992, 100, 11.
(16) Hergeth, W.D. ; Peller, M. ; Hauptmann, P. Acta. Polym. 1986, 37, 468.
(17) Kickelbick, G. ; Schubert, U. Monatsh. Chem. 2001, 132, 13.
(18) Schubert, U. Chem. Mater. 2001, 13, 3487.
(19) Pope, E.J.A. ; Asami, M. ; Mackenzie, J.D. J. Mater. Chem. 1989, 4, 1018.
(20) Lin, H. ; Day, D.E. ; Stoffer, J.O. Polym. Eng. Sci. 1992, 32, 344.
(21) Nishiyama, N. ; Horie, K. ; Schick, R. ; Ishida, H. Polym. Commun. 1990, 31, 380.
(22) Morikawa, A. ; Yamaguchi, H. ; Kakimoto, M. ; Imai, Y. Chem. Mater. 1994, 6, 913.
(23) Dietsch, H. ; Keller, B. submitted 2006.
(24) Scheffold, F. ; and Schurtenberger, P. Soft Materials 2003, 1, 139.
(25) Berne, B. ; and Pecora, R. Dynamic Light Scattering: With Applications to Chemistry, Biology and Physics (Wiley, New York, 1976).
(26) Krall, A. and Weitz, D. A., Phys. Rev. Lett. 1998, 80, 778.
(27) Romer, S., Scheffold, F., and Schurtenberger, P., Phys. Rev. Lett. 2000, 85, 4980.
(28) Schurtenberger, P. ; Bissig, H. ; Rojas, L. ; Vavrin, R. ; Stradner, A. ; Romer, S. ; Scheffold, F. ; and Trappe V. ; "Mesoscale Phenomena in Fluid Systems", ACS Symposium Series 861, F. Case and P. Alexandridis, Eds., pp 143-160 (2003).
(29) Narita, T. ; Knaebel, A. ; Munch, J.-P. ; Zrinyi, M. ; and Candau, S.J. ; Macromol. Symp. 2004, 207, 17.
(30) Ambelard, F. ; Maggs, A. C. ; Yurke, B. ; Pargellis, A. N. ; and Leibler, S. ; Phys. Rev. Lett. 1996, 77, 4470.
(31) Schnurr, B. ; Gittes, F. ; MacKintosh, F.C. ; and Schmidt, C.F. ; Macromolecules, 1997, 30, 7781.
(32) Carnahan, N.F. ; and Starling, K.E., J. Chem. Phys. 1969, 51, 635.
(33) Gazzillo, D. ; and Giacometti, A., J. Chem. Phys. 2000, 113, 9837.

6.2 Influence of the filler size and volume on the glass temperature and friction coefficient in a silica particles-PMMA hybrid composite

Tribological and Differential Scanning Calorimetry measurements on composites gave us the possibility to publish in *Journal of Tribology* [34].

Hervé Dietsch and Beat A. Keller*
Empa, Science and Technology, Ueberlandstrasse 129, CH-8600 Dübendorf, Switzerland
Submitted to the *Journal of Tribology* on August, 8^{th} 2006
*beat.keller@empa.ch

Abstract

Friction coefficient and glass temperature evolution of silica nanoparticles-PMMA hybrid systems for different particle diameters and concentrations was studied. Glass temperature and friction coefficient are expressed as function of particle volume fraction in the polymer matrix relative to the specific surface area of the particles times the volume specific surface area of the total amount of particles. This new ratio parameter revealed an alternative way to characterize the change in mechanical properties in hybrid materials. It allows a comparison between different particle sizes and volume fractions and shows a similarity in the evolution of the glass temperature and friction coefficient.

General Introduction

Due to their unique optical, (1, 2, 3) physical (4) and mechanical properties (5, 6), hybrid materials, which consist of a polymeric matrix and embedded quasi-monodispersively distributed inorganic oxide particles are becoming increasingly popular in industrial applications. Modification of polymer properties by incorporation of inorganic material is not only dependent on size and volume of the fillers (4), but also on dispersion (5, 7) and distribution (6) of the particles in the polymer matrix. In the case of clays (8), the aspect ratio becomes equally important. A linear dependence of the concentration of fillers on the glass temperature was found in the past (4) for PMMA hybrid material modified by SiO_2 particles with diameters less than 100 nm. The main advantage of small particles ($<$ 50 nm) is the possibility to maintain transparency amorphous polymers (PMMA, PS, etc.) when monodispersively distributed. We confirmed this behavior in our laboratory for several systems. However, the effect was only observed for nanoparticles, which diameters are less than 100 nm. In most of the relevant characterization studies in which thermal or mechanical properties were investigated, discussed the influence of the filler volume fraction without comparing different particle sizes. Berriot *et al* studied hybrid systems using silica particles with an average of 50 nm in diameter, with strong emphasis on characterization of the particles-polymer interfaces using ^{1}H-NMR technique (9). Results from rheological measurements indicated a shift of the glass transition close to the particle surface (10) and also a gradient of this parameter suggesting non-linear (11) (transformation conditions) in viscoelastic behavior.

In the past, it has always been proposed that mechanical or thermal properties are a result of the very large specific surface area of nanoparticles used as filler material in hybrid systems. However, only a limited understanding about the influence of particle size in tailored composite material is available, and therefore, we compared the behavior of nanoparticles (diameter $<$ 100 nm) to submicrometer size particles with a higher volume fraction but having the same specific surface. A dependency on the volume fraction as well as from the specific surface area ($=$ size of the particles) was expected. The ratio between volume fraction and specific surface area or size of the particles is a parameter, which was rarely used in the literature for comparisons, but can be used as valuable way to characterize the influence of geometric properties of particles on later mechanical performance of organic/inorganic hybrid materials.

Experiments

The tribological and DSC measurements are performed on poly(methyl methacrylate) macromolecules, cross-linked with 3-(trimethoxysilyl) propyl methacrylate (TPM) surface modified silica particles.
The steps of the preparation have already been published in the past (12, 13) and were adapted to our experimental conditions. Silica particles with diameters of 50.8 nm, 106.7 nm and 515 nm, respectively, were synthesized using a modified Stöber process (14). By this synthetic approach were able to produce monodisperse SiO_2 particles. Diameters were measured with transmission electron microscopy (TEM) (50.8 nm and 106.7 nm), scanning electron microscopy (SEM) (106.7 nm and 515 nm) and dynamic light scattering (DLS) (50.8 nm and 106.7 nm) instruments. Size distributions were then calculated by evaluating 300 individual particle diameters using standard laboratory software. Averaged particle diameters of 50.8 nm $\pm$ 0.7; 106.7 nm $\pm$ 1.5 and 515 nm $\pm$ 15 were obtained by this procedure.

After synthesis, particles were transferred into a water free Stöber milieu (ethanol + ammonia) or alternatively directly grafted in the Stöber solution with TPM silane agent. The SiO_2@TPM modified silica particles were then transferred into methanol through dialysis tubing, dried and further dispersed in methyl methacrylate (MMA) monomer. The concentration of particle was adjusted by dilution with freshly distilled MMA monomer. An amount of 0.2 wt$\%$ of photoinitiator (Irgacure 184, purchased by $Ciba\ SC$, Basel) was added to the mixture and the polymerization step performed using an UV irradiation apparatus.

Tribological tests were performed using a high frequency reciprocating rig apparatus (HFR2, PCS Instruments), with measurements done employing a calibrated steel sphere with a diameter of 6 mm and a weight of 600 g ($\sim$ 6 N). A frequency of 20 Hz over a displacement range of 1 mm was chosen as operating conditions. All samples were evaluated measured twice over a period of 20 minutes. Glass temperature of the composites was determined using differential scanning calorimetry (DSC) in temperature sweep test mode from 65°C up to 160°C. In order to estimate the amount of particles dispersed in the polymer with thermogravimetry measurements, all samples were annealed at 900°C for total decomposition of the organic part. The density of the particles was experimentally evaluated before embedding them into the PMMA matrix and found to be approximately 2.10^3 kg.m^{-3}.

Results

Figure 6.8 is representing the evolution of the friction and glass temperature in function of the ratio fillers volume fraction on its surface area.The specific surface (Ss) is calculated using the equation of the volume of sphere and specific surface of sphere (Ss=6V_{Np}/D_{Np}).

Table 6.1 shows friction (F) and glass temperature (Tg) values obtained for three different particle diameters (D_{Np}) and different volume fractions of particles (V_{Np}).

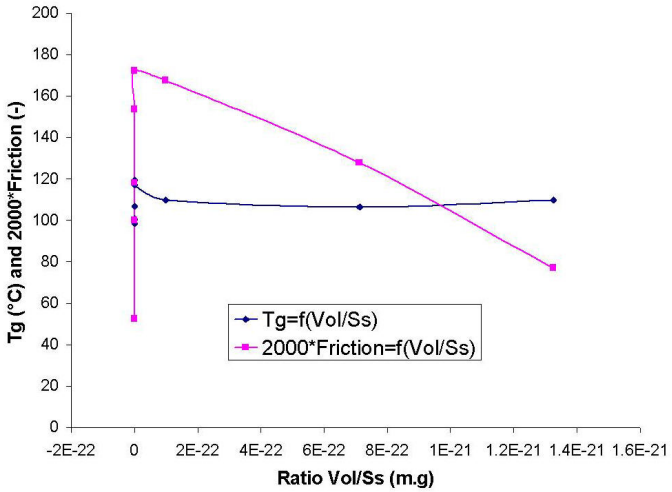

Fig. 6.8: Glass temperature and friction coefficient in function of particle volume fraction in the polymer matrix relative to the specific surface area of the particles times the volume specific surface area of the total amount of particles

Sample	D_{Np} (m)	V_{Np} (%)	Ss ($m^2.g^{-1}$)	F (-)	$Tg(°C)$
REF	0	0	0	0.026	100.6
$515nm_{X/4}$	5.15E-07	0.8	5.83E+00	0.084	109.8
$106.7nm_{X/4}$	1.07E-07	0.6	2.81E+01	0.077	119.2
$515nm_{X/2}$	5.15E-07	5.8	5.83E+00	0.064	106.4
$106.7nm_X$	1.07E-07	2.1	2.81E+01	0.086	117.1
$515nm_X$	5.15E-07	10.8	5.83E+00	0.038	109.7
$50.8nm_{X/4}$	5.08E-08	1.85	5.91E+01	0.050	98.4
$50.8nm_X$	5.08E-08	5.15	5.91E+01	0.059	106.8

Tab. 6.1: Friction and glass temperature in function of particle diameter, volume and specific surface.

Our results confirm that the influence of the specific surface and volume can be expressed as function of thermal property by measurement of the glass temperature (Tg) via DSC and tribology based mechanical property measurements. A number of changes in physical properties was observed tailoring the surface area and the volume fraction of particle filler in a polymer matrix. Our data show that the influence on friction and glass temperature is always increasing and decreasing in parallel.

Moving and orientating polymer chains using the tribological tool show that the viscoelastic properties of the PMMA without fillers induce a small loss of energy as a low friction was

measured for the sample REF. This effect is represented in the drawing 6.9.

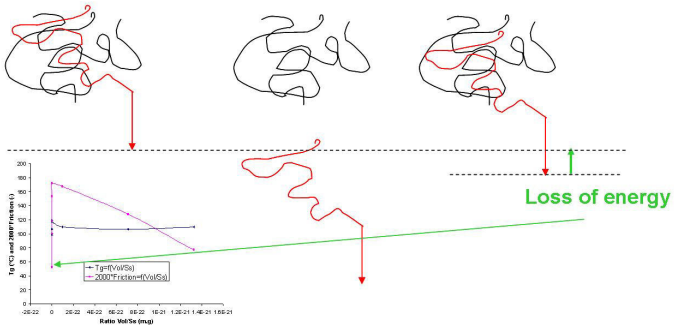

Fig. 6.9: Drawing representing the energy loss during the friction measurement for a non charged PMMA sample

An addition an increase of the glass temperature and friction coefficient is observed immediately after embedding particles in the PMMA matrix. "Low charged composite systems" is defined in our case for polymer matrix containing a small volume fraction and high specific surface of particles (equivalent to a small ratio volume fraction on specific surface). This can be synthesized using small amount of nanoparticles.
Particles bind polymer chains together without increasing a lot the elasticity of the resulting hybrid material.
This means that applying the same force on a low charged composite, deformation stays important and is not be recovered due to high relaxation times. We have a viscous behavior and the friction increase dramatically (representation on 6.10).

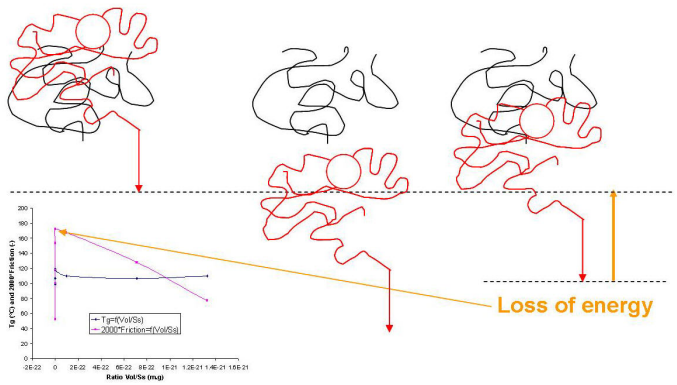

Fig. 6.10: Drawing representing the energy loss during the friction measurement for a low charged PMMA sample

A crosslinked hybrid system using a large amount of particles and/or increasing the particle size in order to decrease the particle specific surface and so increase the ratio volume fraction on specific surface is then measured. We called this system "highly charged composite systems". As the highly charged composites are very elastic, application of the force do not have a big influence on the composite orientation and the loss of energy induced is smaller because deformation is low (see figure 6.11).
As a result the friction is decreasing in comparison with low charged matrix.

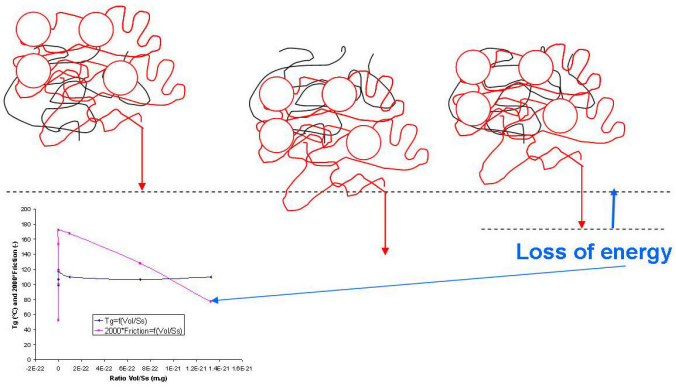

Fig. 6.11: Drawing representing the energy loss during the friction measurement for a highly charged PMMA sample

In conclusion, preliminary work suggests that the total ratio of particles volume to surface area is a relevant parameter to characterize a composite material with respect to mechanical properties. However, the data can presently not confirm this finding on a mathematical basis. Therefore, our future research focuses on computer simulation in combination with additional rheological measurements.
The change from microparticle to nanoparticle filler material induces a disturbing of local internal structure instead of intrinsic structure of the composite material, which can be also the reason why a quantitative formulation of the relationship is quite difficult.

Acknowledgments

Support from the Commission for Technology and Innovation (CTI) through its Technology-Oriented Program TOP NANO 21 is kindly acknowledged by the authors. The author would like to thank Beatrice Fischer for the ATG and DSC measurements and Andreas Mühlebach for the free sample of Irgacure 184.

References

(1) Jethmalani, J., M. ; Ford, W., T., Chem. Mater., 1996, 8, 2138-2146.
(2) Jethmalani, J., M. ; Sunkara, H., B. ; Ford, W., T. ; Willoughby, S., L. ; Ackerson, B., J., Langmuir, 1997, 13, 2633-2639.
(3) Jethmalani, J., M. ; Ford, W., T. ; Beaucage, G., Langmuir, 1997, 13, 3338-3344.
(4) Mauger M. ; Dubault A. ; Halary, J., L., Polym. Intern., 2004, 53, 378-385.
(5) Pu, Z., C. ; Mark, J., M; Jethmalani, J., M. ; Ford, W., T., Polym. Bul., 1996, 37, 545-551.
(6) Bokobza, L; Garnaud, G. ; Marks, J., E. ; Jethmalani, J., M. ; Seabolt E., E. ; Ford, W., T., Chem. Mater., 2002, 14,162-167.
(7) Berriot, J. ; Montes, H. ; Martin, F. ; Mauger, M. ; Pyckhout-Hintzen, W. ; Meier, G. ; Frielinghaus, H., Polym., 2003, 44, 4909-4919.
(8) Sheng, N. ; Boyce M., C. ; Parks D., M. ; Rutledge G., C. ; Abes J., I. ; Cohen R., E., Polym., 2004, 45, 487-506.
(9) Berriot, J. ; Martin, F. ; Montes, H. ; Monnerie, L. ; Sotta, P., Polymer, 2003, 44,1437-1447.
(10) Berriot, J. ; Montes, H. ; Lequeux, F. ; Long, D. ; Sotta, P., Macromolecules, 2002, 35, 9756-9762.
(11) Montes, H. ; Lequeux, F. ; Berriot, J., Macromol., 2003, 36, 8107-8118.
(12) Sunkara, H., B. ; Jethmalani, J., M. ; Ford, W., T., Chem. Mater., 1994, 6, 362-364.
(13) Dietsch, H. ; Lootens, D. ; Keller, B., A., in preparation.
(14) Stöber, W. ; Fink, A., J. Colloid and Interface Sci. 1968, 26, 62-69.

6.3 Synthesis and rheological study of tailored monodisperse and monodistributed SiO_2-PMMA composites

Hervé Dietsch[1], Didier Lootens[2] and Beat A. Keller[1]*
[1] Empa, Science and Technology, Ueberlandstrasse 129, CH-8600 Dübendorf, Switzerland
[2] Sika Technology A. G., Tüffenwies 16, CH-8048 Zürich, Switzerland
Submitted
*beat.keller@empa.ch

Abstract

A synthesis of a monodispersed and monodistributed SiO_2-PMMA with monodisperse SiO_2 silica particles in a range of 30 nm to 1 μm using sol-gel procedure is described.
This synthetic procedure allows staying transparent for an amorphous polymer using particles with diameters lower than 50nm.
Pictures of the particles embedded in a PMMA matrix are shown using TEM, SEM and optical microscopy, depending on the particle size used.
A rheological shear study of the composites obtained tailoring particle size and concentration

is presented in a second part and reveal an enhancement in the relaxation time of the hybrid studied.

Introduction

The fabrication of composites aimed at producing materials with properties, that cannot be achieved with either of the constituents acting alone.
Mechanical (1), thermal (2-5), electrical (6), magnetic (7), photochemical (8), or catalytic (9) can be achieved using fillers in organic materials.
A loss in the original properties such as optical transparency is also possible, but can be avoided with a good dispersion and distribution of small fillers (D $<$ 50nm) (10).
Particulate materials have been used for enhancement polymers. While initially added to safe product cost of polymers, it became soon apparent that properties were considerably changed after adding fillers.
Nanotechnology creates a new challenge for materials science because device properties now depend on size, shape and aspect ratio as much as they depend on the traditional parameters of structure and chemical composition.
Nanocomposites generally have at least one order of magnitude more interfacial area than traditional composites.
As compared with other factors, interaction forces play a major role in nanocomposite design.
Two basic types of interactions are most prominent: particle-particle and particle-matrix interactions. Neighboring particles are interacting via van der Waals (attractive) and electrostatic (repulsive) forces. However, with decreasing particle size, a decrease in interparticle repulsion becomes much more important than decreasing attractive forces.
Size of the fillers control at a determined volume fraction used, the influence of interface area between particles and polymer and the volume of fillers.
We recently proved the importance of this ratio volume of particles of specific surface of the particles used (11).
Therefore controlling attraction between particles becomes the leading design parameter below a certain particle diameter in composite technology. Most of the technical process steps necessary for device fabrication are associated with shear forces in nozzles or heating above the glass temperature of the polymer in extruders.
Well stabilized and appropriately designed surfaces are a prerequisite under such conditions to avoid agglomeration or phase separation processes which cause a breakdown of functionality, particularly in cases where high volume fractions of particles are necessary to achieve sufficient property enhancement. The fabrication of particle-polymer composite materials has been described in detail in the literature (12, 13).
In recent years such inorganic-organic hybrid systems have found increasing interest in various technical applications, principally because the combination between particles with nanometer size dimension and a polymer matrix displays novel and enhanced mechanical, electrical, rheological and optical properties. The degree of influence can be tuned by altering composition,

dimension and internal structure of the involved materials. Industrial applications are found in areas like paints, hard coats, drug delivery, composite materials and catalytic processes (13-16). While changes and improvement in physical properties like hardness and refractive index can also be achieved via thin film technology, it is the polymer-like processability of the hybrid material that makes it suitable for applications on uneven or corrugated surfaces, and in structure design. If they exist, nanoparticle assemblies usually exist in a weakly or strongly bound structure.
They are commonly referred as agglomerates and aggregates.
While the former are built of an assembly of the latter and exhibit a rather open structure which can be disrupted by a considerable amount of energy (e.g. via ultrasonic treatment), the latter are called single particles and form the basic building blocks of the particle ensemble. In order to achieve maximum property enhancement, the resulting nanocomposite should be agglomerate free, contain an optimized volume fraction of nanofillers and maintain the chemical and physical characteristics of its components. Among the various procedures for the preparation of polymer nanocomposites (17), the following approaches are most important:

- direct incorporation of nanoparticles in a polymer solution or melt (18, 19)
- in situ synthesis of nanoparticles in a polymer matrix (20), usually by decomposition of an metalorganic precursor
- polymerization of monomers in presence of monodispersively embedded nanoscale materials (21)
- simultaneous formation of polymer and nanoparticle via sol-gel (22, 23)
- micelle promoted (24) processes

Silica nanoparticles promise to be particularly useful candidates for particle-polymer composite materials because of their availability, low price and chemical inertness.
Stöber (25) synthesized silica nanoparticles by hydrolysis of tetraethylorthosilane ($TEOS$) in presence of ammonia. The alkoxide is injected in a mix of alcohol, water and ammonia under continuous stirring. Particles with sizes ranging from 30 nm to 1 μm are fabricated by this method (26).
The particle size can be controlled with the reaction temperature (27) as well as the water, ammonia and $TEOS$ concentration. Alternatively silica nanoparticles can be fabricated with a narrow size distribution by synthesizing the product in an aqueous colloidal suspension in which uncontrolled spontaneous nucleation is suppressed by vigorous stirring the reaction mixture. Aerosol flame synthesis is also widely used to obtain nanoparticle powder with narrow size distribution and a wide range of different diameters. However, experiments using nanoparticles in powder form suggests a strong tendency for agglomeration. Although the experiment shows that powder particles larger than 400 nm in diameter can be dispersed again in water or

alcohol solution without further surface modification using ultrasonic assisted dispersion technique. Nanometer particles at a powder state (dried or flame produced) form large, irreversibly stacked agglomerates due to large interparticle forces (van der Waals, London) and very large specific surface. Property enhancement is not possible using these materials for production of nanocomposites. Surfactant molecules have been used to stabilize nanoparticle suspensions. The mechanism of this effect is either of ionic nature (electrostatic repulsion) or based on non-ionic molecules (steric stabilization) (28).
In this publication we report on a new synthetic route to fabricate an inorganic-organic hybrid material based on silica nanoparticles with well controllable sizes and a narrow size distribution. The composite is produced by a successive incorporation of the nanoparticles into a various types of polymer matrices. In addition excellent particle dispersion in the polymer matrix and efficient interlinking with the polymer backbone is obtained. This leads to particle-polymer composite materials with modified properties, that are not altered by post-synthesis processes.

Experimental Section

Materials and Instruments

Tetraethylorthosilane (also called tetraethoxyorthosilane $TEOS$), ammonia solution (25 $\%$ in water), ethanol (99.9 $\%$) and methanol (analytic grade) were purchased by VWR Merck. 3-(Trimethoxysilyl) propyl methacrylate (TPM, 98 $\%$) and methyl-methacrylate (MMA) were obtained from $Sigma$-$Aldrich$. All chemicals were used as received.

Particle size and distribution values were measured using dynamic light scattering (DLS) information obtained from a Malvern Zetasizer 4 instrument (29) based on photon correlation spectroscopy (PCS) data taken at 90° scattering angle.
In order to verify the findings from light scattering experiments, the values were compared with imaging data from scanning electron microscopy SEM (SEM, JEOL JSM 6300F instrument) and transmission electron microscopy (TEM, Philips CM30 instrument) measurements.

TEM samples were prepared by slow evaporation of a ten times diluted aqueous suspension of the particles on a standard carbon mesh. Particle size values from electron microscopy images were obtained by averaging over 300 individually estimated particle diameters using the image analyzing tool from Image Access software (Stemmer Imaging GmbH, Puchheim).
Optical microscopy was performed with a Axioscop, Zeiss microscope.

Particle Synthesis and Characterization

For a typical 100 nm diameter particle synthesis, 50 g ammonia solution (25 wt$\%$ in water) were mixed with 500 g ethanol and stirred in a water bath regulated at 40°C.
When the temperature is reached, 135 g $TEOS$ are injected in this solution.
Growth of the particles was made with successive injection of a quantity of under continuous stirring (30, 31). The final particle size and distribution was investigated using light scattering,

TEM, SEM and optical microscopy.

Transmission electron microscopy (TEM) images were performed to measure silica particles diameter using standard data reduction tools.
Statistically relevant values for the particle diameters were obtained by manually measuring 300 individually selected particles. For particles with a diameter < 200 nm, DLS and TEM were chosen rather than SEM. DLS size distribution of silica particles with an average diameter of 31.3 ± 0.9 nm.
Larger particles were analyzed using SEM and/or optical microscopy.

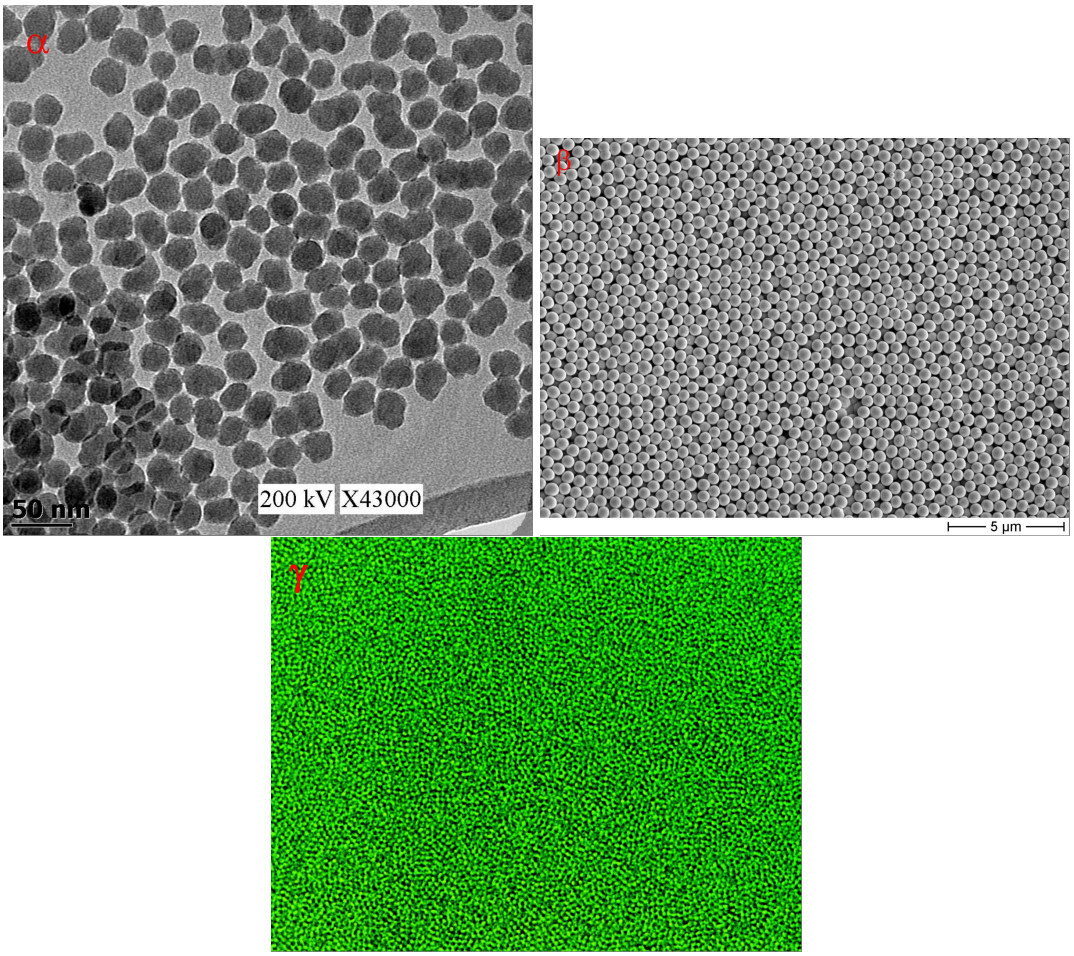

Fig. 6.12: TEM, SEM and OM pictures of particles with respective diameter: α) 31.5 nm, β) 515 nm and γ) 1μm

DLS and TEM are generally used for particle diameters between 30 nm and 200 nm ; SEM is used for particle diameters larger than 200 nm and optical microscopy for particle diameters

larger than 400 nm.
Figure 6.12 shows TEM, SEM and optical microscopy images of silica particles with an average diameter of 31 nm, 515 nm and 1000 nm.
The uniform distribution in a large particle selection is evident from the picture and proves the suitability of our synthetic approach for materials development.
A very concise description of the fabrication of a monodisperse hybrid material by transfer of commercially available modified nanoparticles was published by Ford (32).
Here, we report on the modification of nanoparticles directly in the Stöber solution in which they were initially synthesized. However, in order to establish optimized reaction condition for this reaction, we first calculated the number of theoretically available reaction sites on the surface of the nanoparticles.
Averaged diameter values obtained from size data evaluation allowed to calculate the specific surface of the particles in the solution (in $m^2.g^{-1}$).
Knowing that there are about 6-8 OH group per nm^2 on silica a single particle (33), we calculated the number of hydroxyl groups on the surface. Surface modification was then performed using 3-(trimethoxysilyl) propyl methacrylate (TPM) silane coupling agent to get a methyl methacrylate (MMA) reactive group on the particle surface. This reaction is based on the hydrolysis of the silane agent by adsorbed surface water (34).
However, the overall modification should be carried-out under water-free conditions to avoid aggregation of the silica particles.
The presence of a catalytic amount of base promotes the reaction. The progress and final number of modified surface reaction sites was monitored by $^{29}\mathrm{Si}$ NMR spectrometry (35) and/or carbon analysis.
Figure 6.13 is a non scaled representation of surface modified $\mathrm{Si\,O_2}$ silica particles In order to verify if there was a large difference in particle diameter after surface modification, we analyzed transmission electron microscopy (TEM) images again of the surface modified silica particles.

No relevant changes in the particles size distribution was observed, which means that the surface modification did not induce aggregation between silica particles using TPM alkoxisilane.

In-Situ Polymerization

Ford's method (32) was adapted for the transfer of particles in the methylmethacrylate (MMA) monomer.
For this purpose, TPM-modified silica particles were transferred into a methanol solution using dialysis tubing.
The dialysis bath was changed and freshly prepared five times in an interval of 24 hours. This process had the advantage to remove residual TPM, which did not react on the particle surface and at the same time allowed to transfer the particles into MMA by evaporation the solvent under vacuum conditions.
The suspensions stayed stable over days.

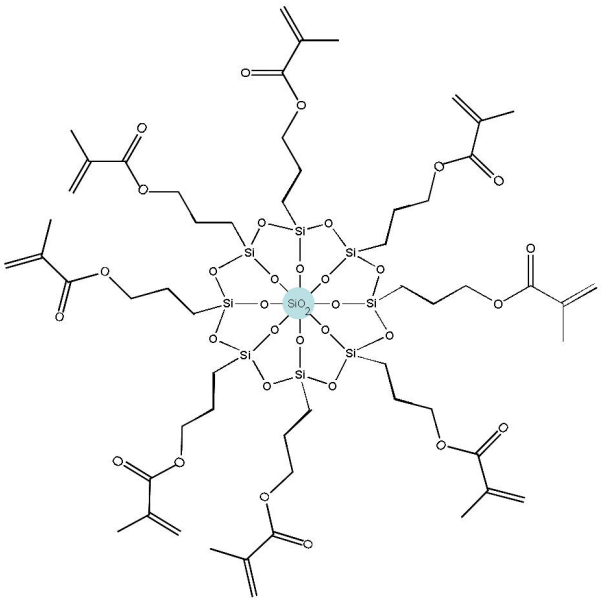

Fig. 6.13: Schematic representation of TPM surface modified silica particles

Frequently the formation of agglomerates with particle diameters larger than 400 nm in diameter was observed. The precipitate sedimentated slowly but could be easily re-dispersed by ultrasonic treatment for 5 minutes. For particles with smaller diameters, no agglomeration was observed at all.
In-situ polymerization in containers with various shapes was than performed under an UV light using Irgacure as photoinitiator in 0.2 wt% concentration.
In order to avoid excessive particle abrasion, the synthesis products (copolymer silica-co-PMMA) were embedded into an epoxy-amine matrix, trailed and polished it with diamond powder.

Figure 6.15 shows a SEM image of monodisperse 515 nm large silica particle copolymerized with MMA in a concentration of 13.3 wt% (6.5 vol%).
SEM imaging and thermogravimetry (TGA) were used to monitor the particle content of the material.

The hybrid system obtained by this reaction (containing up to 20 wt% particle load) appeared perfectly transparent with particles having a diameter less than 50 nm. This proves that the particle distribution in our system remained monodisperse. However, the refractive index did not match perfectly. In the framework of ongoing research, we performed an in-situ polymerization study directly in the measuring cell of a 3D-DLS instrument (36).
Preliminary data from these experiments further supported the finding that no agglomeration process is occurring during the polymerization.

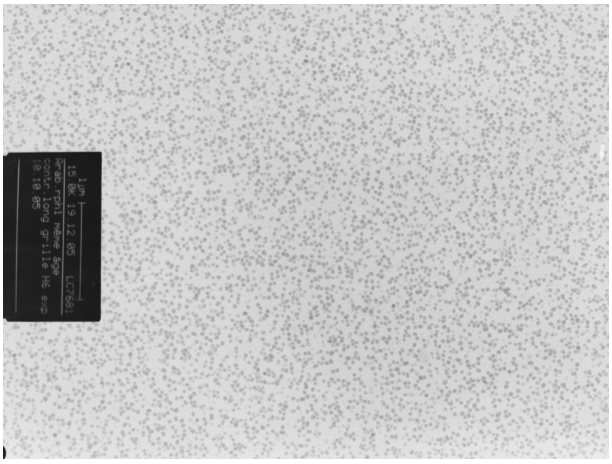

Fig. 6.14: TEM picture of 13.7 wt% SiO_2 particles with a diameter of 50.8nm embedded in PMMA

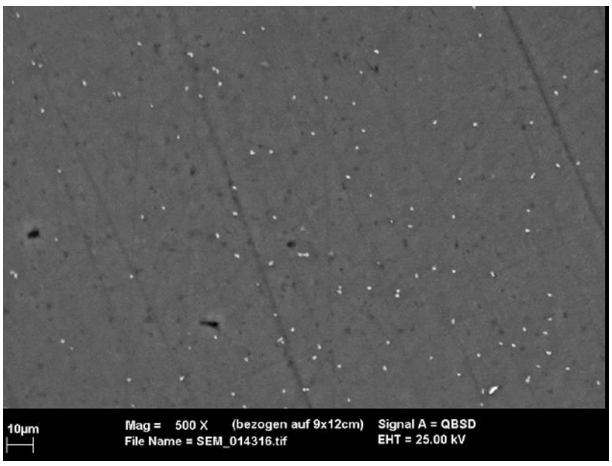

Fig. 6.15: Backscattered SEM picture of 13.3 wt% SiO_2 particles with a diameter of 515 nm embedded in PMMA

Mechanical properties

Dynamic rheological characterizations were performed using a constant strain rheometer from Rheometrics (ARES). The instrument was set up with a shear torsion geometry.
The measurements were conducted in oscillatory mode in a frequency range of 0.01100 rad.s^{-1} at diverse fixed temperatures: 80°C, 100°C, 120°C, 140°C, 160°C, 180°C and 200°C.
The experiments were done in the linear viscoelastic domain using autostress adjustment.
Sample were polymerized using a home-made form with typical dimension in mm: 50 X 12 X 2. All concentrations were controlled by diluting a highly charged monomer with TPM modified silica particles.
Concentrations were checked after polymerization using ATG burning the sample at 900°C.
The time-temperature superposition principle was used to construct master curves with a reference temperature fixed at 80°C.
Payne effect (37) (also called Fletcher-Gent effect (38)), characterized by a decreasing in the storage modulus G' of a hybrid system (typically carbon black in rubber) increasing the amplitude of mechanical oscillations frequency could also be observed for our TPM modified $\mathrm{Si\,O_2}$-PMMA hybrid composite for the 50,8nm diameter large particles, no relevancy between different particle size, specific surface, volume fraction or even ratio volume fraction on specific surface (11) could be established.
Table 6.2 presents the maximum elastic modulus G'$_{max}$ obtained for the highest frequency at the lowest temperature (at 80°C, PMMA is at a glassy state).

Sample	D_{Np} (m)	V_{Np} (%)	Ss (m^2.g^{-1})	$G'_{max}(Pa)$
REF_C	0	0	0	6.01E+08
$50.8nm_{X/4}$	5.08E-08	1.85	5.91E+01	1.16E+09
$50.8nm_X$	5.08E-08	5.15	5.91E+01	7.29E+08
$106.7nm_{X/4}$	1.07E-07	0.6	2.81E+01	5.49E+08
$106.7nm_X$	1.07E-07	2.1	2.81E+01	5.59E+08
$515nm_{X/4}$	5.15E-07	0.8	5.83E+00	7.21E+08
$515nm_{X/2}$	5.15E-07	5.8	5.83E+00	9.75E+08

Tab. 6.2: Maximum elastic modulus G'$_{max}$ (Pa) in function of particle diameter, volume and specific surface.

Relaxation time showing transition between the glass phase and the elastic plateau was slightly increasing by increasing the volume fraction of particles, no relaxation in function of the specific area could be established.

After the construction of the master curves (elastic and loss moduli G' and G" in function of time (t)) with a reference temperature at 80°C, we could determined the displacement factors a_T necessary to build the curves, the logarithm of a_T is defined by the logarithm of the ratio

viscosity at a temperature T and viscosity at a reference temperature T_{Ref}.
Activation energy (E_a, equation 6.6_3) of our composites was determined using Arrhenius relation, plotting $\frac{-1}{log(a_T)}$ in function of $\frac{-1}{T-T_{Ref}}$.

$$\begin{aligned} log(a_T) &= \frac{log(\eta)}{log(\eta_{T_{Ref}})} \\ &= -\frac{C_1(T-T_{Ref})}{C_2+T-T_{Ref}} \\ &= log(K) - \frac{Ea}{RT} \end{aligned} \tag{6.6}$$

Using WLF relation (39) also presented in the equation 6.6, we determined the factor C_1 and C_2 for each composite. These factors are changing in function of the fillers concentration and size, which means that it is not applicable for composites systems.
Results are resumed in table 6.3. With an average E_a of 172 $\pm$ 20 kJ.mol^{-1}, we conclude that the activation energy is independent on the particle sizes and concentrations.

Sample	D_{Np} (m)	V_{Np} (%)	Ss (m^2.g^{-1})	E_a (kJ.mol^{-1})
REF_C	0	0	0	161.2
$515nm_{X/4}$	5.15E-07	0.8	5.83E+00	177.2
$106.7nm_{X/4}$	1.07E-07	0.6	2.81E+01	192.2
$515nm_{X/2}$	5.15E-07	5.8	5.83E+00	165.2
$106.7nm_X$	1.07E-07	2.1	2.81E+01	189.1
$50.8nm_{X/4}$	5.08E-08	1.85	5.91E+01	185.2
$50.8nm_X$	5.08E-08	5.15	5.91E+01	134.5

Tab. 6.3: Activation energy for the different hybrid systems

As an example, we present in figure 6.16 the master curve of the sample 50.8nm$_X$ containing 10.3wt% (5.15 vol%) of particles with a diameter of 50.8nm.

Acknowledgment

Financial support that led to this synthesis has been provided by CTI/KTI (Commission for Technical Innovation) on the contract Nr. 6056.2 TNS (Top Nano 21). Irgacure 184 was kindly

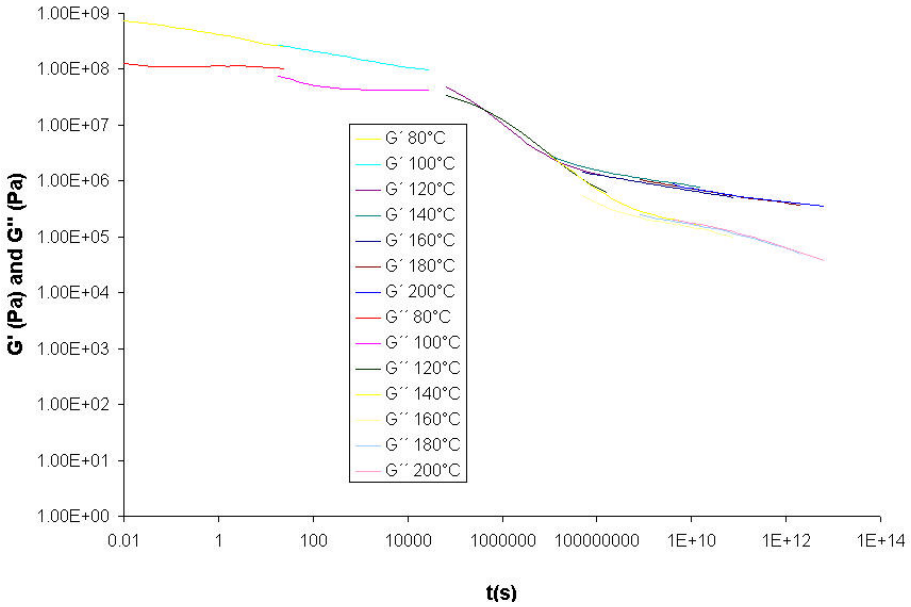

Fig. 6.16: Master curve of the PMMA containing 13.3wt% of 50.8nm diameter large silica nanoparticles

provided by Dr. A. Mühlebach *Ciba SC*, Basel.
Prof. Hans Josef Hug is thanked for his support.

Conclusion

A way to produce composite tailoring particle size, polydispersity and concentration without further agglomeration has been presented.
The in-situ surface modification in the sol-gel synthetic milieu led to compatible particle surface with the monomer medium, an in-situ polymerization avoided any pollution because no solvent was used.
This ”never-dry” technique allowed to fabricate nanocomposites polymerized in the required shape.
Characterization using rheological tool was presented using torsion geometry, Payne effect was observed showing a decrease in the G’ moduli by increasing the particle concentration, but no relevancy comparing different particle sizes could be established.

References

(1) Okada, A. ; Usuki, A., Mater. Sci. Engng. (1995), C3, 109.
(2) Gilman, J. W. Appl. Clay Sci. 15 (1999), 31.
(3) Gilman, J. W. ; Jackson, C. L. ; Morgan, A. B. ; Harris, Jr. R. ; Manias, E. ; Giannelis, E. P.

; Wuthenow, M. ; Hilton, D. ; Phillips, S. H., Chem. Mater. 12 (2000), 1866.
(4) Porter, D. ; Metcalfe, E. ; Thomas, M. J. K., Fire. Mater. 24 (2000), 45.
(5) Zanetti, M. ; Lomakin, S. ; Camino, G., Macromol. Mater. Engng. 279 (2000), 1.
(6) Armes, S. P., Polym. News 20 (1995), 233.
(7) Godovski, D. Y., Adv. Polym. Sci. 119 (1995), 79.
(8) Wirnsberger, G. ; Scott, B. J. ; Chmelka, B. F. ; Stucky, G. D., Adv. Mater. 12 (2000), 1450.
(9) Hanprasopwattana, A. ; Srinivasan, S. ; Sault, A. G. ; Datye, A. K., Langmuir 12 (1996), 3173.
(10) Huang, X. ; Brittain, W. J., Macromol. 34 (2001), 3255.
(11) Dietsch, H. ; Keller, B. A., J. Chem. Mater., submitted.
(12) Sanchez, C. ; Ribot, F., New J. Chem. 18 (1994), 1007.
(13) Schubert, U. ; Huesing, N. ; Lorenz, A., Chem. Mater. 7 (1995), 2010.
(14) Lu, Y. ; Mclellan, J. ; Xia, Y., Langmuir 20 (2004), 3464.
(15) Kamata, K. ; Lu, Y. ; Xia, Y., J. Am. Chem. Soc. 125 (2003), 2384.
(16) Graf, C. ; Vossen, D. ; Imhof, A. Langmuir 19 (2003), 6693.
(17) Tsai, H. L. ; Schindler, J. L. ; Kannewurf, C. R. ; Kanatzidis, M. G., Chem. Mater. 9 (1997), 875.
(18) Shang, S. W. ; Williams, J. W. ; Soderholm, K. J. M., J. Mater. Sci. 27 (1992), 4949.
(19) Dirix, Y. ; Bastiaansen, C. ; Caseri, W. ; Smith, P., J. Mater. Sci. 34 (1999), 3859.
(20) Nakao, Y., J. Colloid Interface Sci. 171 (1995), 386.
(21) Zilg, C. ; Thomann, R. ; Muehlhaupt, R. ; Finter, J., Advanced Materials 11 (1999), 49.
(22) Novak, B. M., Advanced Materials 5 (1993), 422.
(23) Ruys, A. J., Mat. Sci. Eng. A265 (1999), 202.
(24) Palkovits, R. ; Althues, H. ; Rumplecker, A. ; Tesche, B. ; Dreier, A. ; Holle, U. ; Fink, G. ; Cheng, C. H. ; Shanz, D. F. ; Kaskel, S., Langmuir 21 (2005), 604.
(25) Stöber, W. ; Fink, A., J. Colloid and Interface Science 26 (1968), 62.
(26) Pellizetti, E., Fine Particles and Technology, vol. 12 Kluwer Academic Publishers, Dordrecht, (1996).
(27) Tan, C. G. ; Bowen, B. D. ; Epstein, N., J. Colloid Interface Sci. 118 (1987), 290.
(28) Bonini, C. ; Heux, L. ; Cavaillé, J. Y., Proc. MAS Meeting, Polymer Nanocomposites, April 2- 5, San Francisco, (2002).
(29) The Malvern Zetasizer 4 instrument is located at Swiss Federal Institute of Aquatic Science and Technology, Eawag, Dübendorf, Switzerland.
(30) Bogush, G. ; Zukoski, C., J. Colloid Interface Sci. 142 (1991), 1.
(31) Bogush, G. ; Tracy, M. ; Zukoski, C., J. Non-Cryst. Solids 104 (1988), 95.
(32) a) Sunkara, H. B. ; Jethmalani, J. M. ; Ford, W. T., Chem. Mater. 6 (1994), 362.
b) Joseph, R. ; Zhang, S. ; Ford, W. T., Macromolecules 29 (1996), 1305.
c) Jethmalani, J. M. ; Ford, W. T., Chem. Mater. 8 (1996), 2138.
d) Pu, Z. ; Mark, J. E. ; Jethmalani, J. M. ; Ford, W. T., Polym. Bull. 37 (1996), 545.
e) Jethmalani, J. M. ; Sunkara, H. B. ; Ford, W. T., Langmuir 13 (1997), 2633.
f) Jethmalani, J. M. ; Ford, W. T., Langmuir. 13 (1997), 3338.
(33) personal communication $Degussa$ AG, Aerosil and Silanes Division, contact

beata-maria.lortz@degussa.com
(34) Philipse, A. P. ; Vrij, A., J. Colloid Interface Sci. 128 (1989), 121.
(35) Bauer, F., Macromol. Chem. Phys. 1, 2, 3, 4 (2003).
(36) Saric, M. ; Dietsch, H. ; Schurtenberger, P., Coll. Surf. A 291 (2006), 110.
(37) Payne, A. R., J. Appl. Polym. Sc. 9 (1965), 3245.
(38) Fletcher, W. P. ; Gent A. N., Br. J. Appl. Phys. 8 (1957), 194.
(39) Williams, M. L. ; Landel, R. F. ; Ferry, J. D., J. Am. Chem. Soc. 77 (1955), 3701.

7

Conclusion

This work, started on August 2003 first aimed at the investigation of the local structure and interactions in a polymer-particle hybrid system. The establishment of a tailored system required a longer work than expected and force us to synthesize each step of the reaction to get our tailored hybrid system.

Concerning the synthesis of fluorescent particles, we were successful incorporating organic dyes (FITC and RITC) and home-made CdSe quantum dots on the surface of silica nanoparticles. However, photobleaching problems using organic dyes and surface interaction of silica particles modified with quantum dots on their surface led to hybrid systems with particle agglomerates. Nevertheless, the detection of agglomerates could be performed using a fluorescent microscope.

The approach to obtain our tailored hybrid nanocomposite was to synthesize every product, we needed, in order to avoid any undesirable reaction due to a stabilizer not mentioned by the providers and allow getting tailored and well defined nanocomposites. All chemicals were bought by $Sigma\text{-}Aldrich$ and all solutions at a technical grade by VWR international.

Silica particles were all synthesized using sol-gel process always at 40°C, which allows getting monodisperse $\mathrm{SiO_2}$ silica particles in a range between 30 nm and 1 μm. Concentration of water in our milieu was increased to accelerate the kinetics of our reaction, allowing $TEOS$ to condensate very fast on the existing particles to get particles larger than 400 nm [1].
Particle were monodispersed ($\pm$ 5%) and did not build chemical aggregation thank to a constant stirring at 700 rpm during their synthesis.

After modification in the Stöber milieu in the case of little particles (30 nm $<$ D $<$ 400 nm) or in ethanol (400 nm $<$ D $<$ 1000 nm) for larger ones, a transfer in methylmethacrylate (MMA) monomer was performed and photopolymerization was done under UV using 0.2 wt% of Irgacure 184 ($Ciba\ SC$).

Fluorescent marked silica particles with high photostability could also be established using self made quantum dots [36] instead of commercial ones (very expensive) or organic dyes (low photobleaching resistance).
Only a synthetic approach has been presented, low resistance of the quantum dots at high tem-

peratures ($> 100°C$) did not allow the extrusion of our composite product without destroying the emission quantum dots.

As we could tailor the particle sizes and the concentrations of particles embedded in PMMA, characterization during the photopolymerization using SANS and 3 DLS scattering methods [109], after the polymerization process using DSC and tribological apparatus [34] and rheological tools [35] was performed.

In the near future, we can imagine to go on this work by comparing polydisperse systems and monodisperse systems, studying different degree of silane agents on surface (we always saturated the particle surfaces), changing the particle anisotropy and particles properties, which leads to a lot of work on the synthetic and characterization point of views. This future work will hopefully be fulfilled within the new research center for nanomaterials "FriMat".

Outlook:

The next pages have the goal to introduce major ideas, we would like to follow in the next time within the new Fribourg Center for Nanomaterials "FriMat":

"FriMat" will give the opportunity to study the interaction between colloidal particles and polymer matrices, their capability to form ordered structures (for example in an artificial opal form) and their influence on the resulting composite materials formed.
Functionalized nanoparticles will be synthesized at a labor range and agglomeration of the incorporated colloids will be avoided using the knowledge developed in this thesis.
Adaptive polymer colloid nanomaterials with tailored colloid and polymer will allow new optical and mechanical properties.

One of the major goals is to get anisotropic α-Fe_2O_3 magnetic particles-PMMA hybrid systems, controlling the orientation and the monodispersity of the particles and avoid any aggregation in the matrix. A schematic synthetic route is presented in figure 7.1.

These ferromagnetic particles should be then orientated before polymerization and the resulting hybrids will be studied using scattering methods and typical mechanical and rheological tools.
The way used to condensate silica on existing colloids using micelles in water will be adapted to avoid any other nucleation of round shaped silica particle in the synthetic milieu.
Our approach is to tailor the micelle shapes and sizes to fit on the hydrophobic tailored colloids, micelles geometry control in aqueous milieu has already been described in the literature [128].

Another big synthetic effort has to be done to get tailored polymer chain sizes using new techniques like atomic transfer radical polymerization or anionic polymerization.

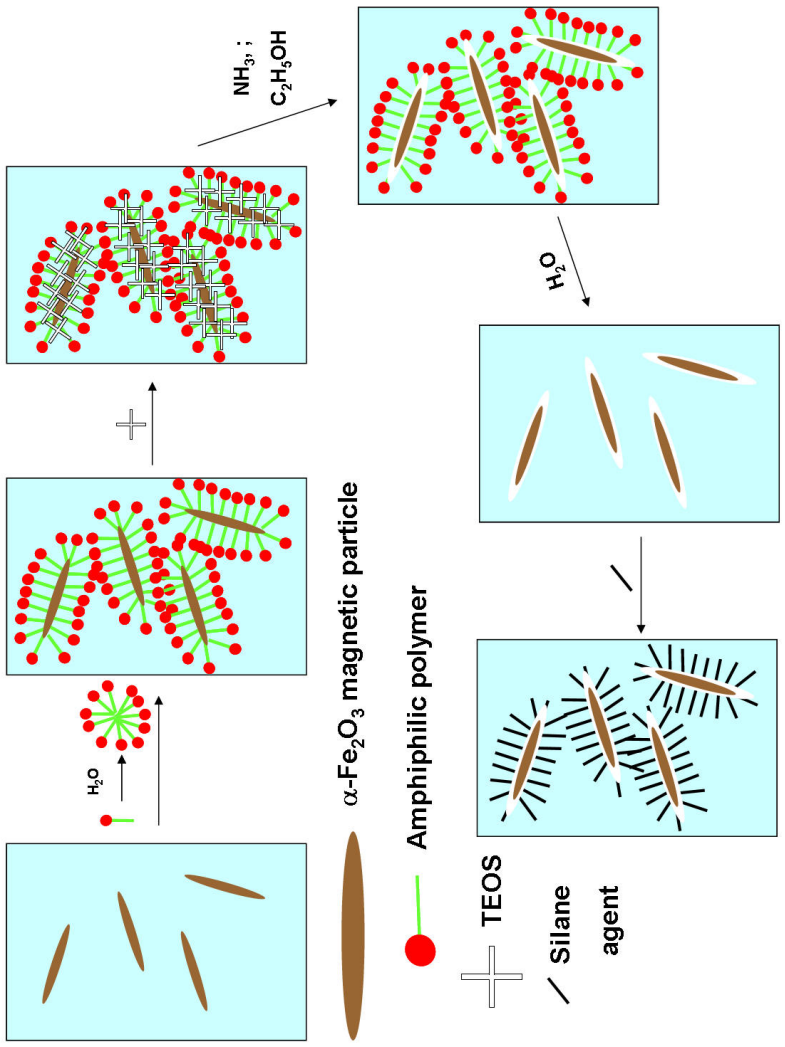

Fig. 7.1: Reaction scheme explaining how to get tailored nanosized magnetic composites

Combining knowledge of chemists with physics will lead to very interesting and useful research works.

List of Figures

3.1 Freeze drying technique: particles in water were frozen with liquid N_2 before evaporating water under vacuum . . . 10
3.2 Difference between agglomerate (α) and aggregate (β): example using TEM pictures of $Ludox\ TMA$, $Sigma\text{-}Aldrich$ . . . 10
3.3 TEM picture of $Aerosil\ OX\ 50$, $Degussa$ . . . 11
3.4 Reaction scheme of Stöber reaction . . . 12
3.5 time t1 . . . 14
3.6 time t2 . . . 14
3.7 time t3 . . . 14
3.8 time t4 . . . 14
3.9 time t5 . . . 15
3.10 SEM pictures of multi nucleations . . . 16
3.11 TEM picture of SiO_2 particles with a diameter about 100 nm . . . 17
3.12 Particle diameter size as a function of the number of day of work . . . 18
3.13 Monodisperse silica particle size distribution and TEM picture . . . 19
3.14 TEM, SEM and OM pictures of particles with respective diameter: α) 31.5 nm, β) 515 nm and γ) 1μm . . . 22
3.15 α) silanol, β) silanediol and γ) silanetriol . . . 23
3.16 General formula of silane agents, with R=OCH_3, as OC_2H_5, as Cl, as CH_3 and respectively R'=SH, as NH_2, as CH_3, as NCO, etc... . . . 23
3.17 3-aminopropyltriethoxysilane, APTES ($ABCR$, Germany) . . . 24
3.18 3-methacryloxy-propyl-trimethoxysilane, TPM ($Sigma\text{-}Aldrich$) . . . 24
3.19 General scheme for particle surface modification with silane agent . . . 25
3.20 Solid-state ^{29}Si NMR spectroscopy of silica nanoparticles modified by silane coupling agents . . . 28

4.1 Representation of optical absorption and emission . . . 31
4.2 Fluroesceinisothiocyanate (FITC) . . . 32
4.3 Reaction scheme of SiO_2@FITC . . . 32
4.4 Optical fluorescent microscope picture of a SiO_2@FITC particle . . . 33
4.5 Tetramethylrhodamineisothiocyanate (TRITC) . . . 33
4.6 α) $Cd(C_2H_5O_2)_2$; $2H_2O$ in $TOPO$ β) Se powder in TOP γ) $TOPO$ . . . 35
4.7 $CdSe$ quantum dots with diameter between 1 and 8 nm. . . . 36
4.8 $CdSe$ quantum dots (size between ca. 1.5 nm and 9 nm from left to right). The bare particles have been irradiated with UV light to show the photoemission . . . 43
4.9 Absorption and emission spectra of the $CdSe$ quantum dots. . . . 44
4.10 Emission spectra of the $CdSe$ and $CdSe(ZnS)$ quantum dots. . . . 45

4.11 Emission of SiO_2@CdSe(ZnS) core-shell fluorescent particles 45
4.12 Different ways of quantum dot incorporation into silica particles. 48
4.13 Reaction scheme of SiO_2@CdSe(ZnS) core-shell synthesis 49
4.14 SiO_2@CdSe(ZnS)@SiO_2 sandwich particles synthesis 50

5.1 Azobisisobutyronitrile (AIBN) 54
5.2 Benzoyl peroxide (BPO) 54
5.3 Reflux set-up 55
5.4 Decomposition of AIBN initiator 56
5.5 Decomposition of BPO initiator 56
5.6 Scheme of the incorporation of SiO_2@FITC in PAA 63
5.7 Raman spectra of α) PAA in DMF and β) FNP labeled PAA in DMF 64
5.8 FT-IR spectra of α) PAA in DMF and β) FNP labeled PAA in DMF 64
5.9 Alignment of FITC modified SiO_2 clusters incorporated in PAA : 10 wt% of $Aerosil\ OX50$ incorporated 65
5.10 Schematic representation of FITC modified SiO_2 clusters incorporated in PAA 66
5.11 The "never dry approach": principe of the synthesis 68

6.1 Selected examples of stable polymer-colloid nanocomposites, where the particles (a) are present in a stable dispersion, (b) form an interpenetrating network, (c) are chemically linked to the polymer matrix, or (d) act as crosslinkers. . . . 71
6.2 Schematic representation of the in-situ polymerization process and the resulting chemically cross-linked particle-PMMA nanocomposite. Also shown is the surface modification of the Silica particles with TPM. 72
6.3 Normalized intensity correlation function of 3.3 wt% TPM-silica nanoparticles measured at a scattering angle = 60° at different polymerization times. Solid symbols indicate Brownian motion of nanoparticles, whereas open symbols indicate subdiffusive motion. Also shown as insets are photographs of the initial and final samples. 75
6.4 (a) Schematic representation of the UV-initiated polymerization process, where the particles are initially freely suspended in the monomer solvent. Polymerization then results in growing polymers both in the melt as well as covalently attached to the particle surface. The functionalized particles act as crosslinkers, and a fully crosslinked polymer gel is formed. (b) Initial time dependence of the mean-square displacement of 3.3 wt% nanoparticles suspended in MMA monomer solvent at different polymerization times at 20°C. (c) Complete representation of the measured MSD over the full range of accessible time scales for all data shown in b). 76
6.5 Master curve $< \Delta r^2(t) > /\delta^2$ vs. t/τ_χ for the MSD obtained for samples at longer polymerization times, i.e., where viscoelastic solids have formed. 77

6.6 Time evolution of parameter p (a) and τc (b) from an analysis of the MSD obtained for the 3.3 wt% TPM-silica nanoparticles in MMA during radical polymerization using eqn. 6.3 78
6.7 (a) Dependence of the q-dependence of the scattering intensity I(q) from time-resolved SANS experiments with TPM-functionalized SiO_2 nanoparticles at a concentration of 13 wt% dispersed in MMA at different polymerization times. Also shown as an in-set is the effective structure factor $S_{eff}(q)$ of the initial particle dispersion. (b) TEM micrographs of the final nanocomposite at two different magnifications. 80
6.8 Glass temperature and friction coefficient in function of particle volume fraction in the polymer matrix relative to the specific surface area of the particles times the volume specific surface area of the total amount of particles 85
6.9 Drawing representing the energy loss during the friction measurement for a non charged PMMA sample 86
6.10 Drawing representing the energy loss during the friction measurement for a low charged PMMA sample 86
6.11 Drawing representing the energy loss during the friction measurement for a highly charged PMMA sample 87
6.12 TEM, SEM and OM pictures of particles with respective diameter: α) 31.5 nm, β) 515 nm and γ) 1μm 92
6.13 Schematic representation of TPM surface modified silica particles 94
6.14 TEM picture of 13.7 wt% SiO_2 particles with a diameter of 50.8nm embedded in PMMA 95
6.15 Backscattered SEM picture of 13.3 wt% SiO_2 particles with a diameter of 515 nm embedded in PMMA 95
6.16 Master curve of the PMMA containing 13.3wt% of 50.8nm diameter large silica nanoparticles 98

7.1 Reaction scheme explaining how to get tailored nanosized magnetic composites 103

List of Tables

3.1 Average Diameter of the nanoparticles obtained by TEM pictures 26
3.2 Specific surface of nanoparticles 27
3.3 BET measurements of nanoparticles specific surface 27
3.4 Comparison between different kinds of $\mathrm{SiO_2}$ silica particles 30

4.1 Comparison of the different synthetic routes towards CdSe quantum dots . . . 37

6.1 Friction and glass temperature in function of particle diameter, volume and specific surface. 85
6.2 Maximum elastic modulus G'$_{max}$ (Pa) in function of particle diameter, volume and specific surface. 96
6.3 Activation energy for the different hybrid systems 97

Bibliography

[1] *Effect, we remark, through our experience* (beat.keller@empa.ch).

[2] *The Malvern Zetasizer 4 instrument is located at Swiss Federal Institute of Aquatic Science and Technology, Eawag, Dübendorf, Switzerland.*

[3] *Method used from Degussa AG, Aerosil and Silanes Division* (beata-maria.lortz@degussa.com).

[4] ALIVISATOS, A. P.
Semiconductor clusters, nanocrystals, and quantum dots.
Science 271, 5251 (1996), 462–466.

[5] AMBLARD, F., MAGGS, A. C., YURKE, B., AND PARGELLIS, A. N.
Subdiffusion and anomalous local viscoelasticity in actin networks.
Physical Review Letters 77 (1996), 4470–4473.

[6] ARMES, S. P.
Electrically conducting polymer colloids.
Polymer News 20 (1995), 233–237.

[7] BARRELET, C. J., WU, Y., BELL, D. C., AND LIEBER, C. M.
Synthesis of CdS and ZnS nanowires using single source molecuzlar precursors.
Journal of the American Chemical Society 125, 38 (2003), 11498–11499.

[8] BATES, F. S., AND FREDRICKSON, G. H.
Block copolymer thermodynamics - theory and experiment.
Annual Review of Physical Chemistry 41 (1990), 525–557.

[9] BERNE, B. J., AND PECORA, R.
Dynamic Light Scattering: With Applications to Chemistry, Biology, and Physics.
Wiley, New York, 1976.

[10] BERRIOT, J., MARTIN, F., MONTES, H., MONNERIE, L., AND SOTTA, P.
Reinforcement of model filled elastomers: characterization of the crosslinking density at the filler-elastomer interface by 1H NMR measurements.
Polymer 44, 5 (2003), 1437–1447.

[11] BERRIOT, J., MONTES, H., LEQUEUX, F., LONG, D., AND SOTTA, P.
Evidence for the shift of the glass transition near the particles in silica-filled elastomers.
Macromolecules 35, 26 (2002), 9756–9762.

[12] BERRIOT, J., MONTES, H., LEQUEUX, F., LONG, D., AND SOTTA, P.
Gradient of glass transition temperature in filled elastomers.
Europhysics letters 64, 1 (2003), 50–56.

[13] BERRIOT, J., MONTES, H., MARTIN, F., MAUGER, M., PYCKHOUT-HINTZEN, W., MEIER, G., AND FRIELINGHAUS, H.
Reinforcement of model filled elastomers: synthesis and characterization of the dispersion state by sans measurements.
Polymer 44, 17 (2003), 4909–4919.

[14] BIRD, R. B., ARMSTRONG, R. C., AND HASSAGER, O.
Dynamics of Polymeric Liquids, vol. 1.
Wiley, New York, 1987.

[15] BLAADEREN, A. V., AND VRIJ, A.
Synthesis and characterisation of colloidal dispersions of fluorescent, monodisperse silica spheres.
Langmuir 8, 12 (1992), 2921–2931.

[16] BOGUSH, G., TRACY, M., AND ZUKOSKI, C.
Preparation of monodisperse silica particles : control of size and mass fraction.
Journal of Non-Crystalline Solids 104 (1988), 95–106.

[17] BOGUSH, G., AND ZUKOSKI, C.
Studies of the kinetics of the precipitation of uniform silica particles trough the hydrolysis and condensation of silicon alkoxides.
Journal of the European Ceramics Society 142, 1 (1991), 1–18.

[18] BOKOBZA, L., GARNAUD, G., MARKS, J. E., JETHMALANI, J. M., SEABOLT, E. E., AND FORD, W. T.
Effects of filler particle/elastomer distribution and interaction on composite mechanical properties.
Chemistry of Materials 14, 1 (2002), 162–167.

[19] BRUCHEZ, M. P., MORONNE, M., GIN, P., WEISS, S., AND ALIVISATOS, A. P.
Semiconductor nanocrystals as fluorescent biological labels.
Science 281 (1998), 2013–2016.

[20] CARNAHAN, N. F., AND STARLING, K. E.
Equation of state for nonattracting rigid spheres.
Journal of Chemical Physics 51 (1997), 635.

[21] CARUSO, F., AND MOHWALD, H.
Preparation and characterization of ordered nanoparticle and polymer composite multilayers on colloids.
Langmuir 15, 23 (1999), 8276–8281.

[22] CHAN, W. C. W., AND NIE, S.
Quantum dot bioconjugates for ultrasensitive nonisotopic detection.
Science 281 (1998), 2016–2018.

[23] CHANG, S., LIU, L., AND ASHER, S.

Preparation and properties of tailored morphology, monodisperse colloidal silica-cadmium sulfide nanocomposites.
Journal of the American Chemical Society 116, 15 (1994), 6739–6744.

[24] CHEN, S., DONG, P., YANG, G., AND YANG, J.
Characteristic aspects of the formation of new particles during the growth of monodisperse silica seeds.
Journal of Colloid and Interface Science 180, 1 (1996), 237–241.

[25] CHUJO, Y., AND SAEGUSA, T.
Organic polymer hybrids with silica-gel formed by means of the sol-gel method.
Advances in Polymer Science 100 (1992), 11–29.

[26] CLAPP, A. R., MEDINTZ, I. L., MAURO, J. M., FISHER, B. R., BAWENDI, M. G., AND MATTOUSSI, H.
Fluorescence resonance energy transfer between quantum dot donors and dye-labeled protein acceptors.
Journal of the American Chemical Society 126 (2004), 301–310.

[27] COE-SULLIVAN, S., WOO, W. K., BAWENDI, M. G., AND BULOVIC, V.
Electroluminescence from single monolayers of nanocrystals in molecular organic devices.
Nature 420, 6917 (2002), 800–803.

[28] CORREA-DUARTE, M., GIERSIG, M., AND LIZ-MARZAN, L.
Stabilization of CdS semiconductor nanoparticles against photodegradation by a silica coating procedure.
Chemical Physics Letters 286, 5-6 (1998), 497–501.

[29] CRIVELLO, J. V.
Cationic polymerization - iodonium and sulfonium salt photoinitiatorsdiaryliodonium salts - new class of photo-initiators for cationic polymerization.
Advanced in Polymer Science 62 (1984), 1–48.

[30] CRIVELLO, J. V., AND LAM, J. H. W.
Diaryliodonium salts - new class of photo-initiators for cationic polymerization.
Macromolecules 10, 6 (1977), 1307–1315.

[31] D., W., PELLER, M., AND HAUPTMANN, P.
Polymerizations in the presence of seeds 2. monitoring the emulsion polymerization in the presence of fillers by means of ultrasound.
Acta Polymerica 37, 7 (1986), 468–469.

[32] DABBOUSI, B. O., RODRIGUEZ-VIEJO, J., MIKULEC, F. V., HEINE, J., MATTOUSSI, R., OBER, R., JENSEN, K. F., AND BAWENDI, M. G.
(CdSe)ZnS core-shell quantum dots: Synthesis and characterization of a size series of highly luminescent nanocrystallites.
Journal of Physical Chemistry B 101, 46 (1997), 9463–9475.

[33] DARBANDI, M., THOMANN, R., AND NANN, T.
Single quantum dots in silica spheres by microemulsion synthesis.
Chemistry of Materials 17, 23 (2005), 5720–5725.

[34] DIETSCH, H., AND KELLER, B. A.
Influence of the filler size and volume on the glass temperature and friction coefficient in a silica particles-pmma hybrid composite.
Journal of Tribology 1111 (2006), submitted on March 14^{th}.

[35] DIETSCH, H., LOOTENS, D., AND KELLER, B. A.
Synthesis and rheological study of tailored monodisperse and monodistributed $\mathrm{Si}\text{ø}_2$-pmma composites.
1111 1111 (2006), in preparation.

[36] DIETSCH, H., LOOTENS, D., AND KELLER, B. A.
Synthetic route to a large amount of CdSe quantum dots at low temperatures for label applications.
Journal of Materials Chemistry 1111 (2006), submitted on June 30^{th}.

[37] DIRIX, Y., BASTIAANSEN, C., CASERI, W., AND SMITH, P.
Preparation, structure and properties of uniaxially oriented polyethylene-silver nanocomposites.
Journal of Materials Science 34 (1999), 3859–3866.

[38] EK, S., IISKOLA, E. I., NIINISTÖ, L., PAKKANEN, T. T., AND ROOT, A.
New bonding modes of gas-phase deposited 3-aminopropyltriethoxysilane on silica by ^{29}Si CP/M as NMR.
Chemical Communication 16 (2003), 2032–2033.

[39] EMPEDOCLES, S. A., AND BAWENDI, M. G.
Spectroscopy of single CdSe nanocrystallites.
Accounts of Chemical Research 32, 5 (1999), 389–396.

[40] FLEMING, M., AND WALT, D.
Stability and exchange studies of alkanethiol monolayers on gold-nanoparticle-coated silica microspheres.
Langmuir 17, 16 (2001), 4836–4843.

[41] FLETCHER, W. P., AND GENT, A. N.
Dynamic shear properties of some rubber-like materials.
British Journal of Applied Physics 8, 5 (1957), 194–201.

[42] GAZZILLO, D., AND GIOCOMETTI, A.
Structure factors for the simplest solvable model of polydisperse colloidal fluids with surface adhesion.
Journal of Chemical Physics 113 (2000), 9837–3848.

[43] GEORGES, J., ARNAUD, N., AND PARISE, L.

Limitations arising from optical saturation in fluorescence and thermal lens spectrometries using pulsed laser excitation: Application to the determination of the fluorescence quantum yield of rhodamine 6G.
Applied Spectroscopy 50 (1996), 1505–1511.

[44] GERION, D., PINAUD, F., AND WILLIAMS, S.
Synthesis and properties of biocompatible water-soluble silica-coated CdSe/ZnS semiconductor quantum dots.
Journal of Physical Chemistry B 105, 37 (2001), 8861–8871.

[45] GIESCHE, H.
Synthesis of monodispersed silica powders ii. controlled growth reaction and continuous production process.
Journal of the European Ceramics Society 14 (1994), 205–214.

[46] GILMAN, J. W.
Flammability and thermal stability studies of polymer layered-silicate (clay) nanocomposites.
Applied Clay Science 15 (1999), 31–49.

[47] GILMAN, J. W., JACKSON, C. L., MORGAN, A. B., HARRIS, R., MANIAS, E., GIANNELIS, E. P., WUTHENOW, M., HILTON, D., AND PHILIPPS, S. H.
Flammability properties of polymer - layered-silicate nanocomposites. polypropylene and polystyrene nanocomposites.
Chemistry of Materials 12 (2000), 1866–1873.

[48] GODOVSKI, D. Y.
Electron behavior and magnetic-properties of polymer nanocomposites.
Thermal and Electrical Conductivity of Polymer Materials Advances in Polymer Science 119 (1995), 79–122.

[49] GRAF, C., VOSSEN, D. L. J., IMHOF, A., AND BLAADEREN, A. V.
A general method to coat colloidal particles with silica.
Langmuir 19 (2003), 6693–6700.

[50] HAIR, M. L.
Chemically Modified Surfaces, Silane surfaces and Interfaces, vol. 1.
New York, 1986.

[51] HANPRASOPWATTANA, A., SRINIVASAN, S., SAULT, A. G., AND DATYE, A. K.
Titania coatings on monodisperse silica spheres (characterization using 2-propanol dehydration and TEM).
Langmuir 12, 13 (1996), 3173–3179.

[52] HANPRASOPWATTANA, A., SRINIVASAN, S., SAULT, A. G., AND DATYE, A. K.

Synthesis and characterization of PMMA nanocomposites by suspension and emulsion polymerization.
Macromolecules 34, 10 (2001), 3255–3260.

[53] HINES, M. A., AND GUYOT-SIONNEST, P.
Synthesis and characterization of strongly luminescing ZnS-capped CdSe nanocrystals.
Journal of Physical Chemistry (Letter) 100 (1996), 468–470.

[54] ILER, R. K.
The Chemistry of Silica.
Wiley, 1979.

[55] IMHOF, A., AND MEGENS, M.
Spectroscopy of fluorescein dye colloidal silica spheres.
Journal of Physical Chemistry B 103, 9 (1999), 1408–1415.

[56] JETHMALANI, J. M., AND FORD, W. T.
Diffraction of visible light by ordered monodisperse silica-poly(methyl acrylate) composite films.
Chemistry of Materials 8, 8 (1996), 2138–2146.

[57] JETHMALANI, J. M., FORD, W. T., AND BEAUCAGE, G.
Crystal structures of monodisperse colloidal silica in poly(methyl acrylate) films.
Langmuir 13, 13 (1997), 3338–3344.

[58] JETHMALANI, J. M., SUNKARA, H. B., FORD, W. T., WILLOUGHBY, S. L., AND ACKERSON, B. J.
Optical diffraction from silica-poly(methyl methacrylate) composite films.
Langmuir 13, 10 (1997), 2633–2639.

[59] JOSEPH, R., ZHANG, S., AND FORD, W. T.
Structure and dynamics of a colloidal silica-poly(methyl methacrylate) composite by ^{13}C and ^{29}Si MAS NMR spectroscopy.
Macromolecules 29, 4 (1996), 1305–1312.

[60] JUDEINSTEIN, P., AND SANCHEZ, C.
Synthesis of nanocomposites - organoceramics.
Journal of Materials Chemistry 6, 4 (1996), 511–525.

[61] KAMATA, K., LU, Y., AND XIA, Y. N.
Synthesis and characterization of monodispersed core-shell spherical colloids with movable cores.
Journal of the American Chemical Society 125 (2003), 2384–2385.

[62] KARSTENS, T., AND KOBS, K.
Rhodamine-B and rhodamine-101 as reference substances for fluorescence quantum yield measurements.
Journal of Physical Chemistry 84 (1980), 1871–1872.

[63] KHANNA, P., MORLEY, C. P., GORTE, R. M., GOKHALE, R., SUBBARAO, V. V. V. S., AND SATYANARAYANA, C. V. V.
A simple and effective synthesis of cadmium selenide in aqueous N,N-dimethylformamide.
Materials Chemistry and Physics 83, 2-3 (2004), 323–327.

[64] KICKELBICK, G., AND SCHUBERT, U.
Synthesis of nanocomposites - organoceramics.
Monatshefte für Chemie 132, 1 (2001), 13–30.

[65] KIM, B. K., SEO, J. W., AND JEONG, H. M.
Morphology and properties of waterborne polyurethane/clay nanocomposites.
European Polymer Journal 39, 1 (2003), 85–91.

[66] KINNEY, D. R., CHUANG, I., AND MACIEL, G. E.
Water and the silica surface as studied by variable-temperature high-resolution proton NMR.
Journal of the American Chemical Society 115, 15 (1993), 6786–6794.

[67] KRALL, A. H., AND WEITZ, D. A.
Internal dynamics and elasticity of fractal colloidal gels.
Physical Review Letters 80 (1998), 778–781.

[68] LI, J. J., WANG, A., GUO, W., KEAY, J. C., MISHIMA, T. D., JOHNSON, M., AND PENG, X.
Large-scale synthesis of nearly monodisperse CdSe/CdS core/shell nanocrystals using air-stable reagents via successive ion layer adsorption and reaction.
Journal of the American Chemical Society 125, 41 (2003), 12567–12575.

[69] LIMBACH, L. K., LI, Y. C., GRASS, R. N., BRUNNER, T. J., HINTERMANN, M. A., MULLER, M., GUNTHER, D., AND STARK, W. J.
Oxide nanoparticle uptake in human lung fibroblasts: Effects of particle size, agglomeration, and diffusion at low concentrations.
Environmental Science and Technology 39, 23 (2005), 9370–9376.

[70] LIN, H., DAY, D. E., AND STOFFER, J. O.
Optical and mechanical-properties of optically transparent poly(methyl methacrylate) composites.
Polymer Engineering and Science 32, 5 (1992), 344–350.

[71] LOOTENS, D.
Ciments et suspensions concentrées modèles: écoulement, encombrement et flocculation.
PhD thesis, Université Pierre et Marie Curie, 2004.

[72] LU, Y., MCLELLAN, J., AND XIA, Y. N.
Synthesis and crystallization of hybrid spherical colloids composed of polystyrene cores and silica shells.
Langmuir 20 (2004), 3464–3470.

[73] MATTOUSSI, H., MAURO, J. M., GOLDMAN, E. R., ANDERSON, G. P., SUNDAR, V. C., MIKULEC, F. V., AND BAWENDI, M. G.
Self-assembly of CdSe-ZnS quantum dot bioconjugates using an engineered recombinant protein.
Journal of the American Chemical Society 122 (2000), 12142–12150.

[74] MAUGER, M., DUBAULT, A., AND HALARY, J. L.
Synthesis and physico-chemical characterization of networks based on methacryloxypropyl-grafted nano-silica and methyl methacrylate.
Polymer International 53, 4 (2004), 378–385.

[75] MAYO, F. R., AND LEWIS, F. M.
Copolymerization I A basis for comparing the behavior of monomers in copolymerization, the copolymerization of styrene and methyl methacrylate.
Journal of the American Chemical Society 66 (1944), 1594–1601.

[76] MEKIS, I., TALAPIN, D. V., KORNOWSKI, A., HAASE, M., AND WELLER, H.
One-pot synthesis of highly luminescent $\mathrm{CdSeCdS}$ core-shell nanocrystals vie organometallic and "greener" approaches.
Journal of Physical Chemistry B 107 (2003), 7454–7462.

[77] MESSERSMITH, P. B., AND STUPP, S. I.
Synthesis of nanocomposites - organoceramics.
Journal of Materials Research 7, 9 (1992), 2599–2611.

[78] MOHAMED, M. B., TONTI, D., AL-SALMAN, A., CHEMSEDDINE, A., AND CHERGUI, M.
Synthesis of high quality zinc blende CdSe nanocrystals.
Journal of Physical Chemistry B 109, 21 (2005), 10533–10537.

[79] MONTES, H., LEQUEUX, F., AND BERRIOT, J.
Influence of the glass transition temperature gradient on the nonlinear viscoelastic behavior in reinforced elastomers.
Macromolecules 36, 21 (2003), 8107–8118.

[80] MORIKAWA, A., YAMAGUCHI, H., KAKIMOTO, M., AND IMAI, Y.
Formation of interconnected globular structure of silica phase in polyimide silica hybrid films prepared by the sol-gel process.
Chemistry of Materials 6, 7 (1994), 913–917.

[81] MURRAY, C., NORRIS, D., AND BAWENDI, M. G.
Synthesis and characterization of nearly monodisperse CdE (E = S, Se, Te) semiconductor nanocrystallites.
Journal of the American Chemical Society 115, 19 (1993), 8706–8715.

[82] MUSIL, J.
Hard and superhard nanocomposite coatings.

Surface and Coatings Technology 125, 1-3 (2000), 322–330.

[83] NAKAO, Y.
Noble-metal solid sols in poly(methyl methacrylate).
Journal of Colloid and Interface Science 171 (1995), 386–391.

[84] NANN, T., AND MULVANEY, P.
Single quantum dots in spherical silica particles.
Angewandte Chemie-International Edition 43, 40 (2004), 5393–5396.

[85] NARITA, T., KNAEBEL, A., MUNCH, J. P., ZRINYI, M., AND CANDAU, S.
Microrheology of chemically crosslinked polymer gels by diffusing-wave spectroscopy.
Macromolecular Symposia 207 (2004), 17–30.

[86] NISHIYAMA, N., HORIE, K., SHICK, R., AND ISHIDA, H.
Influence of adsorption behavior of a silane coupling agent onto silica on viscoelastic properties.
Polymer Communications 31, 10 (1990), 380–383.

[87] NOVAK, B. M.
Hybrid nanocomposite materials - between inorganic glasses and organic polymers.
Advanced Materials 5 (1993), 422–433.

[88] OKADA, A., AND USUKI, A.
The chemistry of polymer-clay hybrids.
Materials Science and Engineering C 3 (1995), 109–115.

[89] OSMAN, M. A., MITTAL, V., MORBIDELLI, M., AND SUTER, U. W.
Polyurethane adhesive nanocomposites as gas permeation barrier.
Macromolecules 36, 26 (2003), 9851–9858.

[90] PALKOVITS, R., ALTHUES, H., RUMPLECKER, A., TESCHE, B., DREIER, A., HOLLE, U., FINK, G., CHENG, C. H., SHANTZ, D. F., AND KASKEL, S.
Polymerization of w/o microemulsions for the preparation of transparent SiO_2-PMMA nanocomposites.
Langmuir 21 (2005), 6048–6053.

[91] PARK, S. J., AND CHO, K. S.
Filler-elastomer interactions: influence of silane coupling agent on crosslink density and thermal stability of silica/rubber composites.
Journal of Colloid and Interface Science, Academic Press 267, 1 (2003), 86–91.

[92] PAYNE, A. R.
Dynamic properties of natural rubber containing heat-treated carbon blacks.
Journal of Applied Polymer Science 9, 10 (1965), 3245–3254.

[93] PELIZETTI, E.
Fine Particles and Technology, vol. 12.
Klunwer Academic Publishers, 1996.

[94] PENG, X., SCHLAMP, M. C., KADAVANICH, A. V., AND ALIVISATOS, A. P.
Epitaxial growth of highly luminescent CdSe/CdS core/shell nanocrystals with photostability and electronic accessibility.
Journal of the American Chemical Society 119 (1997), 7019–7029.

[95] PENG, Z. A., AND PENG, X.
Formation of high-quality CdTe, CdSe, and CdS nanocrystals using CdO as precursor.
Journal of Physical Chemistry (Communication) 123, 1 (2001), 183–184.

[96] PHILIPSE, A., AND VRIJ, A.
Preparation and properties of nonaqueous model dispersions of chemically modified, charged silica spheres.
Journal of Colloid and Interface Science 128, 1 (1989), 121–136.

[97] POKREL, M. R., AND BOSSMANN, S. H.
Synthesis, characterization, and first application of high molecular weight polyacrylic acid derivatives possessing perfluorinated side chains and chemically linked pyrene.
Journal of Physical Chemistry B 104 (2000), 2215–2223.

[98] POPE, E. J. A., ASAMI, M., AND MACKENZIE, J. D.
Transparent silica gel-PMMA composites.
Journal of Materials Chemistry 4, 4 (1989), 1018–1026.

[99] PORTER, D., METCALFE, E., AND THOMAS, M. J. K.
Nanocomposite fire retardants - a review.
Fire and Materials 24 (2000), 45–52.

[100] PRADHAN, N., AND EFRIMA, S.
Single precursor, one-pot versatile synthesis under near ambient conditions of tunable, single and dual band fluorescing metal sulfide nanoparticles.
Journal of the American Chemical Society 125, 8 (2003), 2050–2051.

[101] PU, Z., MARK, J. E., JETHMALANI, J. M., AND FORD, W. T.
Mechanical properties of a poly(methyl acrylate) nanocomposite containing regularly-arranged silica particles.
Polymer Bulletin 37, 4 (1996), 545–551.

[102] QU, L. H., PENG, Z. A., AND PENG, X. G.
Alternative routes toward high quality CdSe nanocrystals.
Nanoletters 1, 6 (2001), 333–337.

[103] REISS, P., BLEUSE, J., AND PRON, A.
Highly luminescent $\mathrm{CdSe/ZnSe}$ core/shell nanocrystals of low size dispersion.
Nanoletters 2, 7 (2002), 781–784.

[104] ROGACH, A., NAGESHA, D., AND OSTRANDER, J.
"raisin bun"-type composite spheres of silica and semiconductor nanocrystals.
Chemistry of Materials 12, 9 (2000), 2676–2685.

[105] ROMER, S., SCHEFFOLD, F., AND SCHURTENBERGER, P.
Sol-gel transition of concentrated colloidal suspensions.
Physical Review Letters 85 (2000), 4980–4983.

[106] RUYS, A. J., AND MAI, Y. W.
The nanoparticle-coating process: a potential sol-gel route to homogeneous nanocomposites.
Materials Science and Engineering A 265 (1999), 202–207.

[107] SANCHEZ, C., AND RIBOT, F.
Design of hybrid organic-inorganic materials synthesized via sol-gel chemistry.
New Journal of Chemistry 18 (1994), 1007–1047.

[108] SANTRA, S., ZHANG, P., AND WANG, K.
Conjugation of biomolecules with luminophoredoped silica nanoparticles for photostable biomarkers.
Analytical Chemistry 73, 20 (2001), 4988–4993.

[109] SARIC, M., DIETSCH, H., AND SCHURTENBERGER, P.
In-situ polymerization as a route towards transparent nanocomposites: Time-resolved light scattering experiments.
Colloids and Surfaces A 291 (2006), 110–116.

[110] SCHEFFOLD, F., AND SCHURTENBERGER, P.
Light scattering probes of viscoelastic fluids and solids.
Soft Materials 1, 2 (2003), 139–165.

[111] SCHNURR, B., GITTES, F., MACKINTOSH, F. C., AND SCHMIDT, C. F.
Determining microscopic viscoelasticity in flexible and semiflexible polymer networks from thermal fluctuations.
Macromolecules 30 (1997), 7781–7792.

[112] SCHUBERT, U.
Polymers reinforced by covalently bonded inorganic clusters.
Chemistry of Materials 13, 10 (2001), 3487–3494.

[113] SCHUBERT, U., AND HÜSING, N.
Synthesis of Inorganic Materials, 2nd, Revised and Updated Edition.
Wiley-VCH, 2005.

[114] SCHUBERT, U., HÜSING, N., AND LORENZ, A.
Hybrid inorganic-organic materials by sol-gel processing of organofunctional metal alkoxides.
Chemistry of Materials 7 (1995), 2010–2027.

[115] SCHURTENBERGER, P., BISSIG, H., ROJAS, L., VAVRIN, R., STRADNER, A., ROMER, S., SCHEFFOLD, F., AND TRAPPE, V.
Aggregation and gelation in colloidal suspensions: Time-resolved light and neutron scattering experiments.

Mesoscale Phenomena in Fluid Systems ACS Symposium Series 861 (2003), 143–160.

[116] SELLINGER, A., WEISS, P. M., NGUYEN, A., LU, Y. F., ASSINK, R. A., GONG, W. L., AND BRINKER, C. J.
Continuous self-assembly of organic-inorganic nanocomposite coatings that mimic nacre.
Nature 394, 6690 (1998), 256–260.

[117] SHANG, S. W., WILLIAMS, J. W., AND SODERHOLM, K. J. M.
Using the bond-energy density to predict the reinforcing ability of a composite.
Journal of Materials Science 27 (1992), 4949–4956.

[118] SHENG, N., BOYCE, M. C., PARKS, D. M., RUTLEDGE, G. C., ABES, J. I., AND COHEN, R. E.
Multiscale micromechanical modeling of polymer/clay nanocomposites and the effective clay particle.
Polymer 45, 2 (2004), 487–506.

[119] SOOKLAL, K., HANUS, L. H., PLOEHN, H. J., AND MURPHY, C. J.
A blue-emitting CdS/dendrimer nanocomposite.
Advanced Materials 10, 14 (1998), 1083–1087.

[120] SOPPIMATH, K. S., AMINABHAVI, T. M., KULKARNI, A. R., AND RUDZINSKI, W. E.
Biodegradable polymeric nanoparticles as drug delivery devices.
Journal of Controlled Release 70, 1-2 (2001), 1–20.

[121] SPEIDEL, M., JONAS, A., AND FLORIN, E. L.
Three-dimensional tracking of fluorescent nanoparticles with subnanometer precision by use of off-focus imaging.
Optical Letters 28 (2003), 69–71.

[122] STECKEL, J. S., ZIMMER, J. P., COE-SULLIVAN, S., STOTT, N. E., BULOVI, V., AND BAWENDI, M. G.
Blue luminescence from (CdS)ZnS core-shell nanocrystals.
Angewandte Chemie International Edition 43 (2004), 2154–2158.

[123] STÖBER, W., AND FINK, A.
Controlled growth of monodisperse silica spheres in the micron size range.
Journal of Colloid and Interface Science 26 (1968), 62–69.

[124] SUGIMOTO, T.
Fine particles. Synthesis, characterisation, and Mechanisms of growth, vol. 92.
2000.

[125] SUNDAR, V. C., LEE, J., HEINE, J. R., BAWENDI, M. G., AND JENSEN, K. F.
Full color emission from II-VI semiconductor quantum dot-polymer composites.
Advanced Materials 12 (2000), 1102–1104.

[126] SUNKARA, H. B., JETHMALANI, J. M., AND FORD, W. T.
Composite of colloidal crystals of silica in poly(methyl methacrylate).
Chemistry of Materials 6, 4 (1994), 362–364.

[127] TAN, C. G., BOWEN, B. D., AND EPSTEIN, N.
Production of monodisperse colloidal silica spheres: effect of temperature.
Journal of Colloid and Interface Science 118, 1 (1987), 290–293.

[128] TANFORD, C.
Micelle shape and size.
The Journal of Physical Chemistry 76, 21 (1972), 3020–3024.

[129] TERRONES, M.
Science and technology of the twenty-first century: Synthesis, properties and applications of carbon nanotubes.
Annual Review of Materials Research 33 (2003), 419–501.

[130] TSAI, H. L., SCHINDLER, J. L., KANNEWURF, C. R., AND KANATZIDIS, M. G.
Plastic superconducting polymer-$NbSe_2$ nanocomposites.
Chemistry of Materials 9 (1997), 875–878.

[131] VARSHNEY, S. K., HAUTEKEER, J. P., FAYT, R., JÉRÔME, R., AND TESSYSSIÉ, P.
Anionic polymerization of (meth)acrylic monomers. 4. effect of lithium salts as ligands on the 2living" polymerization of methyl methycrylate using monofunctional initiators.
Macromolecules 23 (1990), 2618–2622.

[132] VERHAEGH, N. A. M., AND BLAADEREN, A. V.
Dispersions of rhodamine-labeled silica spheres - synthesis, characterization, and fluorescence confocal scanning laser microscopy.
Langmuir 10, 5 (1994), 1427–1438.

[133] WANG, W., AND ASHER, S.
Photochemical incorporation of silver quantum dots in monodisperse silica colloids for photonic crystal applications.
Journal of the American Chemical Society 123, 50 (2001), 12528–12535.

[134] WEN, J. Y., AND WILKES, G. L.
Organic/inorganic hybrid network materials by the sol-gel approach.
Chemistry of Materials 8, 8 (1996), 1667–1681.

[135] WILLIAMS, M. L., LANDEL, R. F., AND FERRY, J. D.
Mechanical properties of substances of high molecular weight .19. the temperature dependence of relaxation mechanisms in amorphous polymers and other glass-forming liquids.
Journal of the American Chemical Society 77, 14 (1955), 3701–3707.

[136] WIRNSBERGER, G., SCOTT, B. J., CHMELKA, B. F., AND STUCKY, G. D.
Fast response photochromic mesostructures.
Advanced Materials 12, 19 (2000), 1450–1454.

[137] WONG, M. S., AND STUCKY, G. D.
The facile synthesis of nanocrystalline semiconductor quantum dots.
Materials Research Society Symposium Proceedings 676 (2001).

[138] WORSFOLD, D. J., AND BYWATER, S.
Anionic polymerization of styrene.
Canadian Journal of Chemistry-Revue Canadienne de Chimie 38, 10 (1960), 1891–1900.

[139] WU, X., LIU, H., LIU, J., HALEY, K. N., LARSON, J. A., GE, N., PEALE, F., AND BRUCHEZ, M. P.
Immunofluorescent labeling of cancer marker Her2 and other cellular targets with semiconductor quantum dots.
Nature Biotechnology 21 (2003), 41–46.

[140] YANG, H., QU, H., AND LIN, P.
Nanometer fluorescent hybrid silica particle as ultrasensitive and photostable biological labels.
Analyst 128, 5 (2003), 462–466.

[141] ZANETTI, M., LOMAKIN, S., AND CAMINO, G.
Polymer layered silicate nanocomposites.
Macromolecular Materials and Engineering 279 (2000), 1–9.

[142] ZILG, C., THOMANN, R., MULHAUPT, R., AND FINTER, J.
Polyurethane nanocomposites containing laminated anisotropic nanoparticles derived from organophilic layered silicates.
Advanced Materials 11 (1999), 49–52.

[143] ZUNDEL, T., TEYSSIÉ, P., AND JÉRÔME, R.
New ligands for the living isotactic anionic polymerization of methyl methacrylate in toluene at 0 °C. 1. ligation of butyllithium by lithium silanolates.
Macromolecules 31 (1998), 2433–2439.

Curriculum Vitae

Date and place of birth:	25 November 1980, Strasbourg, France
Bachelor of Science:	Chemistry, University R. Schuman - Strasbourg Sud, France (1998 – 2000)
Master of Science:	Technology and Transformation of Polymer Materials, University J. Monnet - Saint-Etienne, France (2000 – 2002)
DEA :	Diplôme d'Etudes Approfondies Polymer Materials and Composites, University J. Monnet - Saint-Etienne, France (2002 – 2003)
Doctorate:	Nanoscale Materials Science, Empa, Materials Science and Technology - Dübendorf and University of Physics - Fribourg, Switzerland (2003 – 2006)

List of publications and communications

Publications and Posters

H. Dietsch and B. A. Keller, *Nanoparticles hybrid systems: interactions, local structure and mobility*, March 11^{th} 2004, Poster Presentation, Forschungsmarktplatz, Empa, Dübendorf (Switzerland).

H. Dietsch and B. A. Keller, *Nanoparticles hybrid systems: surface modification and fluorescent* $\mathrm{SiO_2}$ *particles*, October, 21^{st} 2004, Poster Presentation, Polymer Group Switzerland (PGS), Nestlé, Vers-Chez-Les-Blanc, Lausanne (Switzerland).

H. Dietsch and B. A. Keller, *Nanoparticles hybrid systems: interactions, local structure and mobility*, April 11^{th} 2004, Poster Presentation, Centre Löwenberg, Murten (Switzerland).

H. Dietsch and B. A. Keller, *Nanoparticles hybrid systems: synthesis of monodisperse* $\mathrm{SiO_2}$ *particles and incorporation in PMMA Matrix*, November 18^{th} 2005, Poster Presentation, PGS, Université de Neuchâtel, Neuchâtel (Switzerland).

H. Dietsch and B. A. Keller, *Influence of the filler size and volume on the glass temperature and friction coefficient in a silica particles-PMMA hybrid composite*, submitted on August 8^{th} 2006 to the Journal of Tribology.

H. Dietsch, D. Lootens and B. A. Keller, *Synthetic route to a large amount of* CdSe *quantum dots at low temperatures for label applications*, submitted to Nanotechnology.

H. Dietsch, D. Lootens and B. A. Keller, *Synthesis and rheological study of tailored monodisperse and monodistributed* $\mathrm{SiO_2}$*-PMMA composites*, submitted.

M. Saric, H. Dietsch and P. Schurtenberger, *In-situ polymerization as a route towards transparent nanocomposites: time-resolved light scattering experiments*, Colloids and Surfaces A, Physicochemical and Engineering Aspects (2006), 291, 110-116.

Oral communications

07-02-2005: *Quantum dots synthesis*- Novartis, Basel (Switzerland).

15-03-2005: *Nanopartikeln, Herstellung aus dem Stöber Prozess*- Empa, Hochleistungskeramik, Dübendorf (Switzerland).

19-05-2005: *Nanoparticles hybrid systems*- Seminar Gruppe Textor ETH-Abt. 125, ETHZ, Zürich (Switzerland).

15-12-2005: *Einbettung von Nanopartikeln in Polymeren*- mit Prof. Raupach and Prof. Holzer, Empa, Dübendorf (Switzerland).

03-04-2006: *Herstellung von Nanopartikeln mit Sol-Gel Methode*- Nanopowder-day, Empa, Dübendorf (Switzerland).

Invited

01-07-2005: *Synthesis of monodisperse* $\mathrm{Si\,O_2}$ *particles with a modified Stöber sol-gel process*- $Ciba\ SC$, Basel (Switzerland).

19-09-2005: *Nanoparticles hybrid systems*- JEPO, Le Bessat (France).

10-01-2006: *Nanoparticles hybrid systems*- BASF AG, Ludwigshafen (Germany).

Acknowledgments

It is a great pleasure for me to express my sincere gratitude to Prof. Peter Schurtenberger, who supervised this work with discretion. I would like to thank him to let me go in the direction, I have chosen and for the interesting discussions, we had in Fribourg every few weeks.

I would like to express my gratitude to Dr. Max Wolfensberger and Prof. Dr. Hans Josef Hug, team leaders of 132 and 125, to integrate me in their team and always encourage me go in the research direction, I wanted to follow.

Dr. Beat Keller, my supervisor at Empa was always there when I had a theoretical question, his background and is broad knowledge in physico-chemistry helped me a lot in understanding my system. I would like to thank him as well for his kindness, for the barbecue, fondue and aperos, I really enjoyed to share with him.

Dr. Peggy Roßbach, who thought me the half of my current german vocabulary, was always there, when I had a question or a doubt a german expression or science.

Bastian Bommer started surface modification of nanoparticles with Beat before I came at Empa, I want to thank him for the knowledge transfer, his kindness and the nice week of measurements, we spent together at the synchrotron in December 2004.

Every few weeks, I had the opportunity to meet François, Mirko, Silvia and Serge, who worked on the same subject but more concentrated on the physical or computer simulation points, it was always very interesting to see other aspects of the work. Thank to Serge, I was able to understand what is a fractal dimension. As I was in Fribourg, Véronique always had an opened door for me to discuss about my results, I would like to thank her for her kindness.

Beatrice Fischer and Dr. Dani Rentsch did DSC, TGA and $^{29}\mathrm{Si}$ NMR analysis for me, I would like to express my gratitude for the rapidity and the time of work they invest for me. Dereje, Kranthi and Nicolas always helped me for the TEM pictures, a particular thank to Dereje for his time on Sunday morning every few weeks. Thank to Frank Winnefeld and Christian Walder, I am still able to use Rheometer in torsion, Couette-Couette or plate-plate geometries!

I could not stop this acknowledgments without thanking Dr. Didier Lootens, from Sika AG, who teach me the secrets of $\mathrm{Si\,O_2}$ particle synthesis and for the long discussions about the hybrid system. He is a crucial element which leads to this work and I would like to express ma

gratitude because he motivates me every few weeks in order to perform new experiments.

A particular thanks goes to the team 132 Erika, Regula, Paul, Conny, Peter, Markus and Stefan. I really enjoy sharing coffee break and lunch with you, thank you for your explanation about Swiss culture and for the good address to hike or to ski!

I would like to thank Andreas Mühlebach for the free sample of Irgacure 184, he provided me twice.

I am happy to know so many physicist now, Rowena, Raphaëlle, Sébastien, Kalle, Günther, Miguel, Roland, Magdalena, Sigi, Uli, Taryl, Peter, Philipp, Mani, Jörg, Sara, Sasa, Aude and of course my good friend Quang. It was a pleasure to work with you, to try to understand your work and to try to make my work understandable to you. I hope, we are the beginning of a collaboration between physicists and chemists!
Beatrice and Karin made all the administration staffs easier for me, thank you for that.

I am grateful to the thesis committee: Prof. Jean-Claude Dousse, president of Dept. of Physics at the University of Fribourg, my director, Prof. Peter Schurtenberger, my coach at Empa Dr. Beat Keller, my pretty soon colleague Prof. Raffaele Mezzenga from the University of Fribourg and Dr. Frédéric Prochazka from LRMP, Saint-Etienne (France).

I would like to thank Peter Schurtenberger another time because he is giving me the opportunity to integrate the "FriMat" center up to now, I hope I will understand a bit more how the scattering tools are working and hopefully be able to succeed in this new challenge combining chemical and physical work.

Je souhaite conclure ces remerciements dans ma langue maternelle pour deux raisons. D'une part, c'est vraiment plus simple pour moi et d'une autre part cela permettra à mon père de comprendre quelque chose à ce que j'ai écrit! Je veux exprimer tout d'abord toute ma gratitude à mon adorable femme Jana, elle est la seule parmi nous deux qui du début à la fin a cru en moi, les nuits blanches et mon stress ont toujours été atténués voire abolis grâce à ses théories et son écoute. Toujours prêts à m'écouter et à me soutenir moralement et financièrement, Sonia et Philippe, mes parents, ont réussis à faire de moi quelqu'un d'heureux et fier d'avoir suivi les chemins qu'ils m'ont montrés, ce travail est également le leurs (ce qui ne signifie pas dire qu'ils doivent payer l'apéro!). Merci encore à Jérôme et Laure, qui savent toujours me remettre en place (surtout Laure) quand je prends la grosse tête, je leur souhaite de continuer leur bout de route et de pouvoir s'épanouir tout comme moi dans leur couple et dans leur travail.

October 9^{th}, 2006, Fribourg